INSTITUTO POLITÉCNICO DE BRAGANÇA Escola Superior Agrária

UNIVERSIDADE TECNOLÓGICA FEDERAL DO PARANÁ

Alginate-based film blended with propolis loaded sporopollenin exine microcapsules: unveiling the potential of natural substances for wound healing

Maria Eduarda Soares Tofolli Moreira

Dissertation submitted to Escola Superior Agrária de Bragança to obtain the Degree of Master in Biotechnological Engineering under the scope of the double diploma with Federal University of Technology – Paraná - Brazil

Supervised by:

Soraia Isabel Domingues Marcos Falcão

Maria Carolina de Oliveira Ribeiro

Volkan Aylanc

Bragança

2025

I dedicate this to my family,
my pillar throughout this journey.

Acknowledgments

I would like to express my deepest gratitude to my co-advisor, Volkan Aylanc, for his invaluable guidance, support, and encouragement throughout my master's journey. His expertise and insights have been instrumental in shaping my research and helping me to achieve my goals. He has helped me to grow as a researcher and as a person. I am fortunate to have had the opportunity to work with him. I am truly grateful for his mentorship and friendship.

I appreciate my supervisors Soraia Isabel Domingues Marcos Falcão and Maria Carolina de Oliveira Ribeiro for their support. Their willingness to share expertise and provide me with valuable feedback throughout my academic path was really valuable to me.

To my parents, Sandra Maria Soares and Fabiano Tofolli Moreira, I am eternally grateful for your unwavering love and support. You have always believed in me, even when I doubted myself. Your sacrifices have made this possible, and I am forever obliged to you.

To the best sisters I could have ever asked for, Maria Clara Soares Tofolli Moreira and Maria Fernanda Soares Tofolli Moreira. I'm extremely thankful to have you both as my best friends and sisters. Thank you for all your support and encouragement throughout my life. Without your love and advise I would not be as happy as I am with you in my life. Thank you for always supporting me. You are my rock and my greatest motivation to be my best self.

I could not have done this without my friends and family, especially my grandmother Iracy Ferreira and my aunt Silene Aparecida Soares for their encouragement and support throughout my studies. Your kind words and presence have kept me motivated and sane during the challenging times. I am truly blessed to have you in my life.

To my departed grandmother Darcy Tofolli who inspired me to follow the path in this research! Thank you for all the years studying together with me. Your kindness inspired me to be a better person every day and to never give up on my dreams. You made me believe in myself and in my ability to achieve anything I set my mind to. Finally, you made me trust myself to purchase and achieve my goals. I really wish you could be here to see my work. You are missed.

To my dearest Celso Aires Czmola de Lima e Melo Faria, words cannot fully express how grateful I am for your unwavering support and love during my master's program. You have been my rock, my confidant, and my biggest cheerleader throughout this challenging yet rewarding journey. Thank you for always believing in me, even when I doubted myself and for

always celebrating my successes, no matter how small. I am so grateful for your patience, understanding, and willingness to always lend a listening ear. Your encouragement has given me the strength to persevere through tough times and reach for my dreams. I am truly blessed to have you by my side. I love you more than words can describe.

To my boss Marco Festas I express my immense appreciation for your understanding and support. Your flexibility and encouragement have been invaluable in helping me balance my academic and professional responsibilities. I'm truly grateful for the opportunity to continue my research while fulfilling my work commitments. Without your support I could not have completed my thesis while working, it really means a lot to me.

I would also like to thank Universidade Tecnológica Federal do Paraná (UTFPR), Instituto Politécnico de Bragança (IPB) and Centro de Investigação de Montanha (CIMO) for providing me with the resources and opportunities to pursue my research goals. I am grateful for the excellent education and training I have received.

This work is a association between Instituto Politécnico de Bragança (IPB) and Universidade Tecnológica Federal do Paraná (UTFPR). The study was partially funded by the Foundation for Science and Technology (FCT, Portugal) under the financial support to CIMO (UIDB/00690/2020 and UIDP/00690/2020) and SusTEC (LA/P/0007/2020) through national funds FCT/MCTES (PIDDAC).

ABSTRACT

Healing a wound is one of the complex biological processes associated with tissue growth and regeneration, controlled by various biochemical and cellular mechanisms. In recent years, the creation of dressings using biopolymer-based materials with natural extracts has gained prominence. With this in mind, the ideal dressing should promote a moist environment while acting as a barrier against microorganisms. Its composition should include non-toxic, non-allergenic, and adherent substances, being essential to ensure easy removal and high effectiveness in protecting the wound against bacterial infections. Moreover, dressings should possess anti-inflammatory properties while promoting the overall healing process.

This study explores the impact of extracts from two types of propolis on wound healing: red propolis and brown propolis. To produce the dressing, an alginate-based film was created, and propolis was incorporated into its composition through the vacuum-loading method in sporopollenin microcapsules, which are derived from bee pollen grains of *Cytisus* Shrub Species *(Cytisus spp.)*. This incorporation into the film is essential for the controlled release of bioactive compounds into the wound.

Spectrophotometric analyses determined that brown propolis achieved better inhibition results, which align with FTIR assays, where a higher composition of phenolic acids was observed in brown propolis samples compared to red propolis. Brown propolis films showed higher antioxidant activity (76.62% inhibition), outperforming red propolis (60.55%). The encapsulation efficiency of the microcapsules ranged from 67.35% to 74.48%, while the release rate of phenolic compounds reached up to 75% within 48 hours. Cytotoxicity tests indicated cell viability below 20% after 24 hours, evidencing toxicity at high concentrations.

Therefore, it is noted that, for cellular analyses, the results were not satisfactory given that the dressings showed to be toxic to the cells because of the high value of propolis incorporated. Despite of these results, it is possible to conclude that the dressings have great potential as they are full of antioxidants and antibacterial substances. For better results less propolis and loaded SECs should be incorporated into the films. Ultimately, it was possible to develop a dressing with satisfactory quality, although broader studies are necessary for its practical use.

Keywords: Dressing; Propolis; Bee pollen; Sporopollenin microcapsules; Wound; Alginate; Films.

RESUMO

Reparar uma ferida é um dos processos biológicos complexos associados ao crescimento e regeneração dos tecidos, controlados por diversos mecanismos bioquímicos e celulares. Nos últimos anos, criação de curativos utilizando materiais à base de biopolímeros com extratos naturais tem se destacado. Tendo isso em vista, o curativo ideal deve promover um ambiente úmido, atuando como uma barreira contra micro-organismos. A sua composição deve ser com substâncias atóxicas, não alergênicas e aderentes; sendo essencial sua fácil remoção e grande eficácia em proteger a ferida contra infecções bacterianas. Além disso, os curativos devem possuir propriedades anti-inflamatórias, ao mesmo tempo em que promovem o processo geral de cicatrização.

Este estudo explora o impacto do extrato de dois tipos de própolis na cicatrização de feridas, sendo elas: própolis vermelha e própolis castanha. Para a produção do curativo foi feito um filme à base de alginato e em sua composição incorporou-se própolis, pelo método de carregamento a vacuum, em microcápsulas de esporopolenina, que são fabricadas a partir de grãos de pólen de abelha de *Cytisus* Shrub Species *(Cytisus spp.)*. Esta incorporação no filme é importante para a liberação controlada de compostos bioativos no ferimento.

Definiu-se, após análises espectrofotométricas, que a própolis castanha obteve melhores resultados de inibição, o que compactua com os ensaios de FTIR, onde observa-se maior composição de ácidos fenólicos nas amostras de própolis castanha comparada à vermelha. Os filmes com própolis castanha apresentaram maior atividade antioxidante (76,62% de inibição), superior à vermelha (60,55%). A eficiência de encapsulamento das microcápsulas variou entre 67,35% e 74,48%, enquanto a taxa de liberação de compostos fenólicos foi de até 75% em 48 horas. Já os testes de citotoxicidade indicaram viabilidade celular inferior a 20% após 24 horas, evidenciando toxicidade em altas concentrações.

Dessa forma, constata-se que, para análises celulares, os resultados não foram satisfatórios, pois os curativos mostraram-se tóxicos às células devido à alta quantidade de própolis incorporada. Apesar destes resultados, foi possível concluir que os curativos possuem um grande potencial devido à alta quantidade de substâncias antioxidantes e antimicrobianas encontradas. Para melhores resultados menos própolis e biocápsulas carregadas devem ser incorporadas ao filme. Por fim, foi possível obter um curativo de qualidade satisfatória, sendo necessário estudos mais amplos para que possa ser utilizado de fato.

Palavras-chave: Curativo; Própolis; Pólen de abelha; Microcápsulas de esporopolenina; Ferida; Alginato; Filmes.

INDEX

INDEX OF FIGURES

INDEX OF TABLES

INDEX OF ABREVIATIONS

ABS	Absorbance
ABTS	2,2′-Azino-bis(3-ethylbenzothiazoline-6-sulfonic acid)
ATCC	American Type Culture Collection
BP	Brown Propolis
BPF	Brown Propolis Film
cDMEM	Complete Dulbecco's Modified Eagle's Medium
CF	Control Film
CLS	Cell Lines Service GmbH
CTL	Control
Cys	*Cytisus spp.*
DPBS	Dulbecco's Phosphate-Buffered Saline
DPPH	2,2-Diphenyl-1-picrylhydrazyl
DTA	Differential Thermal Analysis
DTG	Derivative Thermogravimetry
DW	Distilled water
EtOH	Ethanol
FTIR	Fourier Transform Infrared Spectroscopy
HaCaT	Human adult low Calcium Temperature
LC/DAD/ESI-MS^n	Liquid Chromatography Diode-Array Detection Electrospray Ionization Tandem Mass Spectrometry
PBS	Phosphate-Buffered Saline
RP	Red Propolis
RPF	Red Propolis Film
SBP	Sporopollenin-loaded Brown Propolis
SBPF	Sporopollenin-loaded Brown Propolis Film
SEC	Sporopollenin Exine Capsules
SEM	Scanning Electron Microscopy
SRP	Sporopollenin-loaded Red Propolis
SRPF	Sporopollenin-loaded Red Propolis Film
TGA	Thermogravimetric Analysis
UV-Vis	Ultraviolet–Visible Spectroscopy

1. INTRODUCTION

The skin is the body's largest organ, serving as both an anatomical and physiological barrier that protects against environmental threats. Constantly exposed to mechanical, biological, physical, and chemical stressors, the skin plays a crucial role as the first line of defense, preventing damage that could compromise the body's internal balance. When injuries occur, a complex healing process is triggered to restore skin integrity, which is essential for maintaining homeostasis. Research by Guo & Dipietro (2010) describes wound healing as a multi-stage process involving four distinct phases: hemostasis, inflammation, proliferation, and remodeling. Each phase plays a vital role in ensuring proper tissue regeneration and recovery.

Currently, antimicrobials are commonly used to treat skin injuries and prevent infections. However, excessive, prolonged, or indiscriminate use of these medications can pose health risks to patients. The first antibiotic ever discovered, benzylpenicillin, was identified by bacteriologist Alexander Fleming in 1928. However, it was not until 1941 that mass production became feasible, thanks to the efforts of scientists Ernst Boris Chain and Howard Walter Florey. Since then, antibiotics have transformed the treatment of bacterial infections, particularly in surgical settings. According to a study published by Bell (2014), the global incidence of diseases treatable with antibiotics decreased by 40% after the introduction of penicillin.

The widespread use of antibiotics over the decades has significantly contributed to the rise of resistant bacteria, posing a major global health challenge. This resistance makes infections harder to treat, leading to increased morbidity and higher healthcare costs (Barreto et al., 2024). Additionally, antibiotics can cause various adverse effects, ranging from mild gastrointestinal discomfort to severe conditions such as toxic epidermal necrolysis and acute hepatitis (de Ávila Reis et al., 2010).

Given these concerns, researchers have been exploring alternative treatments for infections and skin injuries, seeking natural and non-toxic solutions that could replace conventional antibiotics and other chemical-based prophylactic methods. Among these alternatives, propolis—a resinous substance produced by bees—has gained considerable attention. Bees play a crucial ecological role as pollinators, with approximately 87.5% of flowering plants relying on pollination to complete their reproductive cycles (Ollerton et al., 2011). The most commercially significant species, *Apis mellifera L.*, is primarily responsible for honey production and also collects plant resins from the environment, transforming them into propolis.

Often referred to as "bee glue," propolis is a sticky, resinous material produced by worker bees (*Apis mellifera L.*) by mixing plant resins with enzymes from their salivary secretions, wax, and pollen. According to the Brazilian Ministry of Agriculture, Livestock, and Supply (Brasil, Ministério da Agricultura, Pecuária e Abastecimento, 2001), propolis consists of resins from various plant exudates combined with enzymes such as ß-glucosidase, wax, and bee pollen. Inside beehives, propolis serves as both a physical and chemical barrier, thanks to its antiseptic, antimicrobial, and antiviral properties. Bees use it to protect against invading insects and microorganisms while also repairing hive structures (Oliveira, 2021).

The composition of propolis varies depending on the plant species pollinated by the bees, leading to differences in color and chemical profile. In this study, two distinct types of propolis will be analyzed: brown propolis from Portugal and red propolis from northeastern region of Brazil. This resinous substance has drawn increasing interest for its medicinal properties and potential applications in various industries, including cosmetics, pharmaceuticals, and biotechnology (Bankova et al., 2000). Notably, standardized propolis has demonstrated several pharmacological activities in vitro. Research by Touzani et al. (2019) highlighted its antioxidant potential through free radical scavenging assays, as well as its anti-inflammatory effects, which modulate inflammatory cytokine production in lipopolysaccharide-stimulated human peripheral blood mononuclear cells.

Propolis shows promising potential in inhibiting pathogenic bacteria that contribute to wound inflammation. This study aims to evaluate the capacity of red and brown propolis to support the wound healing process. A crucial factor in effective healing is controlled release, which can be achieved by encapsulating propolis within a natural, bioactive microcapsule. Maintaining a consistent concentration of active compounds at the wound site is essential for optimizing treatment outcomes. This controlled release ensures a steady supply of bioactive molecules, preventing fluctuations that could compromise the healing process (Stojko et al., 2021).

Furthermore, this type of drug delivery system can be more convenient for patients, as it reduces the frequency of application and minimizes systemic side effects. This occurs because controlled release in topical applications concentrates the active compound in the affected area, reducing systemic absorption and, consequently, the potential for adverse effects (Fea et al., 2024; Adepu & Ramakrishna, 2021). Moreover, the controlled release of propolis has been shown to provide significant therapeutic advantages. According to Stojko et al. (2021), this method helps prevent infections and promotes faster tissue regeneration, making it a valuable approach for wound healing and skin treatments.

For this study, the selected capsules are derived from bee pollen of the *Cytisus* shrub species (*Cytisus spp.*). After the removal of genetic material from the pollen grains, only the

external capsule structure remains, composed of sporopollenin, which forms the outer layer of plant pollen. These structures are also referred to as sporopollenin exine capsules (SEC) due to their composition. Currently, the use of these capsules for controlled drug delivery has been widely applied in pharmacological, medical, and biotechnological studies. A study published in the Applied Materials Today by Aylanc et al. (2023) investigated the potential of SEC's as natural carrier for the controlled release of pharmaceuticals. This research highlights its biocompatibility and ability to enhance the therapeutical efficiency of encapsulated drugs.

With the production of films for wound dressing applications, this study will evaluate the potential of propolis to inhibit inflammation through its chemical compounds. The chosen film composition was alginate, given that current studies demonstrate that natural polymers (biopolymers) such as alginate, chitosan, and xanthan can degrade more easily when in contact with body fluids because of its biocompatibility and biodegradability characteristics. In addition, they have a lower toxicity potential compared to synthetic polymers (Aylanc et al., 2023). Furthermore, loaded SECs with two different types of propolis will be incorporated into the alginate film acting as a micro-carrier system for the control release of biocompounds during the wound healing process. To control the encapsulation efficacy, but also the released dosage, it is critical to accurately quantify the encapsulated bioactive material throughout spectrophotometry analyses and also Fourier transform infrared (FT-IR) spectroscopy, scanning electron microscope and total phenolics compounds.

To identify new target molecules for wound treatments in vitro and in vivo test systems are required. The in vitro scratch is a procedure that monitors cell migration and skin wound healing in the absence and presence of pharmacologically active compounds. That analysis is crucial to assure that the biocompounds on propolis can help accelerate the regeneration of skin wounds by assisting in cell migration. Thus, it will be determined whether alginate dressings with sporopollenin microcapsules enriched with propolis could be a promising option for wound healing.

2. OBJECTIVES

This study focuses on developing an alginate-based film for use as a wound dressing while investigating the potential of propolis extract - a rich natural source of bioactive compounds - in the wound healing process. The approach involves incorporating two types of hydroalcoholic propolis extracts (brown and red propolis) into sporopollenin exine microcapsules, which are derived from bee pollen pellets of *Cytisus* shrub species (*Cytisus spp.*). These loaded microcapsules are then integrated into alginate films to enable a controlled and sustained release of bioactive compounds at the wound site, optimizing the healing process.

3. LITERATURE REVIEW

3.1. An overview of the skin and its structure

The skin is the largest organ of the human body, with a complex structure composed of multiple layers and components. It is primarily divided into three main layers: the epidermis, dermis, and hypodermis, as illustrated in Figure 1.

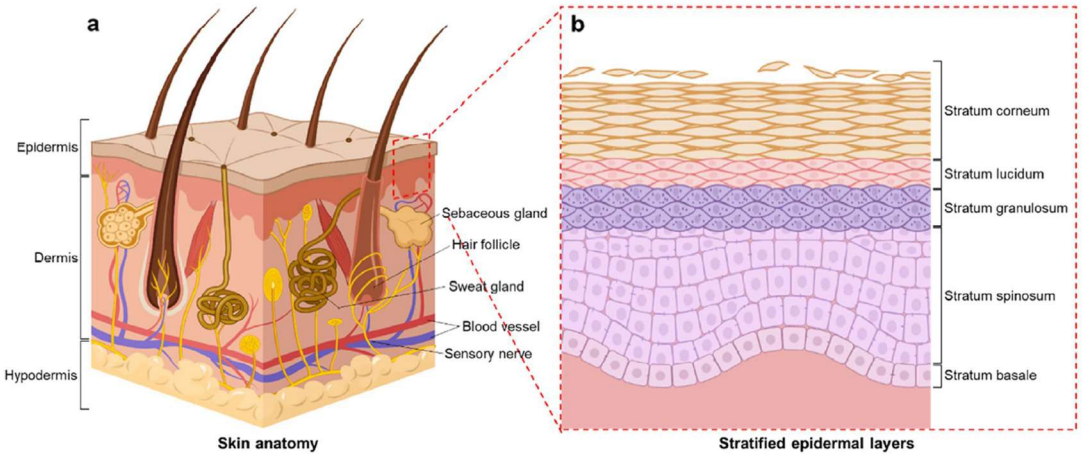

Figure 1 *– Schematic representing the skin structure. a) Anatomy of human skin. b) Stratified epidermis consisting of five distinct layers (Ahn et al., 2023)*

Beyond serving as a protective barrier, the skin plays a crucial role in maintaining homeostasis and defending the body against external threats. Its key functions include protection, temperature regulation, and immune defense, as it houses specialized immune cells that detect and combat pathogens. Additionally, the skin helps regulate body temperature, prevents excessive water loss, and maintains surface hydration. It also participates in metabolic

processes, including the storage of vitamins and lipids, as well as the regulation of blood and lymphatic circulation (Rocha, 2009).

The epidermis, the outermost layer, is a dynamic epithelial structure that continuously regenerates to shield the body from environmental factors (Meyer & Seegers, 2012). Beneath it lies the dermis, a fibrous connective tissue rich in collagen and elastin, which contains blood vessels, nerves, and sensory receptors, providing structural support and elasticity to the skin. The deepest layer, known as the hypodermis or subcutaneous tissue, primarily consists of adipose tissue, acting as a cushion and energy reservoir (Arda et al., 2014).

3.2. Skin lesions

3.2.1. Aging

The aging process affects both the skin and internal organs in similar ways, leading to gradual and irreversible degeneration. Skin aging, in particular, has been widely studied due to its significant social and aesthetic impact. The main contributors to this process include genetic predisposition, external environmental factors, hormonal changes, and random cellular damage, such as mutations in deoxyribonucleic acid (DNA).

According to Puizina-Ivic (2008), extrinsic aging is primarily driven by environmental influences, including prolonged sun exposure, air pollution, smoking, excessive alcohol consumption, and poor nutrition. In contrast, intrinsic aging is determined by genetic factors and the natural passage of time, typically resulting in thinner, smoother skin with the gradual appearance of fine lines.

Visible signs of skin aging - such as wrinkles, deep furrows, and freckles - are clear indicators of accumulated cellular damage (Bolognia, 1995). Chronological aging also brings structural changes, including thinning both the epidermis and dermis, decreased sebum production, and reduced body hair growth.

3.2.2. Cancer

Skin cancer is the most common malignancy among Caucasians worldwide, with its incidence steadily rising. This type of cancer is categorized into two main groups. Non-melanoma skin cancer, which originates from epidermal-derived cells, is more common and generally less aggressive, accounting for approximately 90% of all skin cancer cases.

Melanoma, on the other hand, arises from melanocytes and is much rarer but significantly more aggressive (Zink, 2014).

According to Craythorne (2017), a patient's skin color phenotype plays a crucial role in skin cancer risk. Individuals with a lower Fitzpatrick phototype are at greater susceptibility, particularly those with red hair and freckling, as they often carry two copies of the *R* allele variant of the *MC1R* gene - an inherited factor that increases their vulnerability to skin cancer. Additionally, Xeroderma pigmentosum, a rare autosomal recessive disorder, impairs DNA repair mechanisms in response to ultraviolet (UV) light damage. As a result, affected individuals are significantly more prone to excessive freckling, severe sunburns, and an elevated risk of developing skin malignancies in early childhood.

3.2.3. Eczema

Eczema (Figure 2), also known as atopic dermatitis, is a chronic and recurrent inflammatory skin condition that can be challenging to manage. This condition falls under the broader category of atopy, a genetic predisposition that increases susceptibility to asthma, allergic rhinitis, atopic eczema, and allergic conjunctivitis (Leung & Bieber, 2003).

Figure 2 *– Example of eczema herpeticum (Leung & Bieber, 2003)*

The prevalence of eczema has been rising worldwide, becoming a growing concern in both industrialized regions and urban areas of developing countries. Despite this increase, its exact causes remain unclear. However, researchers suggest that a combination of genetic and environmental factors contributes to its development. In Europe, for example, eczema affects approximately 15% to 20% of children and 2% to 5% of adults (Schmitt et al., 2011).

Atopic eczema manifests differently depending on age and disease stage. In its acute phase, it primarily affects pregnant women and young children, with symptoms such as erythema, vesiculation, and exudation, typically appearing on the scalp and face. In contrast, older children and adults are more commonly affected by the subacute or chronic phase, which is marked by excoriations, lichenification, and significantly less exudation compared to the acute stage. In these cases, lesions tend to appear in flexural areas, such as the elbows and knees (Camelo-Nunes et al., 2004).

3.2.4. Burns

The skin functions as a crucial sensory organ, equipped with specialized nerve endings that allow it to detect and respond to external stimuli. These include tactile receptors, baroreceptors, nociceptors, and thermoreceptors, which play a key role in sensory perception (Guirro et al., 2002; Young et al., 2001, as cited in Rocha, 2009). Thermoreceptors, in particular, are responsible for sensing temperature changes. When exposed to intense heat, these receptors activate pain signals that are transmitted to the brain, alerting the body to potential burn injuries.

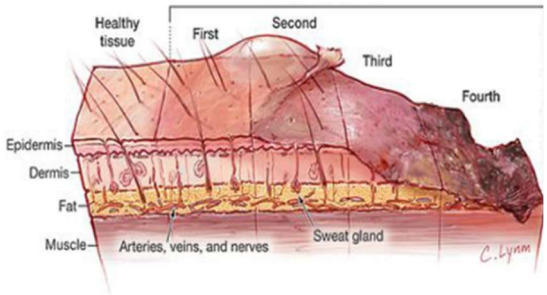

Figure 3 *– Degree of burn analysis relating the four types with the depths of skin. The more into the deepest layers, the degree of burn is higher (Tran et al., 2016)*

Burns can result from various agents, including physical, chemical, electrical, and thermal sources, leading to different degrees of tissue damage (Figure 3). The severity of a burn depends on multiple factors, such as the intensity and duration of exposure to the harmful agent, the thickness of the affected skin, the size of the exposed area, local blood circulation, and even the individual's age (Rocha, 2009).

3.2.5. Other physical injuries

Bedsores, also known as pressure ulcers, are a common type of physical injury that affects thousands of individuals worldwide. They develop when prolonged or continuous pressure is applied to specific areas of the body, leading to damage in both the skin and underlying tissues. These wounds are particularly prevalent in individuals with limited mobility, such as bedridden patients or those who rely on wheelchairs for movement.

Treating bedsores poses a significant challenge due to the complexity of the wounds and the frequent presence of microorganisms that contribute to infection. A wide range of pathogens - including bacteria, fungi, and viruses - can colonize these ulcers. Infection is a major complication that not only worsens the severity of bedsores but also delays healing and increases the risk of systemic complications (Bowler & Davies, 1999).

Among the microorganisms associated with bedsores, bacteria are particularly concerning. *Staphylococcus aureus* and *Enterococcus faecalis* are among the most frequently detected species in these wounds (Heym et al., 2004). The combination of moisture, reduced oxygen supply, and the accumulation of cellular debris creates an ideal environment for bacterial growth, significantly increasing the risk of infection.

3.3. Routes of administration of skin therapeutics

3.3.1. Oral

Skin therapeutics can be administered through various routes, and understanding these delivery methods is essential for optimizing treatment effectiveness and improving patient care. Among them, oral administration remains the most commonly used approach due to its convenience and ability to deliver medications systemically.

Oral medications used in dermatological treatments exert their effects through systemic action. However, their efficacy can be influenced by several factors, including drug metabolism, absorption rates, and interactions with gastrointestinal enzymes, all of which play a crucial role in determining therapeutic outcomes (Dornelas-Figueira et al., 2023).

3.3.2. Subcutaneous

This method involves injecting medications into the subcutaneous tissue, the layer of tissue located just beneath the skin (Figure 4). By bypassing the skin barrier, this route allows the drug to enter systemic circulation more efficiently, leading to faster and more consistent absorption compared to other administration methods (Schiff Jaffe & Freundlich, 2014). It is commonly used for medications that require a moderate absorption rate - slower than intramuscular injections but faster than topical application.

The subcutaneous tissue has lower blood flow than muscle tissue, which results in a slower absorption rate compared to intramuscular injections. However, due to the vascularization of the subcutaneous layer, absorption remains faster than with topical administration (Bechgaard & Nielsen, 2000). According to this study, the predictable pharmacokinetics and stable plasma levels provided by subcutaneous injections make them particularly suitable for conditions that require precise dosing.

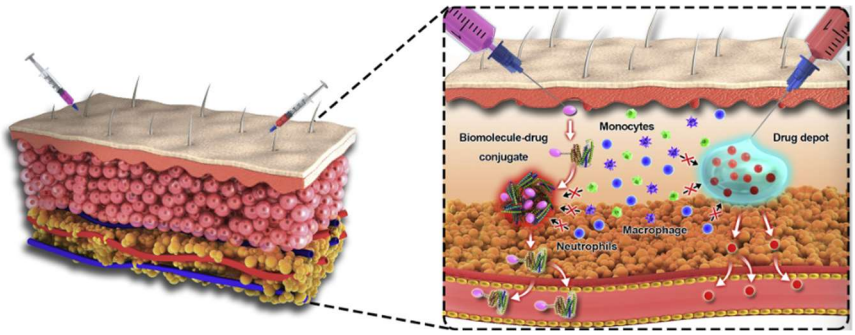

Figure 4 *– Illustration of subcutaneous injections (Chen et al., 2018)*

3.3.3. Intramuscular

This administration route involves injecting medication directly into muscle tissue, typically targeting larger muscle groups such as the deltoid or thigh. According to Bechgaard & Nielsen (2000), this method enables faster absorption compared to subcutaneous injections due to the higher vascularization of muscle tissue. Additionally, it allows for the administration of larger medication volumes, making it particularly suitable for drugs that require rapid systemic effects.

3.3.4. Intravenous

This route involves administering medication directly into a vein, ensuring immediate entry into the bloodstream. As a result, it provides the fastest onset of action, bypassing absorption barriers such as the skin or muscle tissue. Additionally, intravenous administration allows for precise control over drug delivery, making it ideal for medications that require immediate effects or continuous infusion (Wagner & Horn, 2012).

3.3.5. Transdermal controlled delivery

Transdermal drug delivery systems are gaining increasing importance in modern medicine. It's defined as a medicated patch that is placed above the skin and enables the controlled release of medication through the skin and into the bloodstream, ensuring consistent drug delivery and maintaining stable plasma levels (Berner & John, 1994). They offer several advantages, including non-invasive administration, reducing the need for frequent injections or oral dosing, while also improving treatment adherence and minimizing gastrointestinal side effects (Khader & Alany, 2019).

Research by Khader & Alany (2019) highlights that transdermal patches come in various forms, including adhesive systems, polymeric matrices, and controlled-release technologies. Each type differs in drug absorption mechanisms, patch size, and treatment duration, allowing for tailored therapeutic applications. Transdermal drug delivery systems (TDDS) have impressive advantages nevertheless have some limitations. One of the major shortcomings of patches is that it may induce irritation and sensitization of the skin mainly because of the structure composition of the patch (Thacharodi & Rao, 1995).

Other than that, Thacharodi & Rao (1995) informs that many transdermal devices are constructed with synthetic polymers. In the present investigation alginate-glycerol membranes are made to act as a transdermal delivery system. This biopolymer makes the system highly compatible with the skin as it's nontoxic and naturally occurring. Furthermore, according to Zhao & Mao (2021), the natural barrier of the skin is an obstacle to the delivery of most drugs thought the skin. The authors highlight that promising carries for this administration such as ultra-deformable liposomes can overcome the stratum corneum barrier of the skin with a efficiency similar to the subcutaneous injections.

As shown in Figure 5 there are three routes of skin penetration for nanoparticles: intercellular, transcellular and follicular routes. The intracellular route is the most favorable to the transdermic administration when ultra-deformable liposomes are present and that's because of its high fluidity and flexibility. Other than that, the liposomes can pass the skin barrier in the follicular route (Zhao & Mao, 2021).

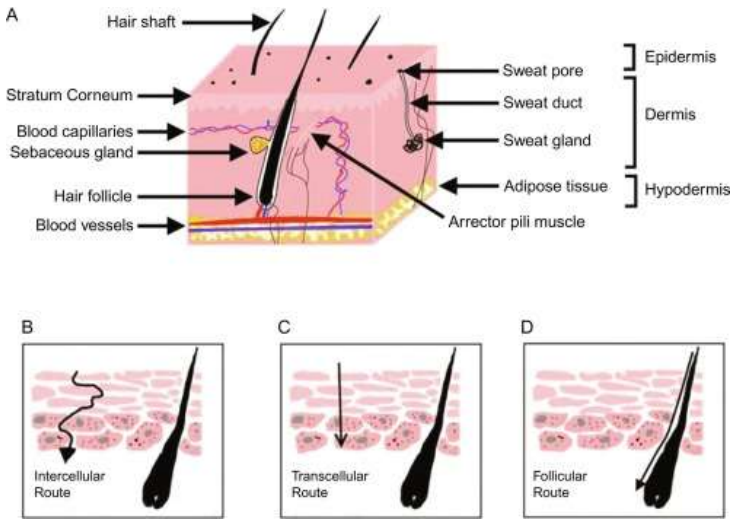

Figure 5 *– Three routes of nanoparticles skin penetration. A) Skin structure. B) Intercellular routes. C) Transcellular routes. D) Follicular route. (Zhao & Mao, 2021)*

3.4. Transdermal film and particle active compounds delivery systems

3.4.1. Inorganic materials

Transdermal films and nanoparticle-based delivery systems have attracted growing interest due to their ability to control drug release, improve bioavailability, and reduce systemic side effects. Among these, inorganic nanoparticles - including gold, silica, and zinc oxide - have been extensively explored for their role in transdermal drug delivery. Their appeal lies in their stability, ease of functionalization, and capacity to enhance skin permeation. A recent study by Rancan et al. (2023) highlighted the potential of silica nanoparticles in enhancing the transdermal delivery of anti-inflammatory drugs. The findings showed that these nanoparticles not only improve skin penetration but also contribute to a more sustained drug release, optimizing therapeutic effects.

3.4.2. Polymer-based systems

Polymer-based transdermal films provide a versatile platform for drug delivery, offering adjustable mechanical properties, biodegradability, and the ability to incorporate a wide range of active compounds. Various polymers, including polyvinyl alcohol (PVA), poly-lactic-co-glycolic acid (PLGA), and chitosan, have been widely used in transdermal film formulations.

A study by Gupta et al. (2023) explored the application of PVA in transdermal films for anti-diabetic drug delivery, demonstrating sustained release and enhanced patient compliance, highlighting its potential for long-term therapeutic use. However, if not well designed the polymer-based system can have low efficiency and notable toxicity that together with a poor understanding of these type of systems scientists were instigated to improve transdermal polymer-based film's chemistry (Schaffert & Wagner, 2008). As a result of new research, natural and biodegradable polymers with reduced toxicity were implemented to improve their chemistry and biocompatibility with the skin.

3.4.2.1. Synthetic polymers

Synthetic polymers such as PVA, PLGA, and polyethylene glycol (PEG) are widely used in transdermal delivery systems due to their favorable mechanical properties and ease of fabrication. These polymers can be tailored to achieve specific drug release profiles while also enhancing drug stability, making them valuable components in pharmaceutical formulations.

A recent study by Liu et al. (2023) explored the use of PLGA nanoparticles in transdermal films for anticancer drug delivery. The study demonstrated enhanced drug stability and prolonged release, highlighting the potential of these systems for sustained therapeutic applications.

3.4.2.2. Natural polymers (bio-based)

Natural polymers, especially those derived from bio-based sources, offer several advantages, including biocompatibility, biodegradability, and a lower risk of toxicity. Among these, alginate, a naturally occurring polysaccharide, stands out for its biocompatibility and gel-forming properties.

Recent research by Chen et al. (2023) explored the potential of alginate-based hydrogels for transdermal insulin delivery, demonstrating enhanced insulin stability and a sustained release profile. These findings suggest that alginate hydrogels could serve as a promising non-

invasive alternative to injections for diabetic patients. Additionally, the study investigated interpenetrating polymer networks, combining alginate with other natural polymers like chitosan, which could further improve mechanical properties and controlled drug release.

Alginate is primarily extracted from Phaeophyceae, a class of multicellular brown algae. It is found in the cell walls of these algae and also in the cellular capsules of certain bacteria, such as Azotobacter vinelandii. This biopolymer consists of two monomeric units and was first discovered in 1883 at Stanford University.

According to Lee & Mooney (2012), Fischer and Dörfel identified the L-guluronate residue, while D-mannuronate was recognized as the major component of alginate. Rather than being a single molecule, alginate is actually a family of linear copolymers, composed of three different building blocks (Figure 6): mannuronic acid residues (M), guluronic acid residues (G), and alternating M-G residues. The sequence and arrangement of these monomers vary depending on the source, allowing for the production of over 200 different types of alginate (Lee & Mooney, 2012).

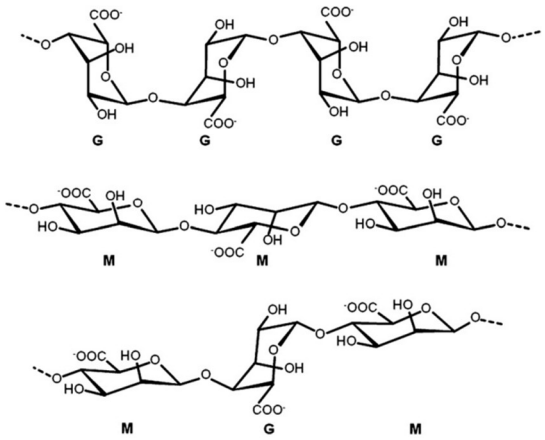

Figure 6 *– Chemical structures of G-block, M-block and alternating block in alginate (Lee & Mooney, 2012)*

Because of its versatile properties, alginate is widely used in the food, pharmaceutical, and medical industries. It serves as a stabilizing agent, thickener, gel former, and pharmaceutical excipient, making it a valuable component in many applications. However, its most significant feature is its ability to form gels, a characteristic that depends on the ratio of G and M blocks in its structure.

3.4.3. Nano and microparticles for delivery

Transdermal delivery systems utilizing nano and microparticles have gained significant attention as innovative technologies for enhancing drug penetration through the skin. Nanoparticles, due to their small size and high surface area, can greatly improve drug permeation, allowing for more efficient absorption. Additionally, they encapsulate active compounds, shielding them from degradation while enabling controlled release.

A study by Liu et al. (2010) demonstrated that PLGA-based nanoparticles successfully delivered anti-inflammatory drugs transdermally, enhancing drug stability and ensuring sustained release over time.

While microparticles are larger than nanoparticles, they offer distinct advantages, such as the capacity to carry larger drug loads and provide extended-release formulations. Research by Zhang et al. (2019) investigated chitosan-alginate microparticles for transdermal insulin delivery. Their findings indicated that these microparticles effectively protected insulin from degradation while enabling sustained release, suggesting a potential non-invasive alternative to insulin injections.

3.4.4. Natural Sporopollenin Microcapsules

Natural sporopollenin microcapsules (Figure 7) have emerged as an innovative biomaterial with significant potential in drug delivery applications (Aylanc et al., 2023). These specialized microcarriers are derived from plant pollen walls, specifically from the exine layer, and are primarily composed of sporopollenin - a highly resilient biopolymer known for its biocompatibility and biodegradability (Khader & Alany, 2019).

What sets these microcapsules apart is their remarkable ability to sustain drug release, making them a breakthrough innovation in biomaterial design for pharmacological and medical applications. Their exceptional stability, controlled release properties, and versatility position them as a highly promising tool in drug formulation and delivery systems (Aylanc et al., 2023).

Additionally, the chemical treatment process used in their production removes pollen proteins and lipid content, eliminating potential allergenic reactions in patients. This further enhances their safety and applicability, reinforcing their potential as a game-changing advancement in drug delivery technologies.

These biocapsules have demonstrated great potential as carriers for a wide range of substances, including drugs, proteins, living cells, oils, and natural extracts like propolis. Their appeal in various industries lies in their allergy-free and non-toxic nature, as well as their versatility for drug encapsulation and delivery. Moreover, their abundant availability from renewable sources makes them a highly sustainable and cost-effective option for large-scale applications (Atalay et al., 2022).

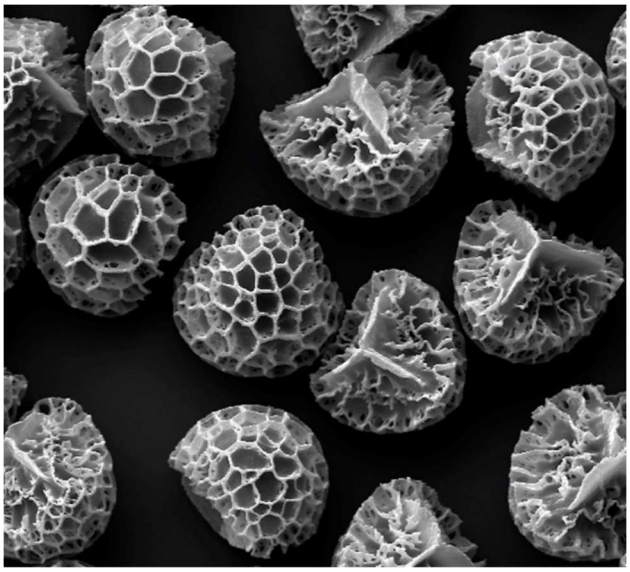

Figure 7 *– Scanning electron microscopy (SEM) picture of Lycopodium clavatum spores with a scale of 10 µm (Diego-Taboada et all., 2014)*

3.5. Use of natural extracts in skin treatment

3.5.1. Plant-based extracts

The use of natural plant-based extracts in skin treatments has gained widespread attention in recent years, thanks to their proven efficacy, safety, and minimal side effects. Botanical extracts provide a variety of skin benefits, ranging from hydration and anti-aging effects to antimicrobial and antioxidant properties. Therefore, it is one of the mains sources in the cosmetic and pharmaceutical industry (Michalak, 2023).

For instance, *Cannabis sativa* can enhance moisture of the skin, while *Aloe Vera* is loaded with regenerative properties that can repair the skin lesions (Michalak, 2023). Additionally, certain plant extracts, such as green tea and rosemary, are packed with antioxidants – such as polyphenols - that help protect the skin from oxidative stress caused by free radicals - one of the key contributors to premature aging (Hoang et al., 2021).

Natural antioxidants that can be found on botanical extracts includes polyphenols, flavonoids, flavanols, stilbenes and terpenes (Hoang et al., 2021). According to them green propolis is a great source of phenolic compounds that is pact with anti-inflammatory, antimicrobial and wound healing characteristics. Likewise, propolis in general have potential activity for wound healing, immunomodulatory and anti-inflammatory. In addition to the previously mentioned benefits, plant-based extracts also exhibit antifungal and anti-cancer properties, expanding their potential therapeutic applications.

3.5.2. Propolis

Propolis demonstrates significant antimicrobial capacity against pathogenic microorganisms. According to Oliveira (2021), this resinous component consists of a chemical composition comprising approximately 50% resin and plant balsam, around 30% wax, and the remainer percentage consists of essential and aromatic oils, pollen, and other substances. These percentages can vary depending on the type of propolis.

Propolis is among the apitherapeutic as it's a natural therapeutical substance and a resinous substance produced by bees (*Apis mellifera*). They mix different parts of plants that are collected and add salivary secretions and enzymes resulting in propolis. More than 300 compounds have been identified in red propolis samples. According to Oliveira et al. (2021), some of the most important bioactive compounds include flavonoids, isoflavonoids, phenolic acids, terpenes, xanthones, propolin, and guttiferones, as also reported by Banskota et al. (1998). The chemical structures of these compounds can be seen in Figures 8, 9, 10, and 11.

Red propolis can be found on the Northeastern Brazil and the bees on that region collect the red exudate from *Dalbergia ecastaphyllum* and *Symphonia globulifera*. Among the substances found in Brazilian red propolis, isoflavonoids are particularly abundant, alongside medicarpin and 3-hydroxy-8,9-dimethoxypterocarpan (Silva et al., 2008). According to Silva et al. (2008), Trusheva et al. (2006) also identified these isoflavonoids, including isosativan. Medicarpin is known as a substance with antifungal and antioxidant properties.

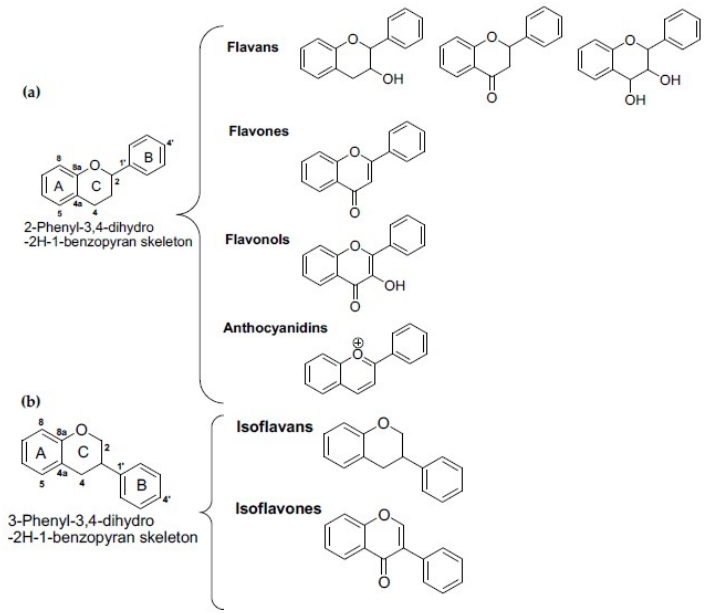

Figure 8 *– Classification of major groups of flavonoids (a) and (b) isoflavonoids (Martin & Touaibia, 2020)*

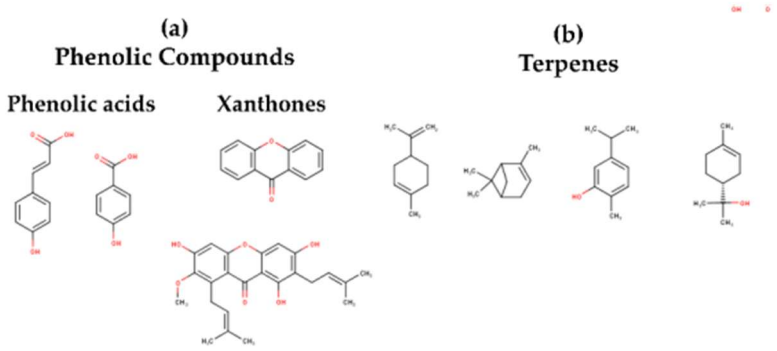

Figure 9 *– Chemical structure of (a) phenolic compounds and (b) terpenes (Leyva-López et al., 2020)*

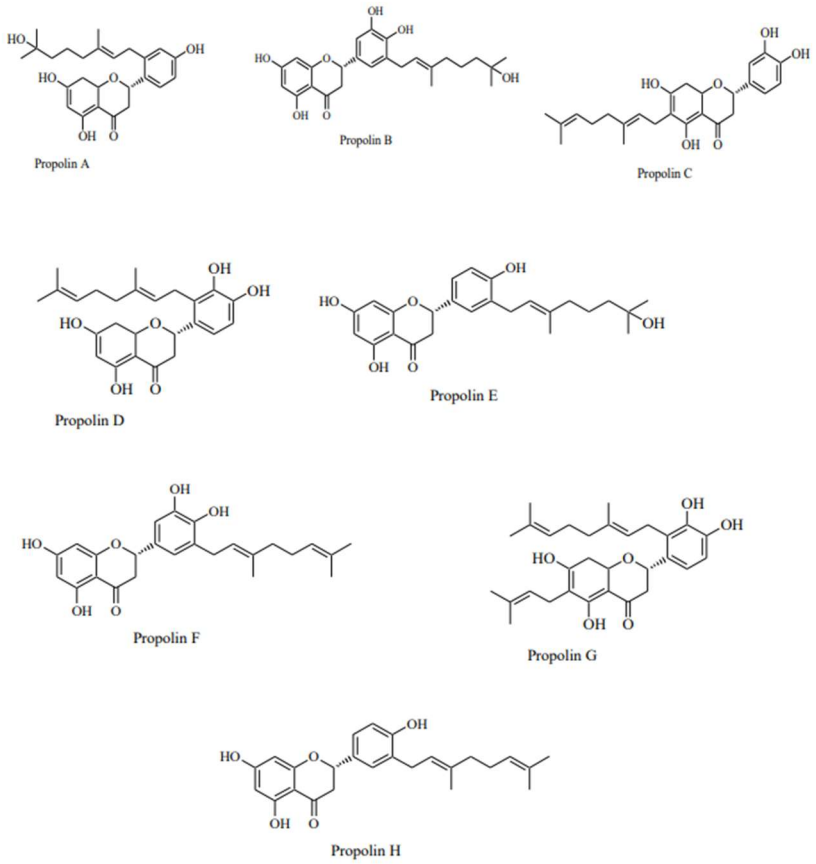

Figure 10 *– Chemical structure of propolin in bee propolis (Okhale et al., 2021)*

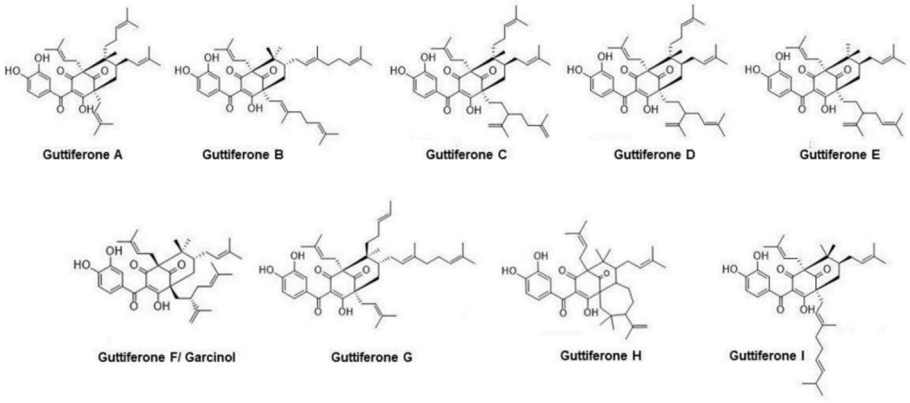

Figure 11 *– Chemical structure of guttiferones (Conceição et al., 2023)*

In temperate zones such as in Europe the most common propolis comes mainly from the tree *Populus spp.* and *Cistus ladanifer L*. leaf (Falcão et al. 2014). The Portuguese propolis has a brown color and has shown antimicrobial activity for bacteria such as *Staphylococcus aureus* and *Pseudomonas aeruginosa* (Silva et al., 2012; cited by Falcão et al., 2014). In general, propolis have similar composition and activities differing mainly because of its plant

source and region. In this work both Portuguese brown propolis and red Brazilian propolis will be studied to elucidate its effects on the wound healing process.

As a result of its medicinal properties and variety around the world, propolis has garnered increasing interest for potential applications across various industries such as biotechnology, cosmetics, pharmaceuticals, and bioproducts (Peixoto, 2023). According to Da Rosa et al. (2022) this natural substance can act in physiological processes such as absorption of vitamins and the healing process as antioxidants. In this aspect, the authors confirmed that clinical studies have shown that propolis had healing power on diabetic ulcers and also decreased inflammatory cytokines.

This resinous substance has demonstrated a wide range of pharmacological activities in vitro, highlighting its potential therapeutic value. Additionally, several studies indicate that isoflavones possess antimicrobial, antifungal, anticancer, and antioxidant properties, while also helping to alleviate symptoms of menopause and osteoporosis (Chen, Ko, & Chen, 2019). Given these attributes, propolis holds significant therapeutic potential in combating pathogenic bacteria associated with skin disorders and diseases. Furthermore, integrating nano and microparticles into a single transdermal delivery system could maximize the advantages of both particle sizes, enhancing drug absorption and controlled release.

4. Materials and methods

4.1. Samples

For the fabrication of alginate/glycerol films containing propolis loaded SECs, pollen from *Cytisus spp.* were collected in Bragança in April 2022 (purity of 99.6%). The brown propolis sample (from *Apis mellifera* hives) was obtained from local beekeepers at Bragança, Northeast of Portugal, in 2020. The red propolis was collected in Brazil.

4.2. Chemicals and reagents

Ethanol (absolute, ≥99.8%), hydrochloric acid (analytical reagent grade), sodium hydroxide (analytical reagent grade), potassium phosphate monobasic (analytical reagent grade), sodium carbonate (analytical reagent grade), di-sodium hydrogen orthophosphate anhydrous (analytical reagent grade), acetone (absolute, ≥99.8%), diethyl ether (grade, ≥99.5%), gallic acid and hydrochloric acid (analytical reagent grade) were purchased from Fisher Scientific (Pittsburgh, PA, USA). Glycerol (G9012, ≥ 99,5%), 2,2-diphenyl-1-picryl hydrazyl (DPPH), alginic acid sodium salt from brown algae (A1112), 2,2′-azino-di-(3-ethylbenzthiazoline sulfonic acid) (ABTS), caffeic acid, p-coumaric acid, kaempferol, pinocembrin and chrysin were purchased from Sigma-Aldrich (St. Louis, MO, USA), and all of them were of analytical grade. Sodium chloride (ACS grade), Folin–Ciocalteu's reagent and potassium chloride (ACS grade) were purchased from PanReac AppliChem ITW Reagents (Barcelona, Spain). Purified water, treated in a Milli-Q water purification system (TGI pure system, Houston, TX, USA), was used in the experiments.

Fetal bovine serum (FBS), penicillin/streptomycin solution (100 U/mL and 100 mg/mL, respectively), non-essential amino acids (NEAA), Trypsin, high-glucose Dulbecco's modified eagle's medium (DMEM), and Hank's balanced salt solution (HBSS) were purchased from PAN-Biotech. Dimethyl sulfoxide (DMSO), resazurin, and trypan blue were purchased from Sigma. Ultra-pure water was obtained from an Aqua-Win purification system.

4.3. Phenolic Compounds Extraction

Prior to the extraction, 10 g of the propolis (PS) was grounded and homogenized with a mortar. The samples were extracted with 60 mL of ethanol/water (80:20, *v/v*) at 50 °C for 3 h in a hot plate with a magnetic stirrer. The resulting mixtures were filtered through Whatman

No 4 filter paper (Figure 12) and the residues were re-extracted in the same conditions. After the second extraction, the filtered solutions were combined and concentrated.

To obtain the concentrated samples, its solvent was evaporated in a rotavapor (Rotary Evaporator model Hei-VAP from Heidolph, Schwabach, Germany) at 40°C with a rotation of 110 rpm; after approximately 20 minutes the ethanol evaporated completely. The propolis extract was placed in containers covered with aluminum to protect them from light, avoiding possible oxidation. Subsequently, the containers were covered with Whatman No 4 filter paper and taken to the freezer at -80°C for an hour and then the extract was freeze-dried using a lyophilizer (FreeZone 4.5 model 7750031 from Labconco, Kansas City, KS, USA) until a powder was obtained.

Figure 12 *– Filtered Red Propolis*

4.4. Liquid Chromatography with Diode-Array Detection and Electrospray Ionization Tandem Mass Spectrometry (LC/DAD/ESI-MS^n) Bioactive Compounds Analysis

For the analysis of bioactive compounds in propolis first, 50 mg of dry extract from red and brown propolis was weighed and placed in two different 5 mL volumetric flasks then were dissolved in EtOH/H_2O (80:20, *v/v*). This is because 10 mg of extract is used for each 1 mL of

ethanol. After dissolving the extract completely (see color in Figure 13) using ultrasonic bath, the samples were filtered and put on the freezer (-32°C) until analysis.

A Dionex UltiMate 3000 ultra-pressure liquid chromatography instrument connected to a diode array and attached to a mass detector was used for LC/DAD/ESI-MS^n analysis (Thermo Fisher Scientific, San Jose, CA, USA). LC was run in a Macherey-Nagel Nucleosil C_{18} column (250 mm × 4 mm id; particles diameter of 5 mm, end-capped) and the temperature was kept constant at 30 ◦C. The conditions applied in the liquid chromatography were based on previous work (Falcão et al. 2014); the flow rate was 1 mL·min^{-1}, and the injection volume was 10 µL. The final spectra data were accumulated in the wavelength interval of 190–600 nm. Quantification was achieved using calibration curves for caffeic acid (0.0187–0.4 mg·mL^{-1}; y =6.0 ×107x 26,360; R^2 =0.996), *p*- coumaric acid (0.0187–0.5 mg·mL^{-1}; y =9.0 ×106x 35,105; R^2 = 0.999), kaempferol (0.075–1.6 mg·mL^{-1}; y =1.0 ×106x 58,666; R^2 = 0.997), pinocembrin (0.0375–0.8 mg·mL^{-1}; y =2.0 ×106x 52,498; R^2 =0.997), and chrysin (0.0375–0.8 mg·mL^{-1}; y =4.0 ×106x 18,959; R^2 =0.999). When the standard was not available, the compounds were quantified using the calibration curve of the structurally closest standard, and the final result was given in equivalent terms, expressed as mg/g of propolis extract. The analysis was performed in triplicate.

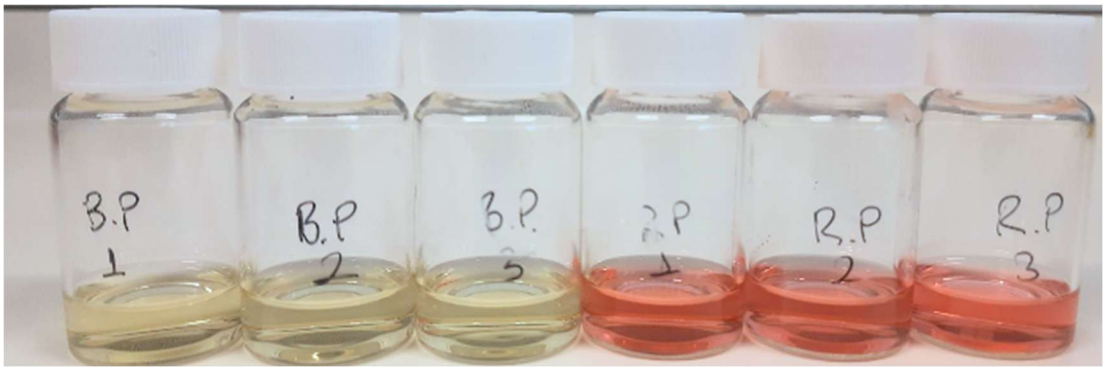

Figure 13 *– Brown and red propolis extract samples prepared in ethanol 80%*

4.5. Defatting of bee pollen and extraction of sporopollenin exine microcapsules (SECs)

This procedure was adapted according to Aylan et al. (2025). Briefly, natural *Cytisus spp.* spores (41.28 g), collected in Bragança in April of 2022, were transferred to a round bottom flask with a magnetic stirring bar, connected to a reflux condenser with water circulation system and water bath. The pollen was defatted by refluxing in acetone (400 mL) at 50°C for 3 h under stirring (220 rpm). The condenser is important to avoid solvent loss. That

step is necessary to remove the pollenkitt, which cover the outer layer of the pollen grains and it's a sticky material consisting mainly of lipids, flavonoids, carotenoids, and polysaccharides (Aylan et al., 2025). The spores were then collected by a vacuum pump filter system (Model DA7C, Charles Austen Pumps Ltd., Byfleet, UK), passing the pollen grains through a glass filter funnel with the sintered disc with ⌀5–15 µm porosity grade (Büchner funnel-BFU3-20D-001, Glassco Co., Ambala, India). To the remaining granules, 350 mL of distilled water was added and the mixture stirred and heated for 1h under the same conditions, repeating the filtration process. This step was repeated by adding another 350 mL of distilled water to the collected residue until the bee pollen aggregates were into individual particles.

After another filtration, 400 mL of acetone was added for a second time, the heating and stirring process was repeated for another 3 hours. The substance was filtered, and the obtained SECs particles were reserved and stored overnight to air-dry for 12 h in a fume hood. The dry sample obtained was resuspended in diethyl ether (350 mL) for 2 hours under stirring (300 rpm) at room temperature. This washing was repeated once more under the same conditions. Finally, 350 mL of fresh diethyl ether was added, stirring for 12 hours at room temperature.

The resulting defatted pollen grains were filtered and washed sequentially with 100 mL portions of water (five times), acetone (twice), 2 M hydrochloric acid (once), 2 M sodium hydroxide (once), water (five times), acetone (once), ethanol (twice) and water (once). The biocapsules were collected by vacuum filtration after each washing step. Samples were poured in a petri dish of 15 cm (± 0.1) diameter and dried under fume hood overnight and then in an oven (Memmert UNE400, Schwabach, Germany) at 60 °C for 3 days. The resulting dried SECs were stored in a desiccator, containing silica gel at room temperature until further characterization.

4.6. Vacuum Loading

75 mg of dry propolis extract was weighed into Falcon tubes in duplicate, and then 1.0 mL of 80% ethanol was added. The propolis was solved and put on a vortex and ultrasonic bath to assure solubility. Then 150mg of SECs was placed in the tubes. The biocapsules were then mixed with the propolis, the mixture was vortexed for 5 minutes and then placed in an ultrasonic bath for 5 minutes. The preparation was placed in the lyophilizer for 2 hours. The samples (Figure 14) were then placed in a freezer at -80°C for 30 minutes before being transferred to a lyophilizer until a dry powder was obtained.

Figure 14 *– Tubes ready with samples to be freeze dried*

4.7. Total Phenolics Content (TPC)

4.7.1. Preparation of standard solution

Gallic acid calibration standard curve was constructed by preparing different dilutions in ethanol. The absorbance was recorded after at 760 nm spectrophotometrically. Table 1 shows the mean absorbance of various concentrations (mg/mL) of gallic acid.

Figure 15 shows the standard gallic acid curve and regression equation used to calculate total phenolic content of the extracts.

Table 1 *– Gallic acid concentrations and absorbances*

Concentration (mg/mL)	Abs 1	Abs 2	Abs 3	Mean	SD
0.10	0.780	0.775	0.778	0.778	0.003
0.08	0.607	0.615	0.616	0.613	0.005
0.06	0.434	0,466	0.466	0.455	0.018
0.04	0.241	0.3	0.291	0.277	0.032
0.02	0.121	0.126	0.131	0.126	0.005
0.01	0.055	0.065	0.056	0.059	0.006
0.005	0.023	0.031	0.024	0.026	0.004

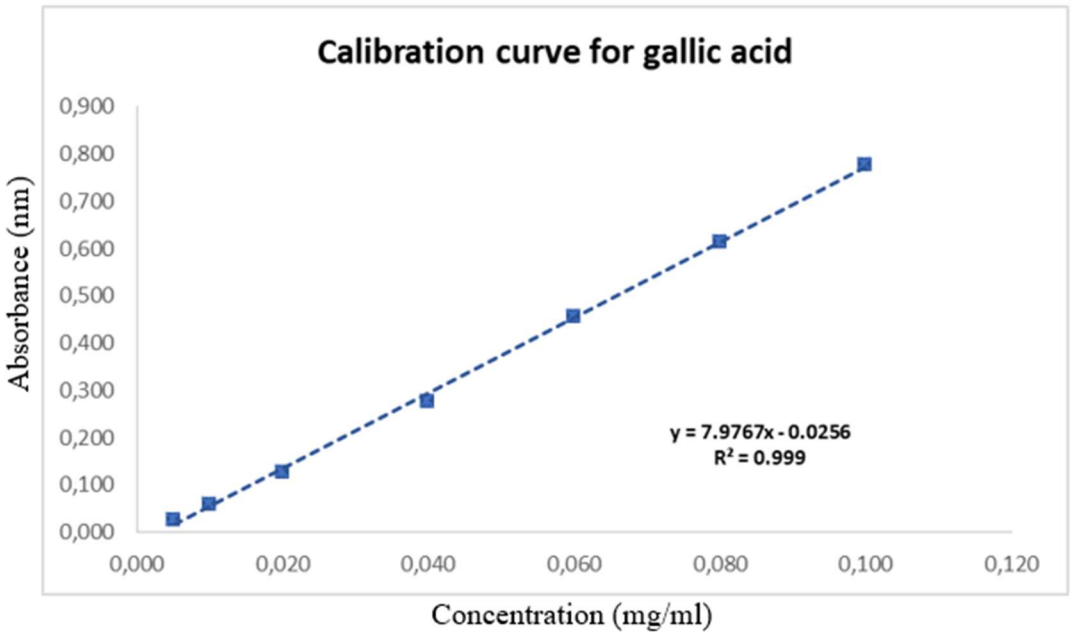

Figure 15 *– Calibration curve for gallic acid*

4.7.2. Preparation of samples and TPC analysis

For this step 25 mg of each RP and BP were added into two individual volumetric flasks along with 100 mL of 80% EtOH. The solution was then placed in an ultrasonic bath until completely homogen. Afterwards, 3 samples in duplicate were prepared, as exemplified in Table 2 below. For the blank was added to a test tube 0,5 mL of ethanol/water (80:20, *v/v*), 0,250 mL of Folin reagent, 1 mL of sodium carbonate (20% w/v) and 3,250 mL of distilled

water. For propolis samples TPC was determined by the Folin–Ciocalteu method (Falcão, Freire & Vilas-Boas, 2013). In the procedure, 0.5 mL of ethanolic extract (0,25 mg/mL) was mixed with 0.25 mL of Folin Ciocalteu reagent. After that, 1 mL of 20% Na_2CO_3 was added and the final volume adjusted to 5 mL with deionized water. The samples were then placed in a water bath at 70°C for 10 minutes and then kept in the dark for 30 minutes at room temperature. Finally, samples were centrifuged at 3500 rpm for 3 minutes. The absorbance was read at 760 nm using a UV/Vis spectrophotometer (Zuzi 4255/50, Auxilab, Beriain, Navarra, Spain). TPC was quantified using a calibration curve for gallic acid (0.045 mg/mL; $y = 7{,}9767x - 0{,}0256$; $R^2 = 0{,}999$). The total phenolic content value of the propolis extract samples were expressed as milligram of gallic acid equivalent per gram of dry weight sample (mg GAE/g).

Table 2 *– Samples prepared for analysis of total phenolic compounds*

Sample	Ethanol (µL)	Extract (µL)	Folin (µL)	Na_2CO_3 (µL)	D.W. (µL)
Blank	500	-	250	1000	3250
RP	500	500	250	1000	3250
BP	500	500	250	1000	3250

For the calculation of TPC the following equations were used:

$$Qty\ of\ PC\ \left(\frac{mg}{mL}\right) equivalent\ to\ gallic\ acid = \frac{Abs + 0{,}0256}{7{,}9767} \quad (1)$$

$$\frac{mg\ of\ PC}{g\ of\ extract} = \left(\frac{\frac{mg}{mL}\ of\ PC}{Samp\ \ 'sconcentration\ \left(\frac{mg}{mL}\right)}\right) \times 1000 \quad (2)$$

4.8. Preparation of Alginate/ Glycerol films with loaded SECs

The methodology for this preparation was adapted from Turbiani et al. (2011). First a solution containing 7 g alginate (2%) was mixed with 350mL DW for 4 hours in the magnetic stirrer at 70°C. After that time 120 µL of glycerol (37,5 %) was added for every 20 mL of film, totalizing 2.1 mL of glycerol. The percentage of glycerol was added based on the dry weight

of alginate per film solution. The mixture stayed in agitation for 10 more minutes until the samples were added. 12 samples (Table 3) each containing 50 mg either of red propolis extract (RP), brown propolis extract (BP), loaded SECs with red propolis extract (SRP) or loaded SECs with brown propolis extract (SBP) were placed in eppendorf's.

Table 3 *– Film Samples in Triplicate*

Sample	Replicate	Mass of dry samples (mg)	Alginate/Glycerol solution (mL)
RPF	1	50	20
	2		
	3		
BPF	1		
	2		
	3		
SRPF	1		
	2		
	3		
SBPF	1		
	2		
	3		
CF	1	-	
	2		
	3		

Then 15 beckers were separated for the triplicate film samples and control films as Table 3 indicates. Each becker was filled with 20 mL alginic solution. For the propolis samples 0.5 mL of EtOH was added to the eppendorf and taken to the ultrasonic bath until completely homogen. Then the propolis solution was poured into the respective becker and mixed for 3 minutes in the magnetic stirrer at room temperature. Finally, the alginate/propolis solution was placed in petri dishes (diameter 89.68 mm (± 0.1) and thickness of 14.91 mm).

The loaded SECs samples were directly added into the respective becker containing 20mL alginate and then 0.5 mL EtOH was added while the solution was stirred at the same conditions as the propolis samples (Figure 16).

Then, the loaded SECs were taken to the ultrasonic bath for a few seconds until they were solved and was again taken to the magnetic stirrer for a few more seconds. Finally, it was poured into the petri dishes with 9,5 cm (± 0.1) diameter.

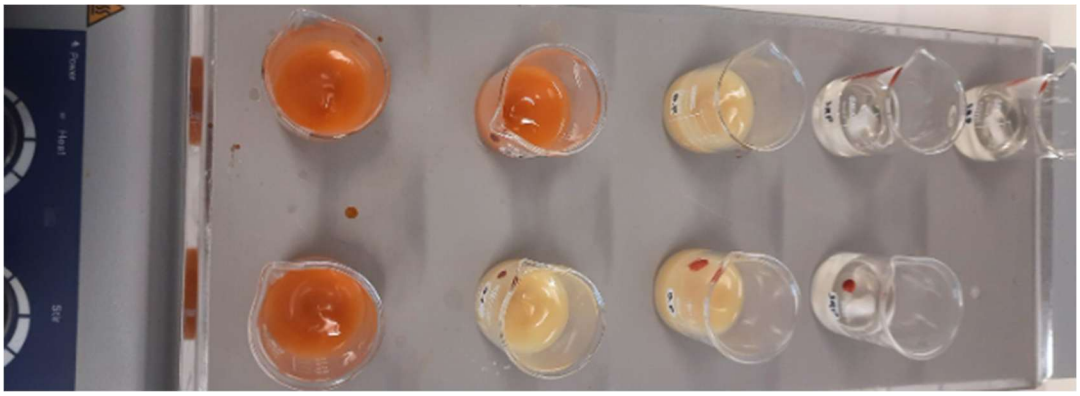

Figure 16 *– Production of the films in the magnetic stirrer*

4.9. Encapsulation efficiency

A total of 10 mg of SECs loaded with red propolis was weighed into Falcon tubes in triplicate. The same procedure was followed for loaded biocapsules with brown propolis, resulting in a total of six samples. Next, 5 mL of 80% ethanol (EtOH) was added to each falcon tube. The solution was then vortexed for 5 minutes, followed by an additional 5 minutes in an ultrasonic bath. It was then subjected to probe sonication (Model CY-500, Optic Ivymen System, Barcelona, Spain) at 50 % amplitude (10 cycles) for 10 s at room temperature. Samples were centrifuged (Centurion K2R series, Chichester, UK) at 4500 rpm for 3 minutes. The supernatant obtained in the process was removed and filtered using a syringe and a 25mm membrane filter 0.22 µm with outer ring (Labfil, China). 200 µL of EtOH was added to the residue, and it was filtered for the second time. The same procedures were performed for the placebo without SECs.

In the second phase of the analysis, the filtered liquids were diluted two-fold. For this step, 250 µL of each sample (filtered SRP and SBP) was transferred to test tubes. Ethanol, Folin reagent, and 20% sodium carbonate were added in the respective amounts specified in Table 4 bellow. The phenolic compounds released from the SECs were quantified using a calibration curve for gallic acid (0.045 mg/mL; $y = 7{,}9767x - 0{,}0256;\ R^2 = 0{,}999$).

Triplicated samples were measured for encapsulation efficiency of phenolic compounds and calculated through the following Equations (Mundargi et al., 2016):

$$Amount\ of\ \ PC\ (mg) = \frac{Absorbance \times Dilution\ factor}{Slope \times 1000} \quad (3)$$

$$Loading\ \% = \left(\frac{Amount\ of\ phenolic\ content\ released}{Weigh\ \ of\ propolis\ loaded\ SECs}\right) \times 100 \quad (4)$$

$$Encapsulation\ efficiency\ (\%) = \left(\frac{Practical\ loading}{Theoretical\ loading}\right) \times 100 \quad (5)$$

Table 4 *– Samples for encapsulation efficiency study*

Samples	Volume of EtOH 80% (µL)	Extract (µL)	Folin (µL)	Sodium Carbonate 20% (mL)
SRP (1)	250	250	250	1
SRP (2)	250	250	250	1
SRP (3)	250	250	250	1
SBP (1)	250	250	250	1
SBP (2)	250	250	250	1
SBP (3)	250	250	250	1
Control	500	-	250	1

After adding all the reagents, the test tubes were placed in a water bath at 70°C for 10 minutes. They were then centrifuged at 3500 rpm for 5 minutes at room temperature. The absorbance was measured at 266 nm using a UV/Vis spectrophotometer (Zuzi 4255/50, Auxilab, Beriain, Navarra, Spain) with the placebo as a blank.

4.10. Physical and appearance of films

4.10.1. UV-Vis light transmittance

The UV–Vis light transmittance of films (2 × 1 cm) was measured from 300 to 800 nm using a spectrophotometer (Zuzi 4255/50, Auxilab, Beriain, Navarra, Spain). The appearance of films before dried and ready to analyze is shown on Figure 17 below.

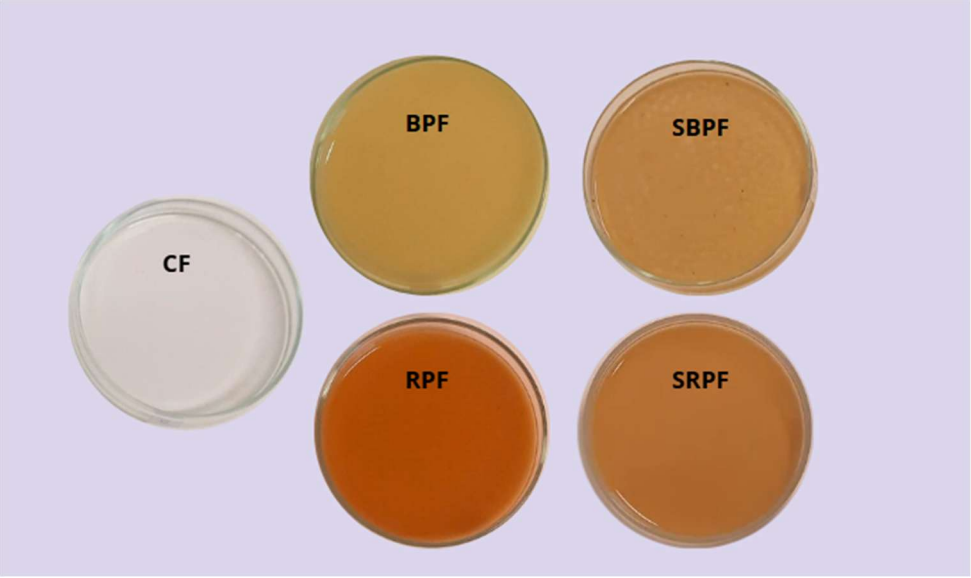

Figure 17 *– Appearance of films before dried*

4.10.2. Color Measurement

Color assay was measured by a portable colorimeter CR400 from Konica Minolta (Chiyoda, Tokyo, Japan) was used. Firstly, a standard calibration must be made on a white plate background. Then the measurement was made in duplicate on the film samples. Additionally, the samples were put on a white background. In Figure 18 below we can check a schematic representation of how the equipment is positioned to collect data. The color was analyzed at three different points at the samples and was evaluated using the CIELAB scale (Figure 19): L^* =0 (black) to L^* =100 (white); $-a^*$ (greenness) to $+a^*$ (redness); and $-b^*$ (blueness) to $+b^*$ (yellowness). The color difference (ΔE*) was calculated according to the following Equation (6) (Ishikawa et al., 2021).

To analyze the color variation between samples — rather than variation from the colorimeter. This allows us to assess how different one sample's color is compared to another.

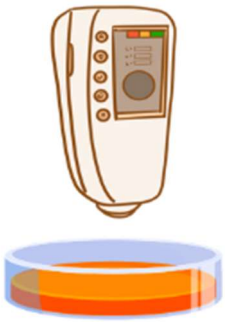

Figure 18 *– Color measurement of alginate films using a colorimetry*

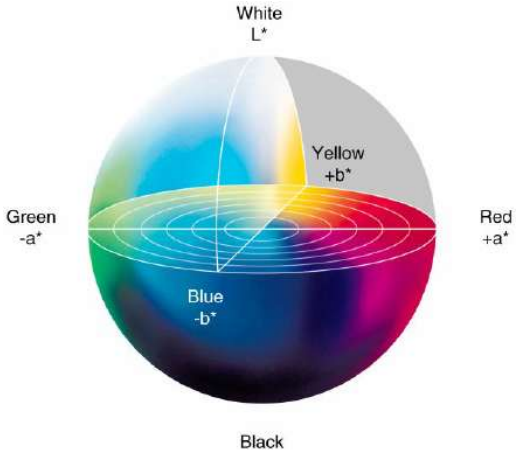

Figure 19 *– CIE LAB 1976 color space (Agudo et al., 2014)*

$$\Delta E = \sqrt{(L^*_{standard} - L^*_{sample})^2 + (a^*_{standard} - a^*_{sample})^2 + (b^*_{standard} - b^*_{sample})^2} \qquad (6)$$

4.10.3. Thickness measurement

For thickness measurement a digital micrometer (Mitutoyo, Kanagawa, Japan) was utilized. Readings were performed in duplicated films, with data collected in six different points of each sample. Results are expressed as mean values ± standard deviation (SD).

4.10.4. Environmental scanning electron microscope (SEM)

Before proceeding with SEM imaging, it was crucial to prepare the samples properly to ensure high-resolution imaging and minimize charging effects. Given the non-conductive nature of the samples, they were placed in conductive carbon tapes and coated with Au/Pd using sputter coater equipment (SPI Module Sputter Coater, PA, US) (15 mA, 100 s).
First, the samples were mounted on aluminum stubs using carbon tape to enhance conductivity and secure them in place. The choice of carbon tape was strategic, as it prevents unwanted charging and ensures a stable imaging process. Then they were carefully cleaned using compressed air to remove any surface contaminants. The samples used for this analysis includes SRPF, SBPF, RPF, BPF, CF and SECs.

The morphology and structural integrity of defatted loaded sporopollenin exine microcapsules were characterized with scanning electron microscopy (SEM), FEI Quanta 400 FEG ESEM/ EDAX Genesis X4M (FEI Inc., OR, USA) instrument at 15.00 kV acceleration voltage under various magnifications. The parameters were adjusted to optimize image resolution and contrast while minimizing beam damage to the sample. The chamber was maintained under high vacuum conditions to prevent electron scattering and enhance imaging clarity.

4.11. Fourier transform infrared (FT-IR) spectroscopy

Fourier-transform infrared (FTIR) spectra were obtained using a FTIR system (Thermo Scientific Nicolet SummitX FTIR Spectrometer 912A1139, Verona, USA). The samples were placed on the plate and pressed for reading results. For powders they were pressed until a thin layer was obtained. The samples used for this analysis includes SRP, SBP, RP, BP, SRPF, SPBPF, RPF, BPF, CF, empty sporopollenin exine microcapsules and alginic acid.

Reflectance spectra were collected at a spectrum of 4 cm^{-1}, by 64 times scanning per measurement over the range from 4000 to 400 cm^{-1}. Background spectra were collected before reading. Data was processed using ThermoScientific Spectrum software.

4.12. Simultaneous thermal analysis

The thermal degradation behavior of RP, BP, SBP, SRP, SRPF, SBPF, RPF, BPF, CF, hollow SECs and alginate was measured by Thermogravimetric analysis (TGA), Derivative Thermogravimetry (DTG) and Differential Thermal Analysis (DTA) using NETZSCH - TG 209 F3 Tarsus (Netzsch, Selb, Germany) thermogravimetric analyzer equipment. The samples were heated from 20 to 700 ºC in a nitrogen atmosphere (40 mL·min 1) at a scanning rate of 5 ºC/min. Thermogravimetric (TG) and derivative curves (DTG) were obtained using Netzsch Proteus thermal analysis (v.5.2.1) software.

4.13. Antioxidant activity

4.13.1. DPPH assays

The antioxidant capacity of the films (RPF, BPF, SRPF and SBPF) were measured by DPPH and ABTS radical scavenging activity assays which were adapted from Aylanc et al. (2020), Zhang et al. (2020) and Aylanc et al. (2022). 20 mg of the film samples were cut into small pieces (< 2.0 mm) and placed in test tubes with 2mL of DPPH solution (concentration: 6×10^{-5}M). Samples were then vortexed for 5 minutes and left in the dark at room temperature for 30 min. After this period, the absorbance was measured using a UV-Vis spectrophotometer (Zuzi 4255/50, Auxilab, Beriain, Navarra, Spain) at 517 nm. The calculation of the inhibition (%) was then made by using the Equation (7) bellow:

$$Inhibition\ (\%) = \left(\frac{Abs_{control} - Abs_{sample}}{Abs_{control}}\right) \times 100 \quad (7)$$

The placebo absorbance ($Abs_{control}$) was the DPPH solution and tests were executed in triplicate.

4.13.2. ABTS assays

For the other assay, ABTS stock solution was prepared reacting ABTS (7mM in deionized water) with 2.45 mM $K_2S_2O_8$. The formulation set over the night (16 h) at room temperature in the dark until a stabilized oxidative state. The work solution ($ABTS \bullet^+$)was then

prepared by adding EtOH. 20 mg of films, cut into small pieces, were added to a test tube along with 5mL of the prepared working solution (tests were achieved by analyzing triplicated samples). Then it was vortexed for 3 min and incubated in the dark for 10 min. The absorbance was measured by the same equipment as in the DPPH assay, but its absorbance was at 734 nm. The calculation results were obtained by using the Equation (7).

4.14. Biodegradability of films and Control release of phenolic compounds

4.14.1. Biodegradability

The biodegradation of the composite films was tested by its phosphate buffered saline (PBS) degradability in different pHs. Films were cut into small squares (1 cm x 1 cm) and placed on Beckers containing 10 mL of the PBS solution in three different pHs (5, 6 and 7). The buffer was made to simulate body fluids, as the dressing goes directly in the skin surface. The solution was prepared by dissolving 8 g NaCl, 0.2g KCl, 1.42 g Na_2HPO_4 and 0.24 g KH_2PO_4 into 1 L of deionized water. pH adjustment was performed using 1 M sodium hydroxide (NaOH) and 2 M hydrochloric acid (HCl). The samples were observed for a period of 5 hours until full degradation occurred. The cut films are shown in Figure 20 bellow.

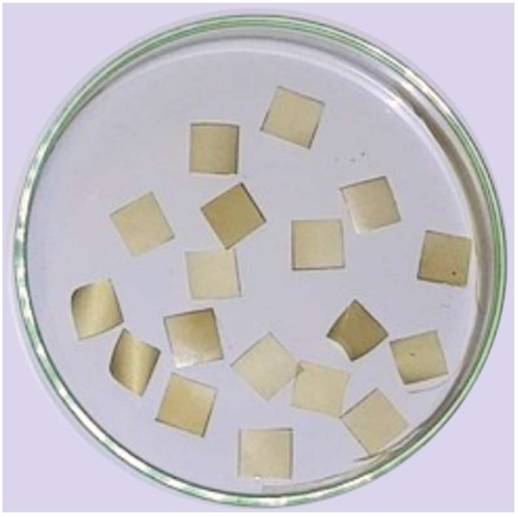

Figure 20 *– Cut films (BPF) for pH biodegradability*

4.14.2. Release experiment

PBS solution adjusted at pH 6.8 was prepared and pH correction was applied with NaOH and HCl as described in Section 4.14.1. The dynamics of releasing propolis-loaded SEC

films were evaluated by successive immersions in simulated body skin fluid (PBS, pH 6.8) and were according to previous literature assays (Aylanc et al., 2025). Propolis loaded biocapsules films (10 mg) were contained in dialysis bags (MWCO 14,000 Da) with 5 mL of PBS. Thereafter, sample bags were placed into flasks containing 50 mL of in vitro simulated fluid and incubated in a thermal orbital shaker (100 rpm) at 37 ºC. Subsequently, 2 mL of the fluid was withdrawn from the 50 mL contained on the flask which was replaced with an equal volume of fresh PBS. This last step described was accomplished at predetermined time points (1 h, 2 h, 3 h, 4 h, 5 h, 24 h and 48 h) for all the film samples (Table 5).

In the following phase, after all the fluid samples were collected, they were filtered by a nylon membrane syringe filter (0.22 μm) and had its absorbance measured by a UV–Vis spectrophotometer at 266 nm with PBS placebo as blank. Release analyses were performed in duplicate for each film type. For calculations (Equations 8, 9 and 10) and results data were plotted with the blank against the absorbance of release compounds. In the equations P (t – 1) referees to the rate of free release before certain time (t). As for Pt it is the rate of free release at t.

Table 5 *– Samples and hours of withdraw*

Samples	Withdrawn hours
CF	1, 2, 3, 4, 5, 24 and 48
BPF	1, 2, 3, 4, 5, 24 and 48
RPF	1, 2, 3, 4, 5, 24 and 48
SRPF	1, 2, 3, 4, 5, 24 and 48
SBPF	1, 2, 3, 4, 5, 24 and 48

$$Concentration\ of\ drug\ \left(\frac{mg}{mL}\right) = (Absorbance\ \times Slope) \pm intercept \quad (8)$$

$$Amount\ of\ released\ compound\ (mg) = (Concentration\ \times Dilution\ bath\ volume) \quad (9)$$

$$Cumulative\ release\ (\%) = \left(\frac{Volume\ of\ sample\ withdrawn\ (mL)}{Bath\ volume\ (mL)}\right) x\ P(t-1)\ + Pt \quad (10)$$

4.15. Total protein content analysis

The protein content of the raw Cys pollen and hollow sporopollenin exine microcapsules were determined by the nitrogen contents of the samples and was calculated according to Aylanc et al. (2025) that uses a methodology in accordance with the macro-Kjel dahl technique. A Kjeldahl steam distillation unit (Pro Nitro A, JP Selecta, Barcelona, Spain) was used for measurements. As stated by Aylanc et al. (2025), recommendation of the Association of Official Analytical Chemists was followed by using a nitrogen conversion factor to obtain the percentage of total protein content. For that, the total Kjeldahl nitrogen conversion factor of 6,25 was used as demonstrated in the Equation (11) bellow:

$$Protein = Nitrogen\ (\%) \times 6{,}25 \tag{11}$$

4.16. Cytocompatibility Evaluation

4.16.1. Cell Culture and Seeding

The cytocompatibility of the films with the human epidermal keratinocyte cell line (HaCaT, 300493, CLS Cell Lines Service GmbH) and the human foreskin fibroblast cell line (HFF-1, SCRC-1041, ATCC) was evaluated following the procedure described by Vieira et al. (2018), with some modifications. Briefly, the HaCaT cell line, at passages 5-7, and the HFF-1 cell line, at passages 15-17, were cultured in high-glucose cDMEM at 37 °C in an atmosphere of 5% CO2. Before performing the seeding, the cells, in a confluency of 80%, were detached from the cell culture flask by using Tripsin: EDTA. HaCaT (25×103 cells/well) and HFF-1 (10×103 cells/well) cell lines were seeded in adherent 24-well culture plates and incubated for 24 h, at 37 °C, in a humidified atmosphere with 5% CO_2. After, the medium containing non-attached cells was removed by aspiration, and a fresh medium was added (500 μL). Then, the different films (10 × 10 mm) were added to the cells. The human keratinocytes and fibroblasts were incubated with the films for 1, 2, and 3 days, and the metabolic activity (Section 4.16.2) of the cells were evaluated for each time point. Cell morphology was analyzed under an inverted microscope (DMi1, Leica, Wetzlar, Germany). Cells cultured without films were used as a negative control of toxicity. All conditions were performed in triplicate.

4.16.2. Metabolic Activity

The metabolic activity of human keratinocytes and fibroblasts incubated with different films was determined by the reduction of the resazurin (blue) to resorufin (pink) by living cells using the resazurin reduction assay. A stock solution of resazurin sodium salt (440 μM) was prepared in DPBS and further sterilized with a 0.22 μm filter under aseptic conditions (Uzarski et al., 2017). Aliquots of the stock solutions were made and stored at –20 °C for no longer than 4 weeks. Resazurin working solution (44 uM) was freshly prepared in a cDMEM culture medium by adding 1/10th volume of the stock solution to the initial cell culture medium volume. After 1, 2, and 3 days of culture, the culture medium was removed, and the cells were gently washed with sterilized warm HBSS three times. Then, 300 uL of freshly prepared resazurin working solution was added to each well. A blank was also made (resazurin without cells). The cells were incubated at 37 °C for 4 h in a humidified atmosphere containing 5% CO2. Thereafter, the absorbance of the resazurin reduction from each sample was recorded at 600 and 570 nm on a microplate reader (SpectraMax iD3 Multi-Mode, Molecular Devices).

4.17. Statistical analysis

The statistical software OriginPro (OriginLab, Northampton, Massachusetts, USA) was used for data analysis. Data were compared using a two-tailed t-test, and $p < 0.05$ was considered significant. For the in vitro assays results were obtained as 3 independent experiments with a minimum of 3 replicates for each condition and are expressed as mean ± standard deviation (SD). Statistical analyses were performed using GraphPad Prism 8.0.1 software. Ordinary one-way Analysis of variance (ANOVA) and Dunnett's multiple comparisons method were used for cell assays. Differences between experimental groups were considered significant with a confidence interval of 95% whenever $p < 0.05$.

5. RESULTS AND DISCUSSION

5.1. Composition of Brown and Red propolis

5.1.1. Total phenolics compounds

The chemical abundance of phenolic compounds can vary according to the botanical origin of propolis. This resinous component contains a variety of substances although not all of these components exhibits antimicrobial, antifungal and antioxidant activity (Socha et al., 2015). The biological efficiency of propolis is directly associated with the presence of flavonoids and phenolic acids. Therefore, it's important to know the availability of phenolic compounds in each sample, as they are primarily responsible for these bioactive properties. Those characteristics are the main target of this work as the dressings are intended to support wound healing by eliminating or reducing pathogens that may be present on the skin during the recovering process. In the present study TPC of red and brown propolis extracts are illustrated in Figure 21 below.

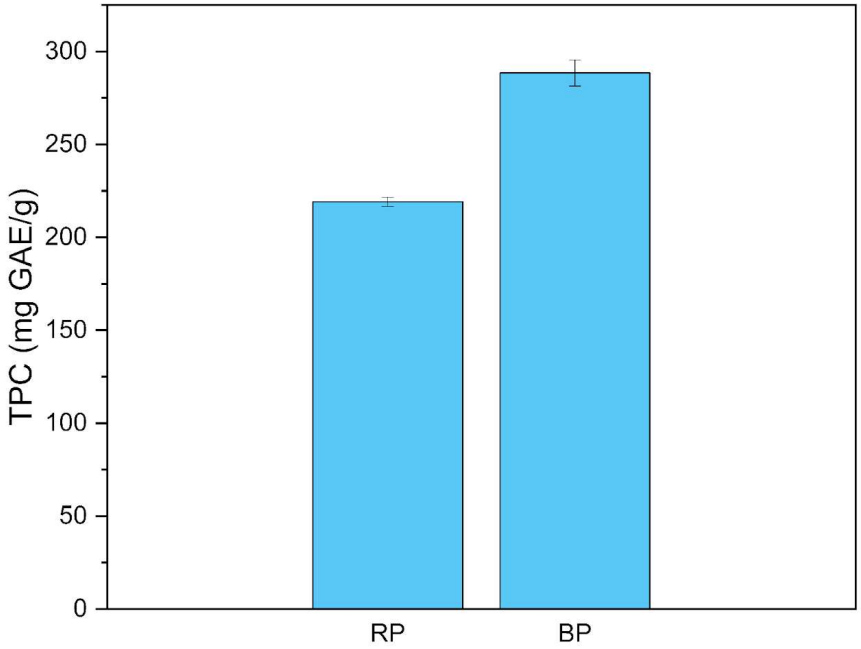

Figure 21 *– TPC of red and brown propolis expressed in milligrams of gallic acid by grams of extract (mg GAE/g*

The total phenolic compounds for RP samples were 219.10 (± 2.5) mg GAE/g, while BP samples was 288.47 (± 7.0) mg GAE/g. All measurements were performed in triplicate for each sample and the results are reported as mean values with their respective standard deviations. The variation observed is associated with the different botanical origins of the samples. Moreover, the TPC for RP samples were more homogenous compared to BP extract.

Additionally, BP presented more TPC indicating it would be a better choice for wound dressing as it presents more bioactive activity. These findings corroborate with previous studies indicating that propolis are an important source of phenolic compounds with antioxidant activity (Altuntaş et al., 2023; Tumbarski et al., 2025; Pobiega et al., 2023).

5.1.2. LC/DAD/ESI-MS^n Bioactive Compounds Analysis

The components and their quantities present in propolis can differ depending on their local and botanical origin. Samples used in this work comes from Brazil and Portugal. Therefore, its bioactive compounds must be identified. The chromatographic profiles (Figures 22 and 23) and compound identification were performed by comparing retention times, UV absorption maxima (λ_max), mass-to-charge ratios ([M−H] $^-$), and fragmentation patterns with literature data and authenticated standards when available (Falcão et al., 2013; Falcão et al., 2010; Omar et al., 2016; Vieira de Morais et al., 2021; Righi et al., 2011; Falcão et al., 2019; Silva et al., 2020).

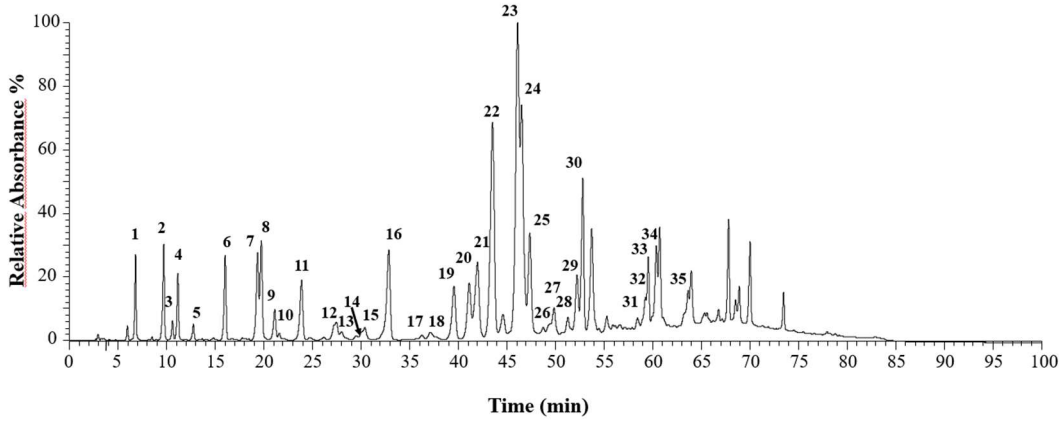

***Figure 22** – LC/DAD/ESI-**MS^n**) resulting profiles for BP*

The chromatogram of BP (Figure 22) revealed a chemically diverse matrix rich in caffeic acid derivatives, flavonoids, and prenylated phenylpropanoids. A total of 35 compounds were identified (Table 6) according to Falcão et al. (2010) and Falcão et al. (2013). Among the identification there are caffeic acid (peak 1), *p*-coumaric acid (peak 2), ferulic acid (peak 3), and isoferulic acid (peak 4) which were detected early in the chromatogram and matched previously reported standards.

Compounds such as pinobanksin-5-methyl ether, quercetin-3-methyl ether, kaempferol-methyl ether, and galangin derivatives (peaks 7, 10, 15, 18) were observed, consistent with the flavonoid profile often found for temperate zone propolis. Several derivatives of pinobanksin (peaks 24 - 35) were detected, confirming their relevance as major constituents. These findings corroborate previous reports on the complexity and biological potential of Portuguese propolis (Falcão et al., 2010; Falcão et al., 2013). The most intense peak was observed at 46.1 min (peak 23), corresponding to chrysin, suggesting a high concentration of this constituent in the BP sample with a 10,471 (± 0,206) mg/g.

Table 6 *- Characterization of the phenolic compounds from Portuguese propolis obtained by LC/DAD/ESI-MS^n. [a]Confirmed with standard, [b]Confirmed with MSn fragmentation, [c](Falcão et al., 2013), [d](Falcão et al., 2010)*

Nº	t_R (min)	λ_{max} (nm)	$[M-H]^-$ m/z	MS^2 (% base peak)	Proposed compound	Family	$\frac{mg}{g}$ Extract
1	6.8	292,.323	179	135	Caffeic acid[a,b]	Phenolic acid	0.691 ± 0.013
2	9.7	310	163	119	*p*-Coumaric acid[a,b]	Phenolic acid	0.635 ± 0.013
3	10.6	295, 322	193	133(100), 149 (49), 177(15)	Ferulic acid[a,b]	Phenolic acid	0.167 ± 0.014
4	11.2	298, 319	193	133(100), 149 (49), 177(15)	Isoferulic acid[a,b]	Phenolic acid	0.608 ± 0.006
5	12.8	228	121	-	Benzoic acid[a,b]	Phenolic acid	0.140 ± 0.001
6	16.1	295sh, 322	207	192(100), 163(62)	3,4-Dimethyl-caffeic acid[a,b]	Phenolic acid	0.987 ± 0.012
7	19.4	287	285	267(100), 239(25), 252(16)	Pinobanksin-5-methyl ether[b,c]	Dihydroflavonol	3.600 ± 0.016
8	19.8	276	147	103	Cinnamic acid[a,b]	Phenolic acid	1.339 ± 0.004
9	21.2	309	177	163(100), 119(16)	*p*-Coumaric acid methyl ester[a,b]	Phenolic acid	0.283 ± 0.004
10	21.6	256, 355	315	300	Quercetin-3-methyl ether[b,c]	Flavonol	0.612 ± 0.021
11	23.9	292	271	253(100), 225(22), 151(8)	Pinobanksin[b,c]	Dihydroflavonol	3.164 ± 0.084

12	27.5	268, 337	269	225(100), 151(20)	Apigenin[a,b]	Flavone	0.434 ± 0.017
13	28.0	266, 366	285	285(100), 257(13), 151(20)	Kaempferol[a,b]	Flavonol	0.885 ± 0.054
14	29.5	253, 370	315	300	Isorhamnetin[a,b]	Flavonol	0.479 ± 0.105
15	30.4	267, 351	299	284	Kaempferol-methyl ether[b,c]	Flavonol	1.357 ± 0.017
16	32.8	311	173	129	Cinnamylidenacetic acid[b,c]	Phenolic acid	1.943 ± 0.001
17	36.3	256, 367	315	165	Rhamnetin[b,c]	Flavonol	0.736 ± 0.219
18	37.2	265, 300sh, 352	283	268(100), 239(76)	Galangin-5-methyl ether[b,c]	Flavonol	1.141 ± 0.170
19	39.6	298, 325	247	179(100), 135(16)	Caffeic acid isoprenyl ester[a,b]	Phenolic acid	1.168 ± 0.028
20	41.2	298, 325	247	179(100), 135(16)	Caffeic acid isoprenyl ester (isomer)[a,b]	Phenolic acid	1.276 ± 0.094
21	42.0	298, 325	269	178(100), 135(96)	Caffeic acid benzyl ester[b,c]	Phenolic acid	2.088 ± 0.089
22	43.5	289	255	213(100), 211(55), 151(36)	Pinocembrin[a,b]	Flavanone	15.706 ± 0.308
23	46.1	268, 313	253	209	Chrysin[a,b]	Flavone	10.471 ± 0.206
24	46.6	294	313	253(100), 271(20)	Pinobanksin-3-*O*-acetate[b,c]	Dihydroflavonol	13.304 ± 0.312
25	47.4	266, 300sh, 359	269	269(100), 241(61)	Galangin[a,b]	Flavonol	12.661 ± 0.214
26	49.4	268, 331	283	269	Acacetin[a,b]	Flavone	0.564 ± 0.037
27	49.9	265, 300sh, 350sh	283	269	6-Methoxychrysin[b,c]	Flavone	1.001 ± 0.037
28	52.2	294, 310	231	163(100), 119(12)	*p*-Coumaric isoprenyl ester[b,c]	Phenolic acid	0.824 ± 0.022

39	52.8	295, 326	295	178(100), 135(60)	Caffeic acid cinnamyl ester[b,c]	Phenolic acid	2.497 ± 0.037
30	53.8	289	327	253(100), 271(10)	Pinobanksin-3-*O*-propionate[b,c]	Dihydroflavonol	6.839 ± 0.148
31	58.4	292	417	297(100), 402(85), 267(67)	Pinobanksin-methyl-ether-3-*O*-phenylpropionate[b,d]	Dihydroflavonol	0.525 ± 0.067
32	59.3	293xx	341	253(100)	Pinobanksin-3-O-butyrate or isobutyrate[b,c]	Dihydroflavonol	1.042 ± 0.101
33	59.6	292	475	415	Pinobansin-3-*O*-acetate-5-*O*-hydroxyphenylpropionate[b,c]	Dihydroflavonol	2.456 ± 0.021
34	60.4	292	475	415	Pinobansin-3-*O*-acetate-7-*O*-hydroxyphenylpropionate (isomer)[b,c]	Dihydroflavonol	3.461 ± 0.258
35	63.7	292	355	253	Pinobanksin-3-*O*-pentanoate or 2-methylbutyrate[b,c]	Dihydroflavonol	1.359 ± 0.085

In contrast, the chromatographic fingerprint of RP (Figure 23) displayed a distinct chemical profile, characterized predominantly by isoflavonoids, pterocarpans, and benzophenones. Among the 17 identified compounds (Table 7), vestitone, liquiritigenin, formononetin and biochanin A, were found between 17.4 and 33.3 minutes.

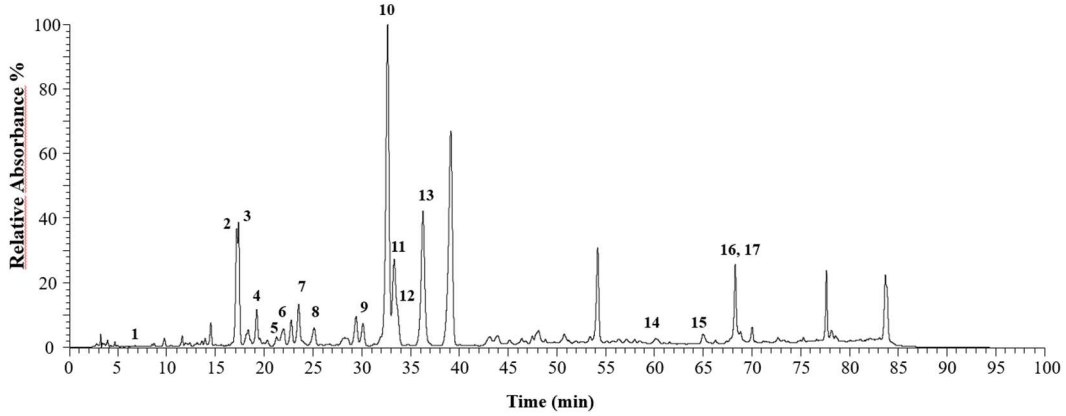

***Figure 23** – LC/DAD/ESI-**MS^n**) resulting profiles for RP*

These compounds are known for their estrogenic and anti-inflammatory properties and are commonly associated

with Dalbergia-derived propolis. The results were processed according to previous literature (Omar et al., 2016; Vieira de Morais et al., 2021; Righi et al., 2011; Falcão et al., 2019; Falcão et al., 2013; Silva et al., 2020).

The most prominent peak (peak 10, 32.6 min) corresponded to vestitol, a characteristic compound of RP. Other notable constituents included neovestitol and formononetin derivatives (peaks 11 and 13), which contribute significantly to the biological activity of red propolis.

Furthermore, RP samples revealed the presence of polyisoprenylated benzophenones such as gutiferone E, oblongifolin B, and xanthochymol (peaks 16 - 17), compounds that are often associated with high cytotoxic and antioxidant potential (Omar et al., 2016; Silva et al., 2020).

Both propolis types exhibited rich phenolic profiles, the chemical classes were distinct. BP showed higher diversity in flavonoids and phenolic acids, reflecting its European botanical origin. RP, on the other hand, presented a fingerprint dominated by isoflavones and benzophenones, matching with its northeastern botanical origin. These differences influence their antioxidant behavior and different applications.

***Table 7** - Characterization of the phenolic compounds from Brazilian red propolis obtained by LC/DAD/ESI-MS^n. [a]Confirmed with standard, [b]Confirmed with MSn fragmentation, [c](Omar et al., 2016), [d](Vieira de Morais et al., 2021), [e](Righi et al., 2011), [f](Falcão et*

Nº	t_R (min)	λ_{max} (nm)	$[M-H]^-$ m/z	MS^2 (% base peak)	Proposed compound	Family	$\frac{mg}{g}$ Extract
1	6.7	292, 323	179	135	Caffeic acid[a,b]	Phenolic acid	Detected
2	17.4	276, 312	255	135(100), 119(10)	Liquiritigenin[b,c]	Flavanone	3.247 ± 0.028
3	18.3	279, 310	285	270	Vestitone[b,d]	Isoflavanone	0.110 ± 0.000
4	19.2	289	283	268	Calycosin[b,c]	Isoflavanone	0.165 ± 0.010
5	21.4	276, 309	315	300	Violanone[b,e]	Isoflavanone	0.042 ± 0.008
6	21.9	280, 342	285	270(100), 267(17), 179(4)	3,4-Dihydroxy-9-methoxypterocarpan[b, e]	pterocarpan	0.120 ± 0.002
7	23.5	291	271	151	Naringenin[a,b]	Flavanone	0.748 ± 0.105

8	25.1	280	283	268	Biochanin A[b,d]	Isoflavone	0.125 ± 0.003
9	30.1	281	299	284	Sativanone[b,f]	Isoflavanone	0.150 ± 0.003
10	32.6	283	271	227(100), 109(86), 135(83)	Vestitol[b,d]	Isoflavan	2.624 ± 0.004
11	33.3	280, 320	267	252	Formononetin[b,d]	Isoflavone	0.698 ± 0.013
12	33.7	240, 370	255	135(100), 119(25)	Isoliquiritigenin[b,d]	Chalcone	0.598 ± 0.093
13	36.3	282	271	135(100), 227(74), 109(62)	Neovestitol[b,d]	Isoflavan	1.227 ± 0.009
14	60.2	285, 481	521	397(100), 491(45)	Retusapurpurin B[b,h]	isoflavan der	0.047 ± 0.013
15	64.9	284, 481	521	397(100), 491(60)	Retusapurpurin A[b,h]	isoflavan der	0.069 ± 0.002
16	83.7	244, 351	601	465	Guttiferone E/Xanthochymol[b,d]	isoflavan der	0.306 ± 0.024
17	84.0	244, 351	601	327(100), 273(26), 271(15)	Oblongifolin B[b,d]	isoflavan der	0.172 ± 0.020

5.2. Protein content in pollen grains

Pollen is a common allergen that affects the immune system triggering allergic reactions in the body because of its protein and glycoprotein content. These molecules are recognized by the immune system as foreign and potentially harmful, leading to exaggerated immune response (Platts-Mills & Woodfolk, 2011). Because of the side effects pollen grains (Figure 24) can cause in the body, it's important to remove it's protein content so the dressing can be used by patients minimizing drastically the risks of allergic reactions. For that, the extraction process of SECs is very important. The protocol is divided into two main steps: removing the inside components and isolating the external structure (exine). The methodology for obtaining hollow exine microcapsules from pollen grains involves the progressive removal of internal cellular contents, leaving behind a robust and porous exine shell. This procedure is

based on the method described in Section 4.5, which consists in a sequence of physical and chemical treatments designed to isolate the exine while preserving its structural integrity and removing the allergenic protein content.

Pollen presents the pollenkitt which is a lipidic-rich material composed of flavonoids, carotenoids and polysaccharides being the external content of the grain (Pacini & Hesse, 2005). The raw grains also contain the exine (resistant external layer), intine (internal layer), protoplasm (cytoplasmatic content) and nanochannels. Initially, pollenkitt is removed by defatting with organic solvents. Followed by hydrations steps that induces the turgor pressure inside the grains, facilitating the breakdown of internal membranes. The alkaline and acidic treatments that follow promotes the digestion and removal of cytoplasmatic content and intine. The schematic pathway for conventional methodology to obtain the biocapsules can be observed in Figure 25 and the methodology representation to obtain hollow SECs is shown in Figure 26. After several washes and filtration, the hollow exine biocapsules (Figure 27) are collected.

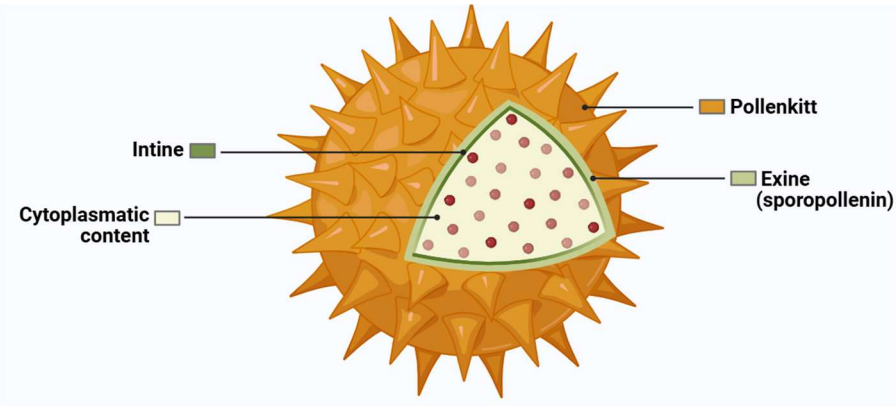

Figure 24 *– Schematic representation for pollen's layers structure*

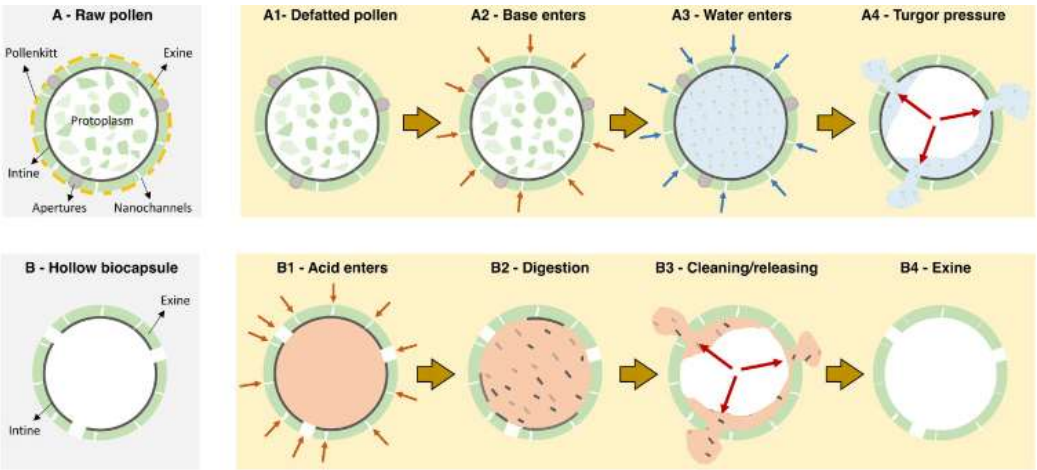

Figure 25 *– Schematic pathway for the conventional methodology to obtain SECs (Aylanc et al., 2023)*

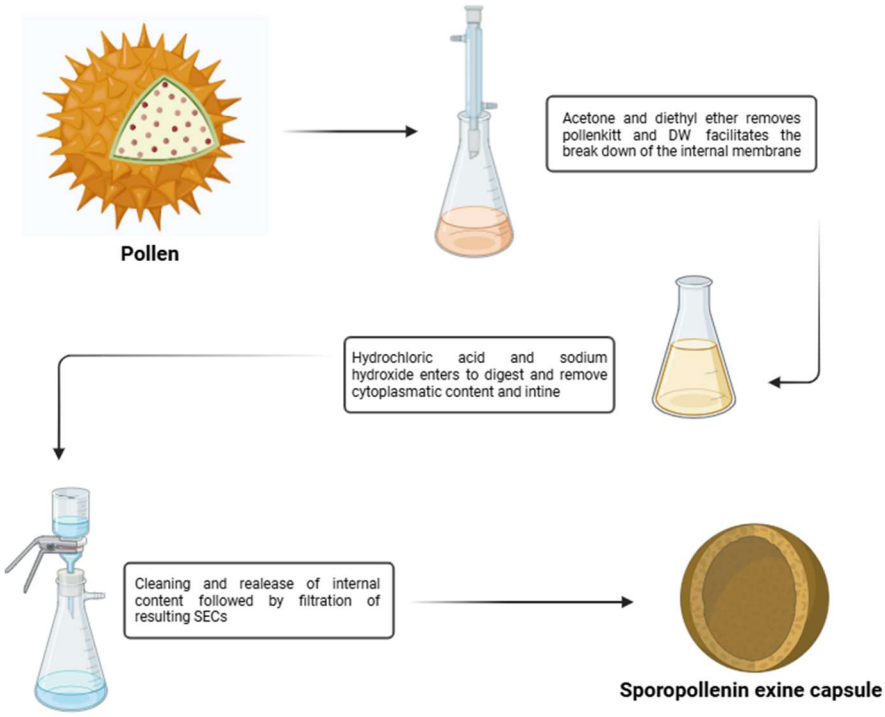

Figure 26 *– Schematic representation of the methodology for obtention of hollow exine structure*

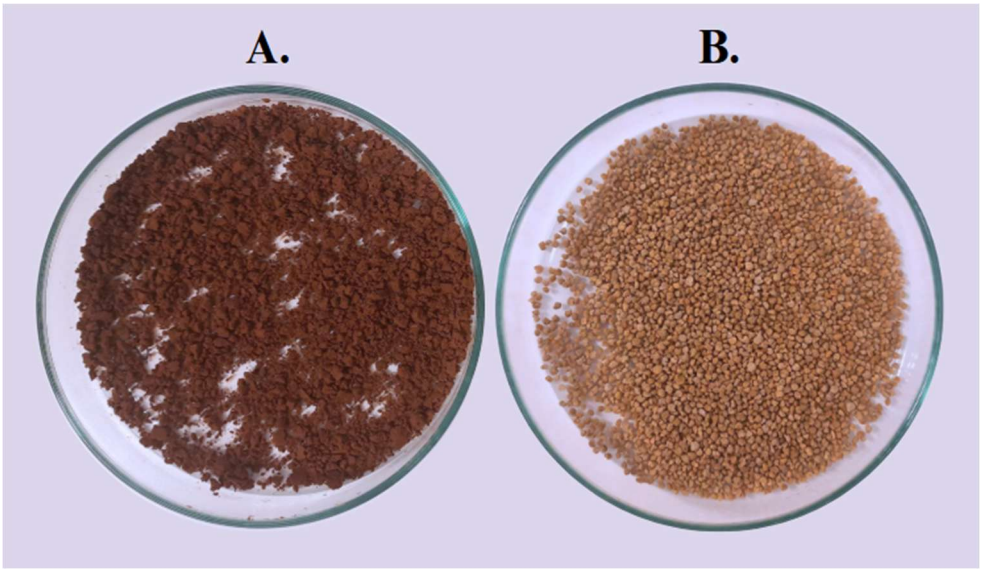

Figure 27 *– A. SECs after last filtration and before completely dried. B. dried SECs ready for loading procedure*

Raw pollen had its protein content compared with the produced sporopollenin exine microcapsules. Total protein content of the first sample was 29.74 % (± 0.16), whereas the SECs showed a significantly lower value of 5.34 % (± 0.25) as shown in Figure 28. This result confirms the efficiency in removing most of the protein components which corroborate with the multi-step procedure described regarding the digestion and removal of the pollen content (which includes allergenic proteins).

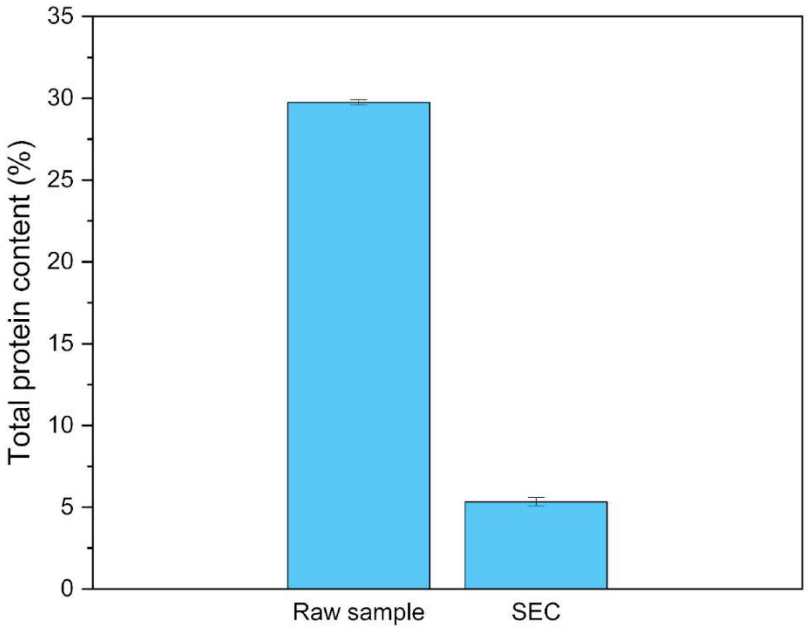

Figure 28 *– Graph representing the percentage of total protein content and its standard deviation*

5.3. Encapsulation efficiency (%EE)

During the vacuum-assisted loading of propolis into the SECs, not all of the encapsulated material necessarily contains phenolic compounds. Therefore, it is essential to determine the encapsulation efficiency specifically for the TPC within the biocapsules. This directly influences the amount of bioactive compounds available in the wound dressing to support the skin during the healing process. For the SRP the EE was 30.34% (± 1.09) and as for the SBP samples the efficiency obtained was higher presenting a result of 40.67% (± 6.68). All the measurements were in triplicate, and the results (Figure 29) given in mean value with standard deviation. The higher SD observed in the biocapsules loaded with brown propolis is likely associated with the material's inability to form a homogeneous powder even after freeze-drying, due to its persistent resinous and sticky nature. These characteristics differ from those

of red propolis (RP), which remained as a homogeneous powder. The results obtained are consistent with findings in Section 5.1.1, where the brown propolis exhibited higher TPC compared to red propolis samples.

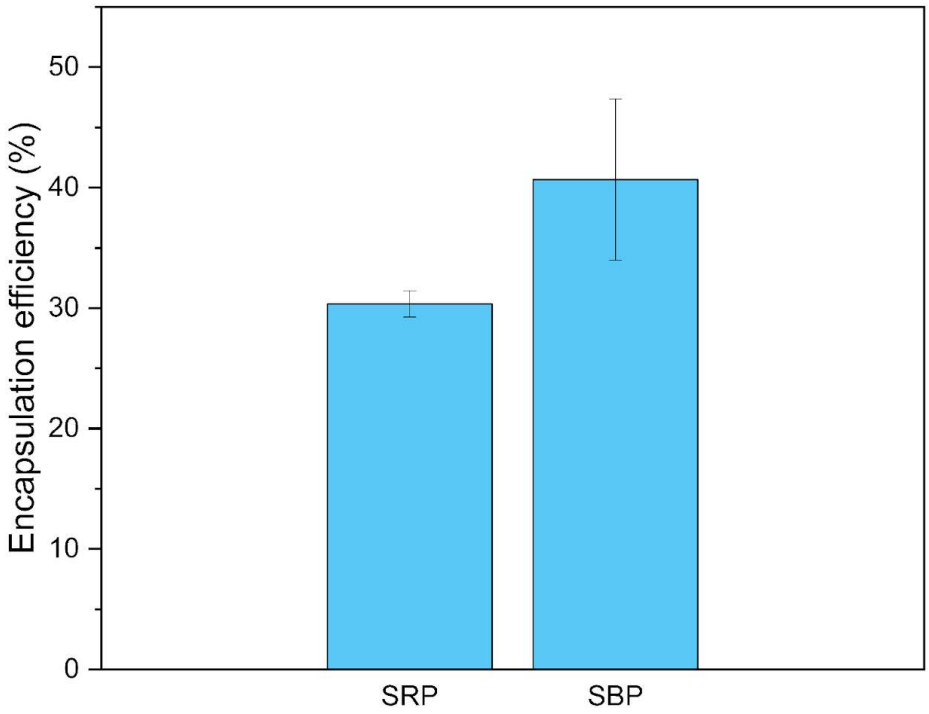

Figure 29 *– Graphical results for the encapsulation efficiency percentage of vacuum loaded TPC*

5.4. Appearance of films

5.4.1. Color and thickness

In the wound care industry, both color and thickness parameters can significantly influence their functionality, usability and patient acceptance. The color can promote psychological comfort in patients as neutral and skin-tones dressings are more discreet, therefore often preferred. Color parameters on the CIELAB spectra including L^*, a^*, b^* and ΔE values of all the film samples are given in Table 8. Values are given in mean ± SD and measurements were in triplicate for each film.

The control film (CF) exhibited the highest lightness value ($L^* = 90.10 \pm 0.44$), indicating a bright and translucent appearance. In comparison, all other formulations incorporating propolis showed significantly lower L^* values ($p < 0.05$), suggesting a darkening effect associated with the addition of bioactive extracts and loaded SECs, particularly RPF ($L^* = 62.36 \pm 3.82$). This result is associated with the homogeneity of the film containing only red propolis extract. Due to its well-uniformed surface, the film exhibited a color more closely

matched with the natural shade of the extract. The *a** values varied considerably among samples, with BPF sample presenting a slightly negative value of -0.87 (± 0.41), indicating a slight shift toward green tones. RPF showed the highest *a** (23.45 ± 2.02), indicating a significant reddish color. In terms of *b**, all films containing propolis extract presented higher values compared to CF, especially RPF, SBPF, and SRPF, all of which had *b** values above 43, reflecting a strong yellow component. Regarding color difference (ΔE), the CF film had the highest value (42.42 ± 1.05), while SRPF showed the lowest (3.03 ± 2.46), suggesting a closer color resemblance between SRPF and the reference standard (white background). These results highlight how the type of propolis extract distinctly influences the visual appearance of the films. That occurs mainly because of their individual unique phenolic compositions and natural pigments, consistent with observations reported in previous studies (Grassi et al., 2023; Sarapa et al., 2025).

Table 8 *– L*, a*, b* and ΔE* parameters for the color of the produced films (p < 0.001)*

Film Sample	*L**	*a**	*b**	ΔE
CF	90.10 ± 0.44	1.17 ± 0.08	5.88 ± 1.00	42.42 ± 1.05
BPF	80.00 ± 2.21	-0.87 ± 0.41	28.30 ± 2.12	20.30 ± 2.61
RPF	62.36 ± 3.82	23.45 ± 2.02	43.67 ± 3.34	17.91 ± 3.63
SBPF	72.79 ± 1.80	3.49 ± 1.03	43.04 ± 2.15	7.08 ± 1.80
SRPF	69.71 ± 2.09	11.88 ± 1.68	43.44 ± 1.39	3.03 ± 2.46

Thickness is another parameter with considerable influence in the wound care industry. It interferes with the absorption capacity of the dressing because greater thickness holds more wound fluids also offering a mechanical protection reducing pain from friction or pressure (Boateng et al., 2008). The thinner the material is, more flexibility is observed which is important for greater mobile application.

The appearance of the CF and propolis-loaded films are shown in Figure 30, and their thickness results are expressed in µm as shown in Table 9. The control film (CF) presented a thickness of 74.17 (± 19.86) µm. Films incorporated with propolis extracts exhibited varying thicknesses, with BPF showing the lowest value (55.00 ± 7.89 µm) and RPF the highest (95.00 ± 10.06 µm). SBPF and SRPF films also demonstrated increased thickness, with 89.17 (± 10.81) µm and 90.00 (± 5.59) µm, respectively. The results suggest that the incorporation of propolis extracts tends to increase film thickness in comparison to the control.

This behavior may be attributed to the structural contribution of the extracts and potential differences in intermolecular interactions and crosslinking between the film matrix and each type of propolis used, as similarly reported in studies involving plant-derived additives in polymer-based films (Marangoni et al., 2022).

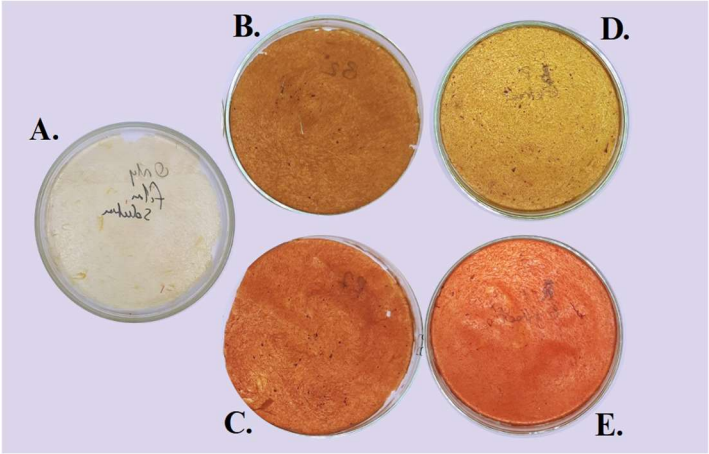

Figure 30 *– Film's appearance after dried.* ***A.*** *Control film.* ***B.*** *SBPF.* ***C.*** *SRPF.* ***D.*** *BPF.* ***E.*** *RPF*

Table 9 *– Thickness of* the films expressed in mean with standard deviation

Sample	Mean	SD
CF	74.17	19.86
BPF	55.00	7.89
RPF	95.00	10.06
SBPF	89.17	10.81
SRPF	90.00	5.59

5.4.2. UV-Vis light transmittance

The transparency of dressings allows professionals to monitor the wound without removing it. This reduces drastically the risk of contamination. Therefore, optical transmittance was evaluated in the range of 300 to 800 nm, aiming to assess their transparency and light-blocking capabilities within the ultraviolet-visible spectrum. Figure 31 presents the transmittance curves obtained for each formulation: control film (CF), brown propolis film (BPF), red propolis film (RPF), and the corresponding films containing microcapsules loaded with brown and red propolis (SBPF and SRPF, respectively).

Control film (CF) presented the highest transmittance across the entire spectrum, reaching approximately 50.16% at 800 nm. This behavior is expected for biopolymeric films composed solely of alginate, which is naturally transparent and does not contain ligh-absorbing groups that absorb in the UV-visible region.

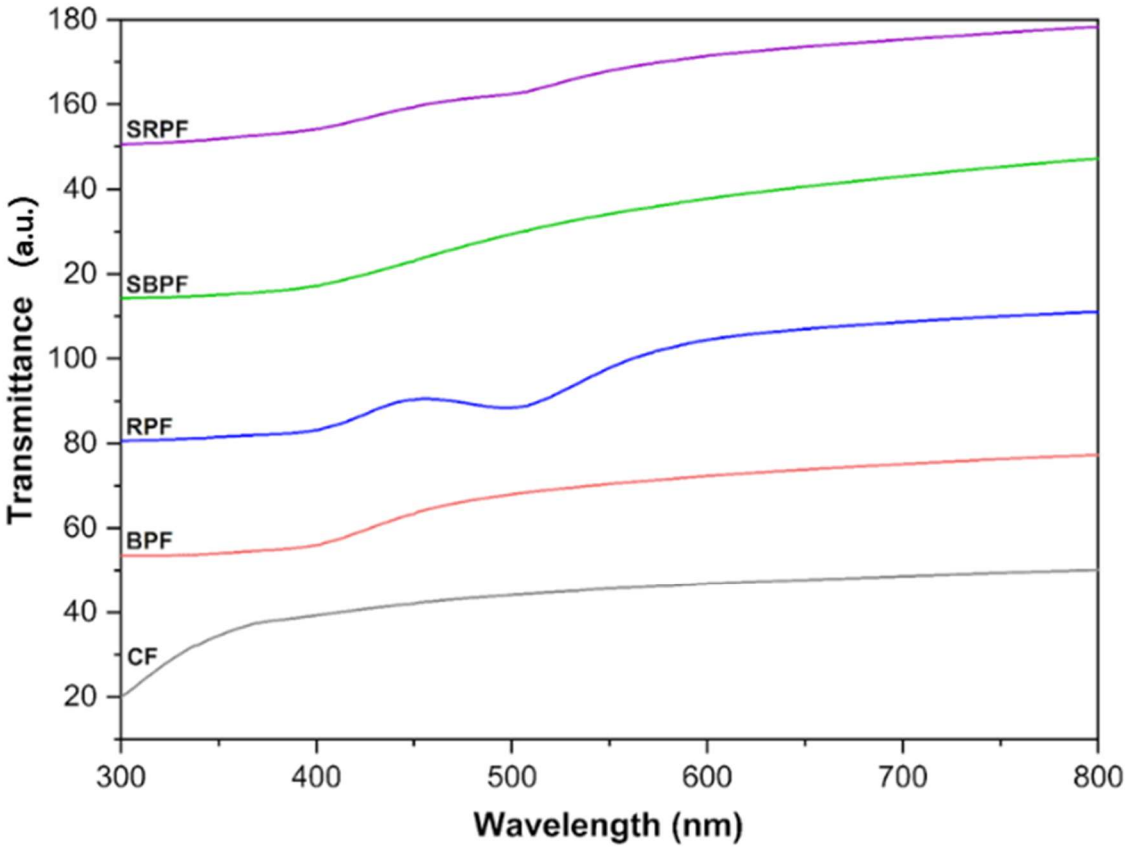

Figure 31 *– Graph representation of the spectrum for each film composition*

In contrast, both BPF and RPF films exhibited significantly lower transmittance values, especially in the ultraviolet region (300–400 nm), confirming the presence of absorbing compounds within the propolis extracts. At 300 nm, BPF showed transmittance values of 0.37 and RPF 0.28. These low values indicate strong absorption in the UV region, which can be attributed to the presence of polyphenols and flavonoids with conjugated aromatic systems known to absorb UV radiation (Bankova, 2005). Throughout the visible range, transmittance gradually increased, with BPF and RPF reaching approximately 24.22 and 30.75 at 800 nm. The higher absorbance observed in RPF compared to BPF suggests that red propolis contains a greater concentration or diversity of light-absorbing compounds, possibly linked to its distinct phenolic profile.

The films containing microcapsules, SBPF and SRPF, exhibited intermediate behavior between the control and extract-loaded films. Their transmittance curves were consistently lower than CF, but slightly higher than the directly loaded films, especially in the UV region.

This may be attributed to the challenge of obtaining a completely homogen film containing microcapsules. At 300 nm, SBPF showed a transmittance of 0.44, while SRPF reached 0.89. These values increased progressively across the spectrum, culminating in values of 33.32 and 28.71 at 800 nm for SBPF and SRPF, respectively.

While the SRPF film had slightly higher transmittance than RPF throughout the spectrum, its curve maintained a similar shape, suggesting that the encapsulation process preserved most of the optical properties of the extract, but possibly limited the direct interaction between active compounds and the incident light due to the exine shell. SBPF, on the other hand, followed the profile of BPF but with slightly higher transmittance values, especially above 500 nm, indicating partial attenuation of light-blocking capacity after encapsulation.

The strong absorption observed in the UV region (<400 nm) for all samples containing propolis is particularly relevant in the context of UV-protective applications. The incorporation of propolis and biocapsules reduces UV transmittance, enhancing the film's potential as a natural photoprotective barrier. This protective effect is consistent with findings reported in the literature for other propolis-based systems and reflects the chemical nature of polyphenols as effective UV absorbers (Marangoni et al., 2022). This suggests that these films, especially BPF and SBPF, may serve as promising materials for applications in wound dressings that requires UV filtration.

5.4.3. SEM

The surface morphology of the hollow sporopollenin exine microcapsules (SECs), control film (CF), propolis-loaded films (RPF and BPF), and microcapsule-loaded films (SRPF and SBPF) was analyzed by SEM at different magnifications to assess structural integrity, dispersion, and surface homogeneity (Figures 32 and 33).

The hollow sporopollenin exine microcapsules, visualized at 6,500× and 14,000× magnifications, exhibited a characteristic spherical morphology with porous external shells and highly visible surface texture, consistent with natural pollen wall architecture (Cao et al., 2024; Raish et al. 2021; Mundargi et al., 2016). Fractures and ruptures on the shell surface confirmed their hollow structure, which is critical for loading and releasing applications. Their rigid, textured architecture offers mechanical stability while preserving internal void space.

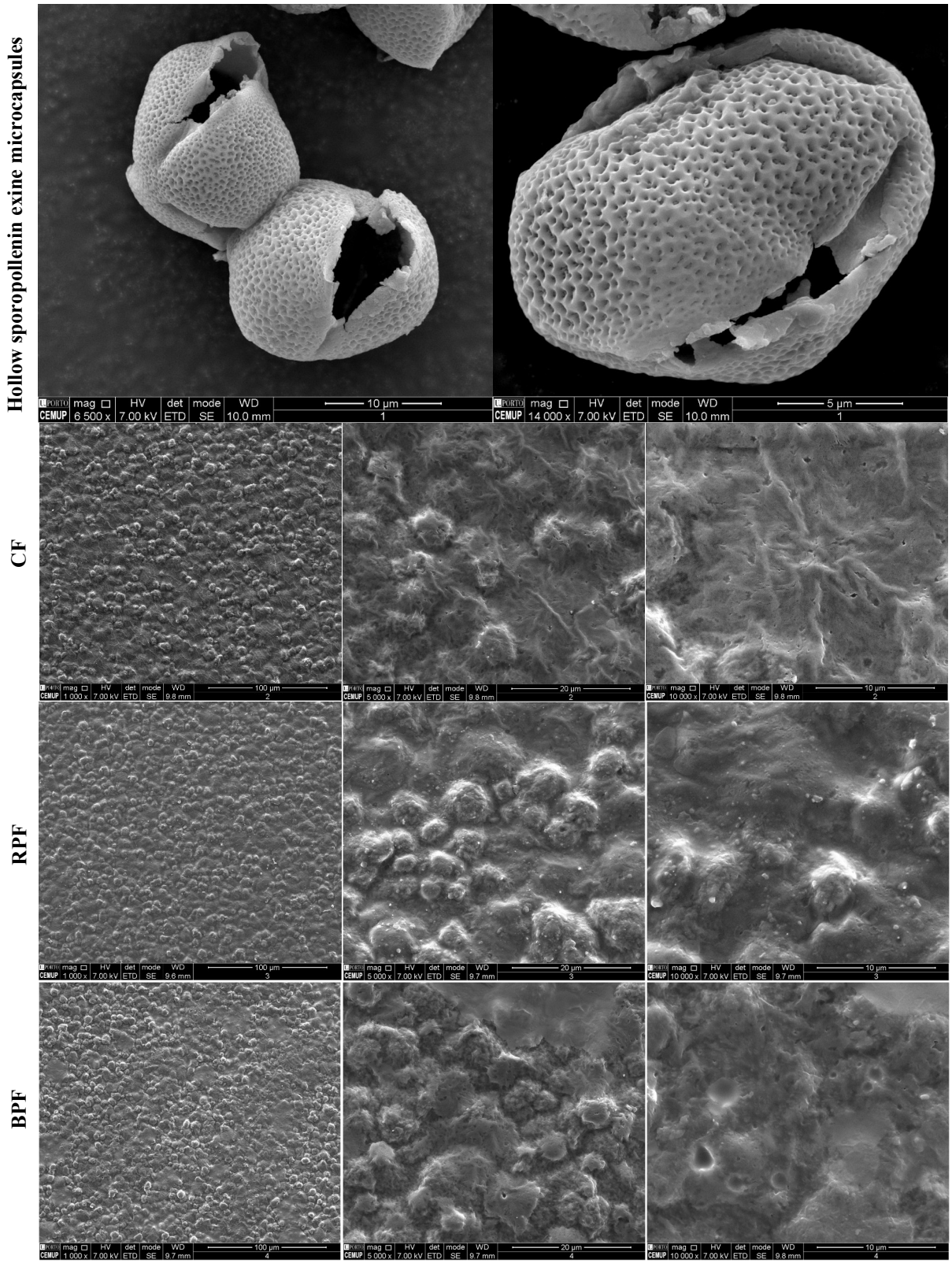

Figure 32 *– Morphology of the samples' surface for hollow SECs, CF, RPF and BPF*

The control film (CF) presented a smooth and homogeneous surface morphology across all magnifications, as expected for a polymeric alginate matrix. The absence of irregularities reflects the film's uniform internal structure and lack of microstructural complexity.

In contrast, the red propolis (RPF) and brown propolis (BPF) films displayed rough, porous surfaces with visible agglomerates, especially at 5,000× and 10,000× magnifications. These features are indicative of the incorporation of propolis extracts into the polymeric network, resulting in the formation of particle agglomerates and intensified surface complexity. The presence of localized accumulations is attributed to the partial aggregation of propolis constituents during film formation.

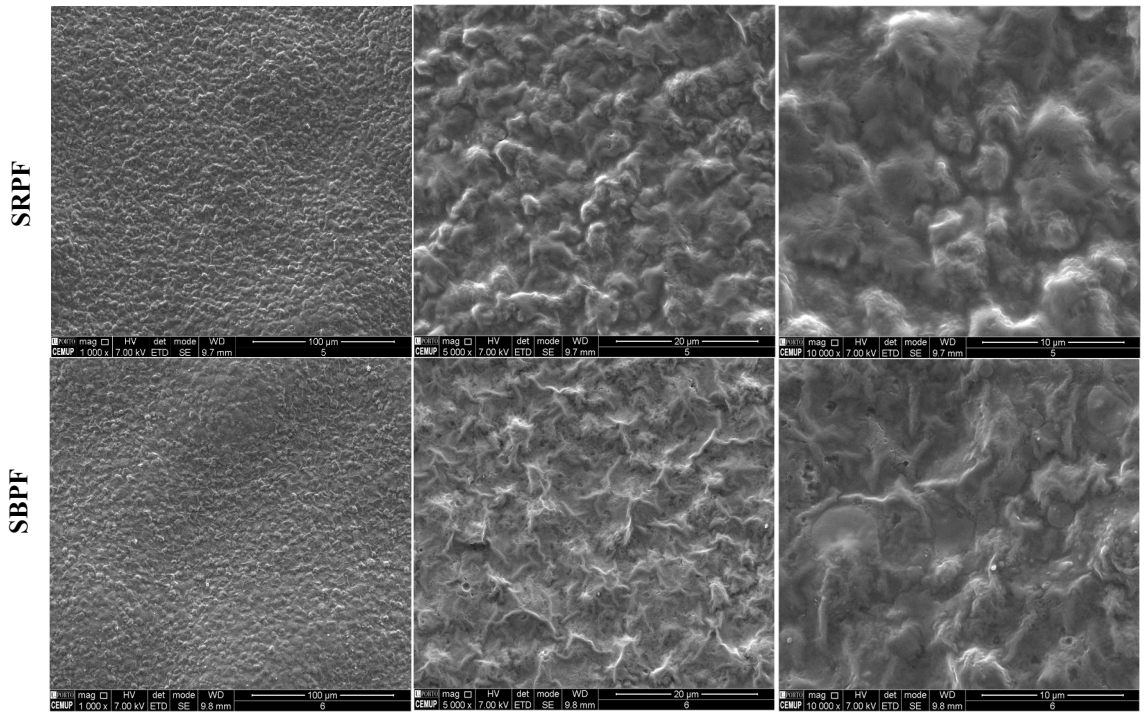

Figure 33 *– Morphology of the samples' surface for SRPF and SBPF*

The incorporation of microcapsules into alginate films (SRPF and SBPF) contributed to evident changes in surface morphology. Both samples exhibited a granular and fibrous texture, with visible topographical irregularities. The microcapsules formed interconnected agglomerates that increased overall surface roughness and in general was well-integrated into the alginate if compared with the films containing extracts. Even so, samples SRPF and SBPF were not completely homogeneous. At higher magnifications, partial integration of the capsules into the matrix was visible, suggesting strong interaction between SECs and alginate.

5.5. Physicochemical properties of films

5.5.1. FTIR

The Fourier-Transform Infrared Spectroscopy (FTIR) analysis was conducted to investigate the chemical structures and interactions among the components of ten samples, including pure alginate, control films, brown and red propolis extracts (BP and RP), microcapsules loaded with propolis (SBP and SRP), and their respective film formulations with only propolis and with the loaded SECs. The obtained spectra (Figure 34) enabled the identification of key functional groups (Table 10, 11, 12, 13, 14, 15, 16 and 17) and possible intermolecular interactions based on the position and intensity of characteristic vibrational bands, supported by comparative data from the literature (Oliveira et al., 2016; Cebi et al., 2020; Erdoğan, 2023; Soliman et al., 2023; Nandiyanto, Oktiani & Ragadhita, 2019; Lawrie et al., 2007).

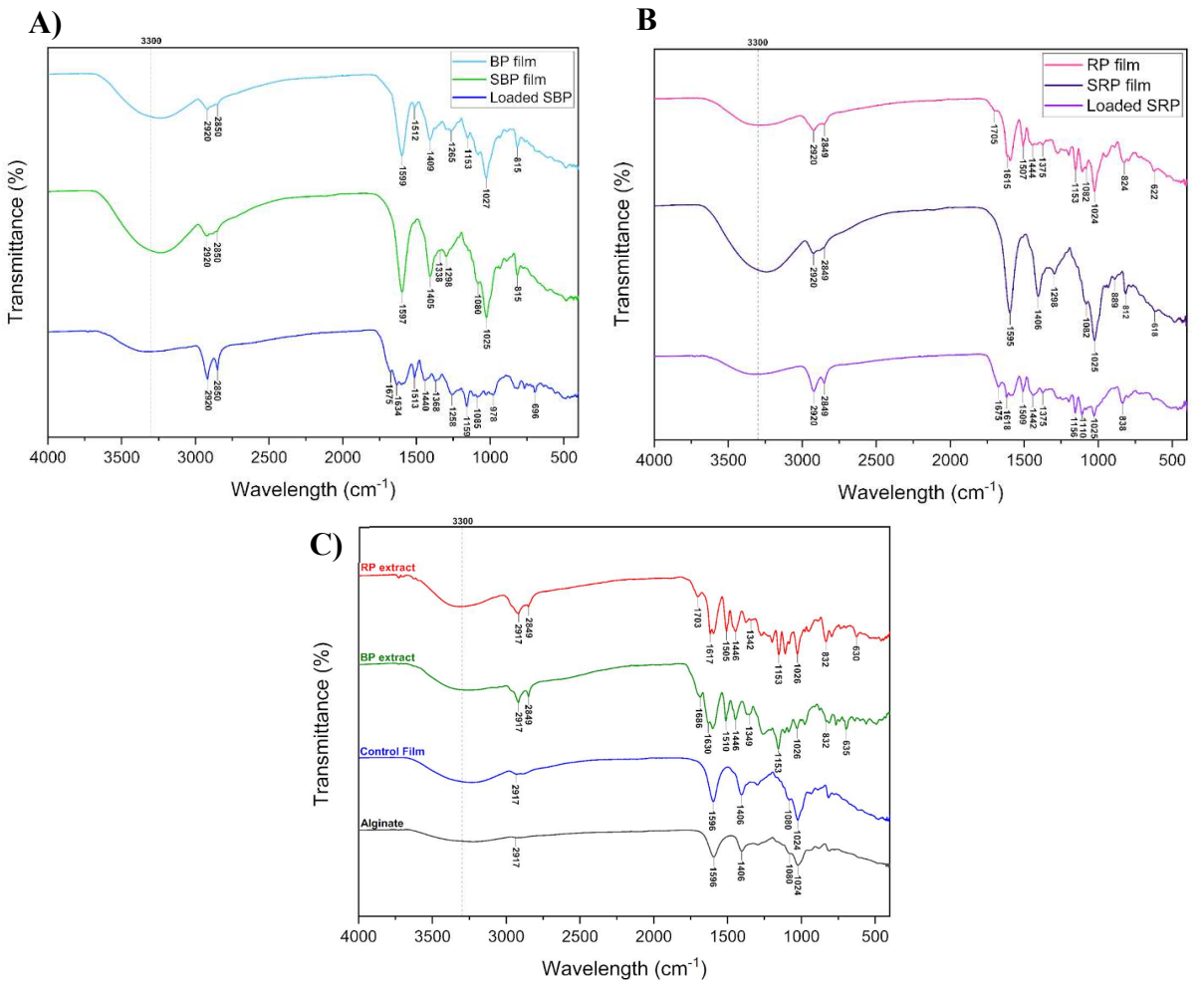

Figure 34 *– A) Spectrum of the produced samples containing BP (SBP, BPF and SBPF). B) Bands of RPF, SRPF and RPF. C) FTIR results for standard samples (extracts, alginate and control film with only alginate in its matrix*

Table 10 *– Peak ranges and its respective functional groups for alginate and control film*

Peak Ranges (cm^{-1})	Functional Group/ Assignment
3500 - 3200 (broad)	Intermolecular hydrogen bonding (O-H stretching vibrations)
2917	C–H asymmetric stretch (aliphatic hydrocarbons)
1596	COO^- asymmetric stretching (alginate)
1406	COO^- symmetric stretching (carboxylate)
1080	C–O stretching (polysaccharide or alcohols)
1024	C–O stretching vibration

Table 11 *– Peak ranges and its respective functional groups for BP and RP extracts*

Peak Ranges (cm^{-1})	Functional Group/ Assignment
3500 - 3200 (broad)	Intermolecular hydrogen bonding (O-H stretching vibrations)
2935 - 2915	Methylene C-H asymmetric stretch (aliphatic hydrocarbons)
2865 - 2845	Methylene C-H symmetric stretch (alkyl chains)
1703	C=O stretching (carbonyls from esters or acids)
1686	C=O stretching (aromatic or carboxylic acids)
1630 - 1617	C=C stretching (phenolic or aromatic compounds)
1510	C=C stretching (conjugated aromatics)
1505	C=C stretching (substituted phenols)
1446	Methyl (CH_3) asymmetric bending (organic molecules)
1349 - 1342	C-O-H bending (phenol or tertiary alcohol)
1153	C–O stretching (tertiary alcohol or ethers)
1026	C–O stretching vibration
860-800	C–H (out-of-plane). Aromatic ring (C-H 1,4-disubstitution (para))
635-630	Out-of-plane bending (aromatics or C–Cl/C–Br)

Table 12 *– Peak ranges and its respective functional groups for loaded SRP*

Peak Ranges (cm^{-1})	Functional Group/ Assignment
3500 - 3200 (broad)	Intermolecular hydrogen bonding (O-H stretching vibrations)
2935 – 2915	Methylene C-H asymmetric stretch (aliphatic hydrocarbons)
2865 – 2845	Methylene C-H symmetric stretch (alkyl chains)
1675	C=O stretching (conjugated or aromatic systems)
1618	C=C stretching (aromatic compounds)
1509	C=C stretching (conjugated aromatics)
1442	C–H bending (phenolic or aromatic structures
1375	C–H bending (alkyl groups)
1156	C–O–H bending (secondary alcohols or phenolic OH)
1110	C–O stretching (esters or secondary alcohols)
1025	C–O stretching vibrations
860-800	C–H (out-of-plane). Aromatic ring (C-H 1,4-disubstitution (para))

Table 13 *– Peak ranges and its respective functional groups for loaded SBP*

Peak Ranges (cm^{-1})	Functional Group/ Assignment
3500 - 3200 (broad)	Intermolecular hydrogen bonding (O-H stretching vibrations)
2935 - 2915	Methylene C-H asymmetric stretch (aliphatic hydrocarbons)
2865 - 2845	Methylene C-H symmetric stretch (alkyl chains)
1675	C=O stretching (conjugated or aromatic systems)
1634	C=C stretching (aromatic or phenolic compounds)
1513	C=C stretching (conjugated aromatics)
1440	C–H bending (phenolic or aromatic structures
1368	C–H bending (alkyl groups)
1258	C–O stretching vibrations
1159	C–O stretching vibrations
1085	C–O stretching vibrations
970–960	Trans-C-H out-of-plane bend
900–670 (several)	Aromatic C-H out-of-plane bend

Table 14 *– Peak ranges and its respective functional groups for RP film*

Peak Ranges (cm^{-1})	Functional Group/ Assignment
3500 - 3200 (broad)	Intermolecular hydrogen bonding (O-H stretching vibrations)
2935 - 2915	Methylene C-H asymmetric stretch (aliphatic hydrocarbons)
2865 - 2845	Methylene C-H symmetric stretch alkyl chains)
1705	C=O stretching (carbonyls from esters or acids)
1630 - 1617	C=C stretching (phenolic or aromatic compounds)
1507	C=C stretching (substituted phenols)
1444	C–H bending (methyl or phenolic structures)
1375	C–H bending
1153	C–O stretching (tertiary alcohol or ethers)
1082	C–O stretching vibration
1024	C–O stretching vibration
860-800	C–H (out-of-plane). Aromatic ring (C-H 1,4-disubstitution (para))
622	Out-of-plane bending (aromatics or C–Cl/C–Br)

Table 15 *– Peak ranges and its respective functional groups for BP film*

Peak Ranges (cm^{-1})	Functional Group/ Assignment
3500 - 3200 (broad)	Intermolecular hydrogen bonding (O-H stretching vibrations)
2935 - 2915	Methylene C-H asymmetric stretch (aliphatic hydrocarbons)
2865 - 2845	Methylene C-H symmetric stretch alkyl chains)
1705	C=O stretching (carbonyls from esters or acids)
1630 - 1617	C=C stretching (phenolic or aromatic compounds)
1599	C=C stretching (aromatic ring)
1512	C=C stretching (phenolic or aromatic compounds)
1409	C–H bending (alkyl or phenolic structures)
1265	C–O–C bending (ethers, esters)
1153	C–O stretching (tertiary alcohol or ethers)
1027	C–O stretching vibration
860-800	C–H (out-of-plane). Aromatic ring (C-H 1,4-disubstitution (para))

Table 16 *– Peak ranges and its respective functional groups for SBP film*

Peak Ranges (cm^{-1})	Functional Group/ Assignment
3500 - 3200 (broad)	Intermolecular hydrogen bonding (O-H stretching vibrations)
2935 – 2915	Methylene C-H asymmetric stretch (aliphatic hydrocarbons)
2865 – 2845	Methylene C-H symmetric stretch (alkyl chains)
1597	COO^- asymmetric stretching (carboxylates)
1406	COO^- asymmetric stretching (carboxylates)
1338	C–O–H bending (phenols/alcohols)
1298	C–O stretching (tertiary alcohol or ethers)
1080	C–O stretching vibration
1025	C–O stretching vibration
860-800	C–H (out-of-plane). Aromatic ring (C-H 1,4-disubstitution (para))

Table 17 *– Peak ranges and its respective functional groups for SRP film*

Peak Ranges (cm^{-1})	Functional Group/ Assignment
3500 - 3200 (broad)	Intermolecular hydrogen bonding (O-H stretching vibrations)
2935 – 2915	Methylene C-H asymmetric stretch (aliphatic hydrocarbons)
2865 – 2845	Methylene C-H symmetric stretch (alkyl chains)
1595	COO^- asymmetric stretching (carboxylates)
1406	COO^- asymmetric stretching (carboxylates)
1298	C–O stretching or aromatic ether linkage
1082	C–O stretching vibration
1025	C–O stretching vibration
889	C–H (out-of-plane).
860 – 800	C–H (out-of-plane). Aromatic ring (C-H 1,4-disubstitution (para))
618	Out-of-plane bending (aromatics or C–Cl/C–Br)

The spectrum of pure alginate exhibited a broad absorption band between 3500 and 3200 cm^{-1}, attributed to O–H stretching vibrations involved in extensive intermolecular hydrogen bonding, commonly found in polysaccharides. A small but distinct absorption band was observed at 2917 cm^{-1} in the FTIR spectrum of pure alginate, corresponding to the asymmetric stretching vibration of C–H bonds in aliphatic hydrocarbon chains. This band is typically attributed to methylene ($–CH_2–$) groups present in the polymer backbone and reflects the presence of minor hydrophobic regions within the otherwise hydrophilic alginate structure. Although alginate is primarily composed of polysaccharide chains rich in hydroxyl and carboxyl groups, the presence of C–H stretching bands indicates the contribution of saturated carbon chains, consistent with its natural origin and molecular structure. In addition, distinct bands at 1596 cm^{-1} and 1406 cm^{-1} were associated with the asymmetric and symmetric

stretching of carboxylate (COO^-) groups, respectively, confirming the presence of ionized carboxylic functionalities in the alginate backbone. The bands at 1080 and 1024 cm^{-1} were assigned to C–O stretching vibrations typical of saccharide units and hydroxyl-bearing groups. The control film composed solely of alginate showed similar spectral features, indicating that the film-forming process did not significantly alter the alginate's chemical structure.

The brown propolis (BP) and red propolis (RP) extracts presented FTIR spectra characteristic of polyphenol-rich natural products. A broad O–H stretching band between 3500 and 3200 cm^{-1} confirmed the presence of alcohol and phenol groups capable of forming hydrogen bonds. Prominent C–H stretching vibrations were observed at 2935–2915 cm^{-1} (asymmetric) and 2865–2845 cm^{-1} (symmetric), corresponding to aliphatic CH_2 and CH_3 groups present in the propolis matrix. The C=O stretching bands appeared near 1703 cm^{-1} in BP and 1686 cm^{-1} in RP, indicating the presence of esters, carboxylic acids, or flavonoid carbonyls. The region from 1630 to 1505 cm^{-1} contained several bands attributed to C=C aromatic stretching, consistent with phenolic rings and conjugated systems. The absorption band observed at 1446 cm^{-1} in the spectra of both brown and red propolis corresponds to the asymmetric bending vibration of methyl groups ($–CH_3$). This vibrational mode involves angular deformation of the C–H bonds in the methyl group, where two hydrogen atoms move in opposite directions while the third remains relatively fixed. Unlike stretching vibrations, bending modes do not change the bond length but rather the bond angle. The presence of this peak is indicative of aliphatic chains or methyl-substituted aromatic compounds, which are common in natural substances such as flavonoids, terpenoids, and other phenolic constituents found in propolis. The 1446 cm^{-1} band is therefore consistent with the molecular complexity of the propolis extracts and confirms the presence of organic structures containing terminal methyl groups, as also reported in previous FTIR studies of natural resins and plant-derived materials. Additional features below 1350 cm^{-1}, such as C–O–C, C–OH, and C–H bending vibrations, further supported the presence of alcohols, ethers, and substituted aromatic compounds, in agreement with studies on Brazilian and UK propolis (Oliveira et al., 2016).

The spectrum of exine microcapsules loaded with red (SRP) and brown (SBP) propolis preserved key bands from both the propolis and the exine matrix, confirming the successful loading of bioactive constituents into the microcapsule matrix. Strong O–H stretching, as in the raw extracts, was observed between 3500–3200 cm^{-1}, while C–H asymmetric and symmetric stretching remained evident between 2935 and 2845 cm^{-1}. Notably, increased absorption in the region between 1298 and 1025 cm^{-1}, including contributions from aromatic ether linkages and tertiary alcohols, suggested potential hydrogen bonding or physical interactions between the exine structure and propolis components. These interactions may have contributed to the chemical stabilization of the encapsulated extracts. As in the extracts, C=O signal was detected

at 1675 cm^{-1}. The spectrum also revealed C=C stretching at 1618 - 1509 cm^{-1} and well-defined C–O vibrations between 1298 and 1025 cm^{-1}, along with aromatic C–H out-of-plane bending at 970–670 cm^{-1}. Additionally, for both samples, it showed C–H stretching bands 1440 – 1368 cm^{-1} and for SRP the spectrum reveled C–OH bending peaks at 1156 cm^{-1}. The absence of bands typically associated with carboxylate groups COO^- at ~1595 and 1406 cm^{-1} in both SRP and SBP spectra confirms that these functionalities were not prominent in the microcapsule formulations.

The RP and BP films, obtained by incorporating the respective extracts into the alginate matrix, maintained the fundamental spectral features of polyphenolic extracts while suggested interaction with polymeric network. O-H stretching vibrations were attributed to a broad absorption band between 3500-3200 cm^{-1} which indicates the presence of hydroxyl groups and hydrogen bonding. As found in the extracts, their films maintained C-H stretching from aliphatic chains (2935-2845 cm^{-1}), strong C=O bands from esters or carboxylic acids (1705 cm^{-1}), C=C vibrations that indicates aromatic or phenolic structures between 1630 and 1507 cm^{-1}. Additionally, peaks related to the fingerprint region (~1500-800 cm^{-1}) confirmed the presence of alcohol and ether groups (C-H bending and C-O stretching) as it also showed out-of-plane C-H bending consistent with para-substituted aromatic rings, commonly found in flavonoids. Subtle changes in band intensity and width suggests intermolecular interaction between the alginate chains and phenolic compounds, particularly in the hydroxyl and carbonyl regions.

The films containing microcapsules loaded with red and brown propolis (SRP film and SBP film) revealed complex vibrational profiles, combining signals from alginate, exine structure, and the incorporated extracts. It showed important spectral modifications on new or shifted bands which indicated significant molecular interactions. In these samples, the O–H and C–H stretching regions were consistent with the other materials (3500-2845 cm^{-1}). In the SRP film, a strong absorption band at 1595 cm^{-1} was attributed to the asymmetric stretching of carboxylate groups (COO^-), while a second band at 1406 cm^{-1} confirmed the corresponding symmetric COO^- stretching, suggesting the presence of deprotonated carboxylic acids, likely originating from the interaction between the red propolis and the alginate. Additional bands at 1298, 1082, and 1025 cm^{-1} were assigned to C–O stretching vibrations from ethers, tertiary alcohols, or aromatic linkages. The fingerprint region included prominent peaks between 889 and 800 cm^{-1}, attributed to C–H out-of-plane deformations of aromatic rings, particularly para-substituted structures, which are common in flavonoid-rich propolis extracts. A further low-intensity band at 618 cm^{-1} was associated with out-of-plane bending of aromatic or halogenated structures, though the latter is unlikely to be predominant. The SBP film exhibited a highly similar spectral profile. The band at 1597 cm^{-1} was also assigned to the asymmetric stretching

of COO^{-}, with a corresponding symmetric stretch at 1406 cm^{-1}, confirming the presence of carboxylate groups in this formulation as well. Other relevant peaks included 1338 cm^{-1}, associated with C–O–H bending of phenols or alcohols, and 1298, 1080, and 1025 cm^{-1}, corresponding to C–O stretching vibrations. The fingerprint region showed a clear C–H out-of-plane deformation band between 860–800 cm^{-1}, characteristic of para-substituted aromatic rings, reinforcing the structural similarity between the two films and confirming the preservation of the phenolic structures from brown propolis.

In summary, the FTIR results demonstrate the successful incorporation of both brown and red propolis extracts into alginate-based matrices and microcapsules, indicating that the encapsulated propolis compounds remained chemically stable within the film matrices. It also reveals the emergence or enhancement of specific bands, particularly, for SRPF and SBPF in the COO^{-} and C–O regions where new spectral patterns con be observed reflecting new intermolecular interactions between propolis constituents, alginate and the biocapsules. The spectral features observed are in good agreement with previous studies involving propolis extracts, polysaccharides, and phenolic compound identification by FTIR (Oliveira et al., 2016; Cebi et al., 2020; Erdoğan, 2023; Soliman et al., 2023; Nandiyanto, Oktiani & Ragadhita, 2019; Lawrie et al., 2007). These findings confirm the compatibility between the bioactive extracts and the delivery system and support the effectiveness of the encapsulation and film-forming processes.

5.5.2. TGA

Thermogravimetric analysis (TGA) was performed to evaluate the thermal stability and decomposition behavior of the isolated and combined components of the film formulations. The TGA curves, which show weight loss (%) as a function of temperature (°C), are presented in Figure 35.

The sporopollenin exine capsules (SEC) exhibited the highest thermal stability, with a gradual weight loss and significant residual mass beyond 500 °C, consistent with their known high carbon content and robust aromatic structure. The weight loss initiated around 200 °C until nearly 500 °C, demonstrating the material's resistance to thermal degradation, which is attributed to the complex, crosslinked nature of sporopollenin biopolymers (Bernard et al., 2015).

The alginate sample revealed a typical two-step degradation behavior. The first event occurred below 150 °C, associated with the evaporation of bound water. The second, more significant mass loss took place between 200–300 °C, corresponding to the breakdown of the polysaccharide backbone and depolymerization of alginate chains. This behavior was mirrored by the control film (CF).

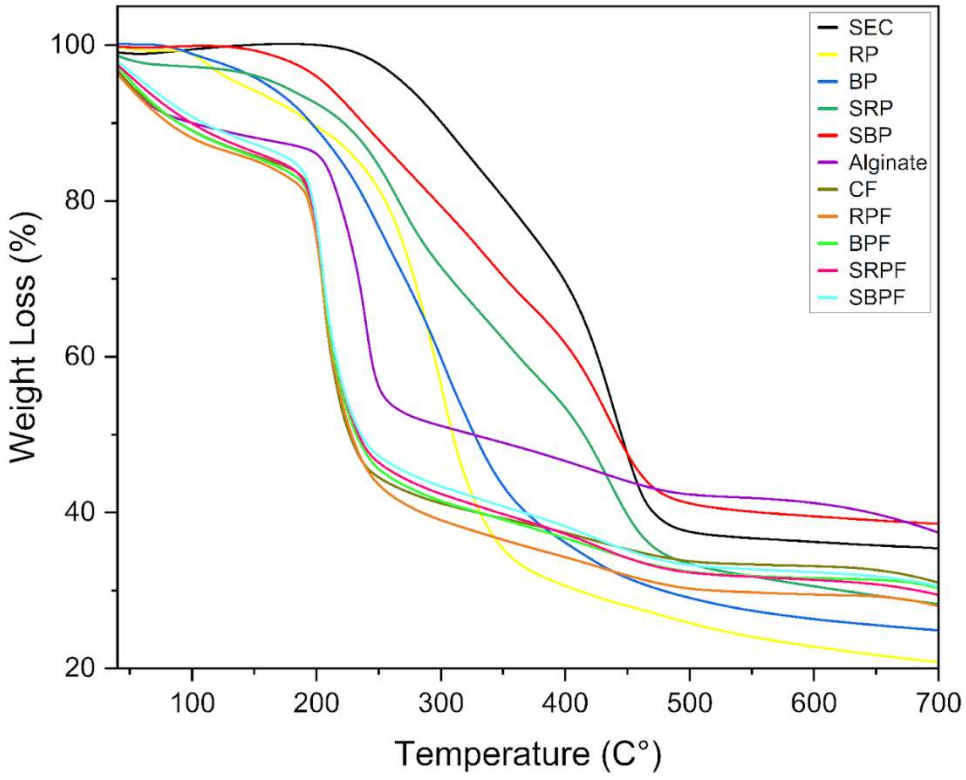

Figure 35 *– Graph showing TGA results for all samples involving the dressing production*

The red and brown propolis extracts samples presented lower thermal stability compared to SEC and alginate. Initial degradation started earlier, around 150–200 °C, with rapid weight loss occurring up to 400 °C. This behavior is characteristic of phenolic and flavonoid-rich materials, which tend to degrade at relatively lower temperatures due to their volatile and thermolabile constituents (Silva et al., 2020). Notably, RP and BP left minimal residual mass, indicating near-complete thermal decomposition.

Loaded sporopollenin capsules (SRP and SBP) demonstrated improved thermal stability compared to the pure extracts. Their weight loss curves showed a delayed beginning and broader degradation profiles. This suggests that encapsulation protected propolis compounds. The SBP sample retained more mass at higher temperatures than the SRP, indicating a potentially more stable encapsulation system for brown propolis.

The films incorporating propolis (RPF and BPF) showed multistep degradation profiles, combining characteristics of both alginate and their respective propolis extract. The initial loss of mass occurred around 100–150 °C (moisture), followed by more substantial weight losses between 200–350 °C and again between 400–500 °C. These steps reflect the simultaneous degradation of the alginate network and propolis components. BPF exhibited slightly enhanced thermal resistance over RPF, possibly because of their different phenolic composition and interactions with the alginate film.

Finally, the films containing encapsulated propolis (SRPF and SBPF) presented the most complex degradation curves. These profiles included the typical polysaccharide moisture loss, followed by two distinct degradation phases. The first, between 200–350 °C, was associated with the degradation of both the alginate matrix and free propolis fractions. The second, extending from 350 °C to over 500 °C, is attributed to the stability of SECs. The thermal behavior of SBPF showed better retention of mass at elevated temperatures compared to SRPF, reinforcing the observation that brown propolis maintains higher thermal integrity within the biocapsules.

In summary, the TGA results confirm that sporopollenin microcapsules significantly enhance the thermal stability of propolis, and their integration into alginate-based films provides an improved heat resistance.

5.5.3. Biodegradability on different pHs and Control release

To evaluate the pH-sensitivity and biodegradability of the films, all formulations (RPF, BPF, SRPF, SBPF, and CF) were immersed in buffer solutions at pH 5, 6, and 7, and their complete degradation time (min) was recorded. This test simulates different physiological and pathological environments, as wound exudates or tissue fluids may vary in acidity depending on the inflammatory or healing phase. The results are shown in Figures 36.

Across all formulations, a clear pH-dependent degradation profile was observed. In general, the degradation time decreased as the pH increased, indicating that the films degrade more rapidly under neutral conditions and more slowly in acidic environments. This behavior reflects the sensitivity of the alginate matrix to the ionic environment and may be associated with protonation of carboxyl groups and reduced solubility at lower pH values.

For instance, the SRPF film exhibited the longest degradation time at pH 5 (~220 min) and the shortest at pH 7 (~100 min). A similar pattern was observed in the RPF and BPF films, with degradation times dropping from approximately 210–220 min at pH 5 to ~100 min at pH 7. The SBPF also followed this trend, with slightly lower degradation times overall but a

consistent decline from acidic to neutral conditions. The control film (CF) presented the most rapid degradation, especially at pH 7, suggesting that the presence of propolis and/or microcapsules contributes to improved film stability.

The statistical significance of the differences between degradation times at different pH levels was assessed, suggesting that the observed variations were highly significant (Figure 36).

These findings demonstrate that the films presents pH-responsive degradation behavior, which may be advantageous for biomedical applications such as wound dressings for drug delivery systems. In particular, their longer persistence under lower acidic conditions (pH 5–6), which are often found in wounded tissues, may help prolong bioactive release and improve therapeutic efficacy before natural degradation occurs (Huang et al., 2024; Moreno-Rivas et al., 2024).

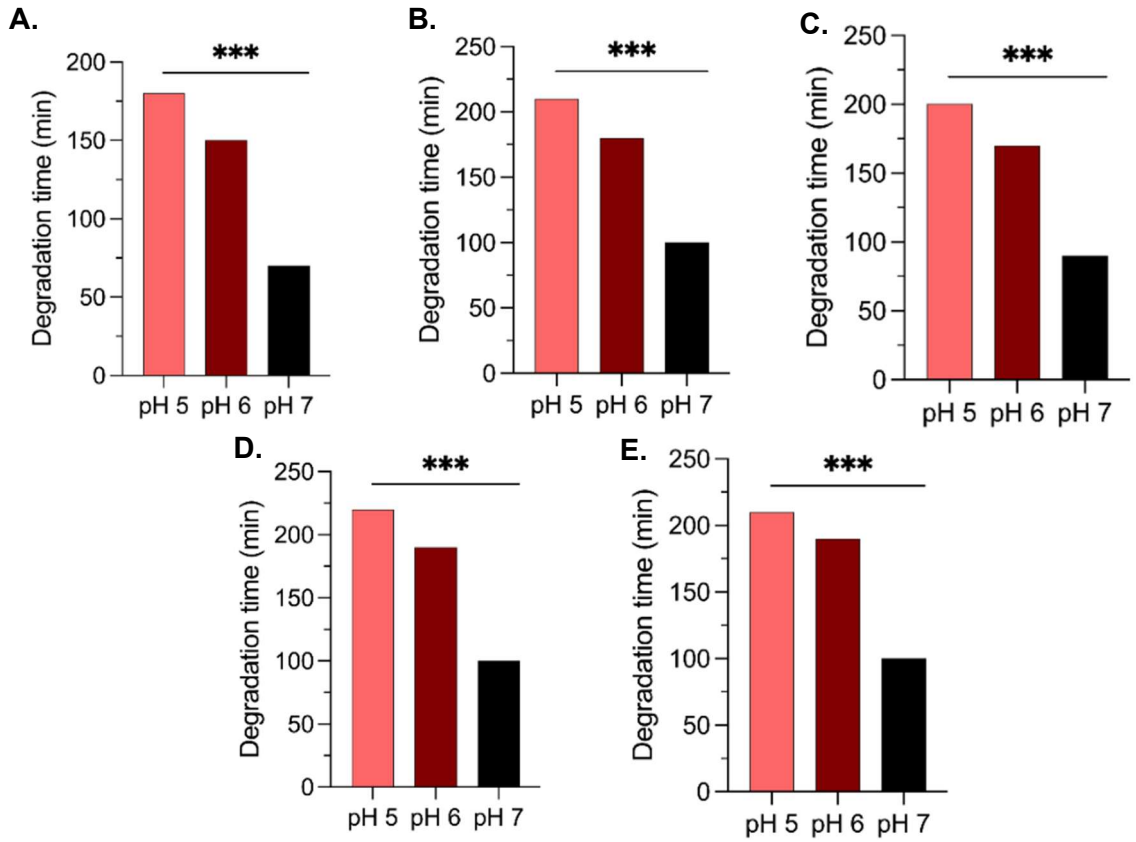

Figure 36 *– pH degradation time for each film composition. A. CF. B. RPF. C. BPF. D. SRPF and E. SBPRF. *** indicates p < 0.001*

The release kinetics differed significantly among the four formulations of films containing either propolis extracts or loaded SECs (Figure 37). The profile of bioactive phenolic compounds from the prepared films was evaluated under aqueous conditions using phosphate-buffered saline (PBS) solution (pH 6.8). PBS contains sodium (Na^+), potassium (K^+), chloride (Cl^-), and phosphate ions in concentrations that mimic those found in bodily

fluids. Being isotonic and non-toxic, PBS does not damage cells or interfere with native molecular interactions, making it highly suitable for studies aiming to simulate conditions on wounded skin or within moist tissue environments (Martin et al., 2006).

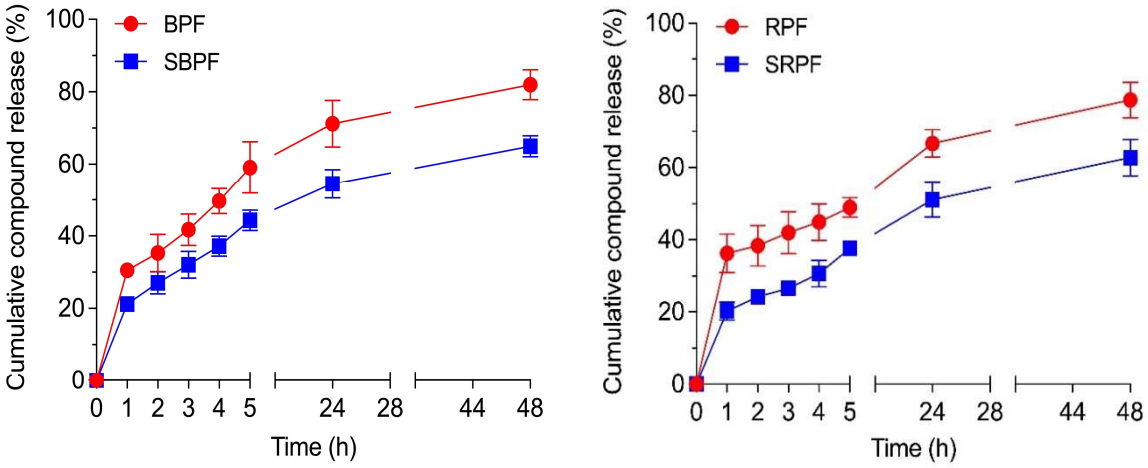

***Figure 37** – **A.** Cumulative compound release (%) for BPF and SBPF. **B.** Cumulative compound release (%) for RPF and SRPF. Results are expressed in mean value with standard deviation and analysis were made in duplicate*

In this context, the immersion of films in PBS not only provided insight into their compound release behavior but also served as a basis for evaluating their biodegradability and potential in vivo performance. This is especially relevant for biodegradable wound dressings, which are expected to degrade naturally without causing additional trauma, thereby supporting the healing process. Monitoring compound release in PBS over time helps determine the functional lifespan of the films and their ability to maintain controlled delivery.

The release kinetics differed significantly among the four formulations. Films containing non-encapsulated propolis (RPF and BPF) exhibited faster and more pronounced release profiles when compared to the microcapsule-loaded counterparts (SRPF and SBPF). After 48 h, the cumulative release from RPF reached approximately 78.77%, while BPF reached 81.97%. In contrast, the SRPF and SBPF films showed slower and more sustained release, achieving 62.77% and 65.02%, respectively. This difference can be attributed to the presence of sporopollenin microcapsules, which form a more compact barrier, limiting the immediate diffusion of phenolic compounds and promoting a more controlled release.

These findings are consistent with studies reporting that micro structured carriers like sporopollenin can modulate drug diffusion by acting as a porous and chemically interactive matrix (Aylanc et al., 2025). The encapsulated systems (SRPF and SBPF) presented a typical diffusion-limited profile, which aligns with release models such as Higuchi or Korsmeyer–

Peppas. Although not fitted here, such models are valuable tools to further interpret the release mechanism and should be explored in future studies (Bańkosz, (2024).

The slower release observed in SRPF and SBPF highlights the protective effect of the encapsulation strategy, which can be advantageous in biomedical applications where prolonged antioxidant delivery is desired. Furthermore, the higher release rates of films containing brown propolis on their formulation compared to the films with red propolis, corresponds to previous analysis of this study such as TPC as it confirms the higher amount of phenolic compounds in brown propolis. That explain the higher percentage of compound release over time for brown propolis.

5.6. Biological properties of films

5.6.1. Antioxidant assays

The antioxidant activity of the developed formulations was evaluated using the DPPH radical scavenging assay, a widely employed method for assessing the free radical neutralization potential of bioactive compounds. The results, expressed as percentage of DPPH inhibition, are presented in Figure 38.

The control film (CF), composed solely of the alginate matrix without the incorporation of active substances, exhibited minimal antioxidant activity, with a mean inhibition value of 9.32% (± 4.31), as expected for a polysaccharide-based film lacking phenolic constituents.

In contrast, films containing pure propolis extracts demonstrated significantly higher radical scavenging activity. The BPF (Brown Propolis Film) presented the highest inhibition rate, reaching 85.42% (± 4.89), followed by the RPF (Red Propolis Film) with 58.15% (± 4.53). These results are in line with literature reports and previous analysis indicating that brown propolis contains higher concentrations of flavonoids and phenolic acids, which are potent radical scavengers (Çelekli, Akhras & Bozkurt, 2024).

The incorporation of propolis into exine microcapsule films also preserved strong antioxidant activity. The SBPF showed 78.58% (± 6.61) inhibition, while the SRPF (Red Propolis Microcapsule Film) reached 76.63% (± 4.81). The release kinetics indicated a trend toward more sustained delivery in SBPF samples compared to BPF, which may reflect the encapsulation's role in protecting and gradually releasing bioactive compounds, although further studies are required to confirm this statistically as in the DPPH analysis no statistically significant difference was found. In the case of SRPF, the higher inhibition percentage observed may be attributed to the experimental sequence. Since the SRPF sample was analyzed

after the RPF, it remained in contact with the DPPH solution for a longer period, potentially allowing more time for the antioxidant compounds to interact the free radicals. This extended exposure time could have contributed to the increased radical scavenging activity recorded.

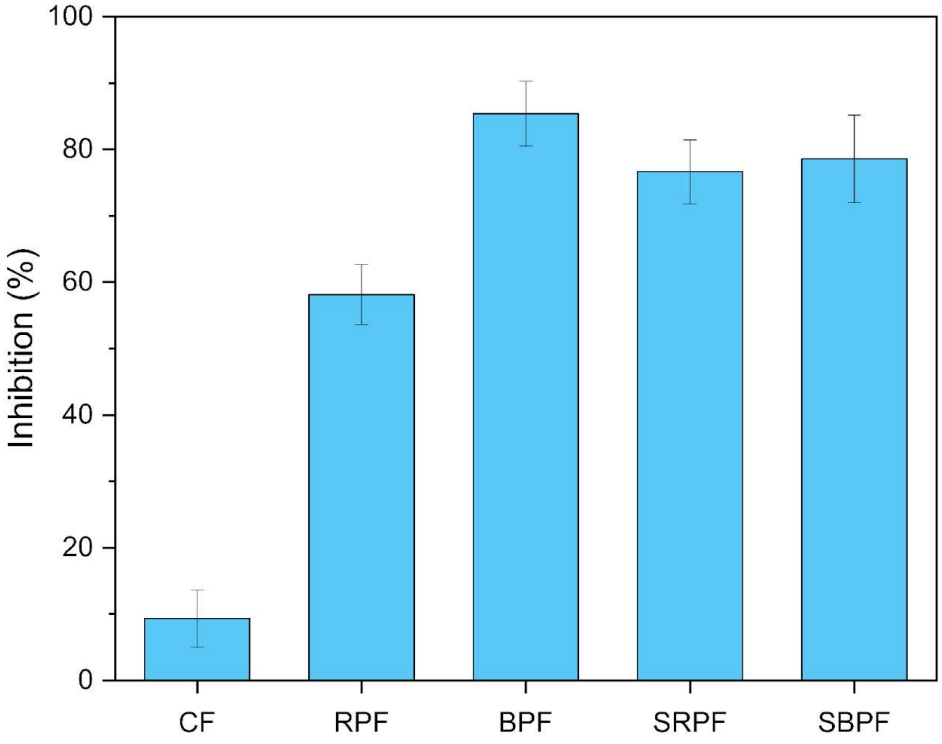

Figure 38 *– DPPH scavenging assay results expressed with its standard deviation. Measurements were taken in triplicate for each sample*

The antioxidant capacity of the samples was further assessed using the ABTS radical cation ($ABTS^{+}$ •) scavenging assay. This method complements DPPH analysis by allowing the evaluation of both lipophilic and hydrophilic antioxidants in a larger polarity range. The results, expressed as the percentage of ABTS inhibition, are shown in Figure 39 and reflect the average values obtained from triplicate measurements.

As expected, the control films (CF) exhibited negligible antioxidant activity, with mean inhibition values consistently around 9.36% (± 2.93), confirming the absence of antioxidant compounds. These values are aligned with the results observed in the DPPH assay and serve as a baseline for comparison.

The pure red and brown propolis extracts demonstrated exceptionally high ABTS radical scavenging capacity. RPF samples showed values ranging from 95.01% to 96.52%, while brown propolis ranged between 94.98% and 96.82%, with minimal standard deviation. These results confirm the antioxidant richness of propolis, as a result of its content of flavonoids and phenolic acids with high electron-donating potential (Kurek-Górecka et al., 2013). The

slightly higher inhibition observed for brown propolis supports previously reported leading to the assurance of a more diverse or potent polyphenolic profile.

For the films containing exine microcapsules loaded with propolis (SRPF and SBPF), the results reflects a complex perspective. The SBPF samples maintained high antioxidant activity, with inhibition value of 92.67% (± 1.81). This suggests excellent retention of antioxidant compounds after encapsulated, and strong compatibility with the exine structure.

In contrast, the SRPF presented significantly lower activity, with a mean of 59.71% (± 14.75). This discrepancy in standard deviation may be attributed to the experimental timeline, possibly facing partial oxidation or loss of activity prior to measurement. Another potential explanation lies in encapsulation efficiency or interactions between specific red propolis compounds and the exine wall, which may have restricted the release in the ABTS system.

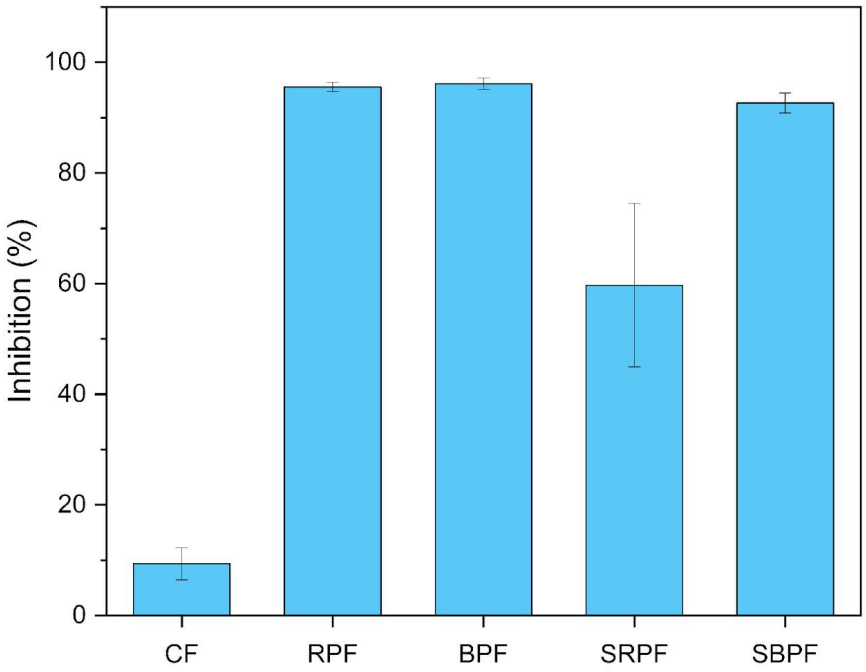

Figure 39 *– ($ABTS^{+}$ •) scavenging assay results*

5.6.2. Cytocompatibility

The cytocompatibility of the films was assessed using human epidermal keratinocyte (HaCaT) and human foreskin fibroblast (HFF-1). The metabolic activity of both cell lines after 1, 3, and 3 days of culture in the presence or absence of the films is presented in Figure 40.

In the control condition (CTL), both keratinocytes and fibroblasts showed an increase in metabolic activity over time, indicating continuous cell proliferation. Film A (CF) was shown to be cytocompatible with keratinocyte and fibroblast over 3 days of culture. Moreover, it promoted cell proliferation, as evidenced by a higher metabolic activity compared to the

control. In contrast, films B (RPF), C (BPF), D (SRPF), and E (SBPF) showed marked cytotoxicity, particularly, film B which was initially considered cytocompatible. In keratinocytes, a reduction of approximately 40% in metabolic activity was observed on day 1 compared to the control, although the difference was not statistically significant. By day 2, metabolic activity remained lower and became statistically different from the control, with a drastically decline by day 3, confirming its cytotoxic effect. In contrast, fibroblasts maintained metabolic activity levels similar to the control on day 1, indicating short-term cytocompatibility. However, no increase was observed on day 2, suggesting an absence of proliferation. By day 3, metabolic activity had decreased by approximately 80%. These findings demonstrate that film B is cytotoxic to both cell types.

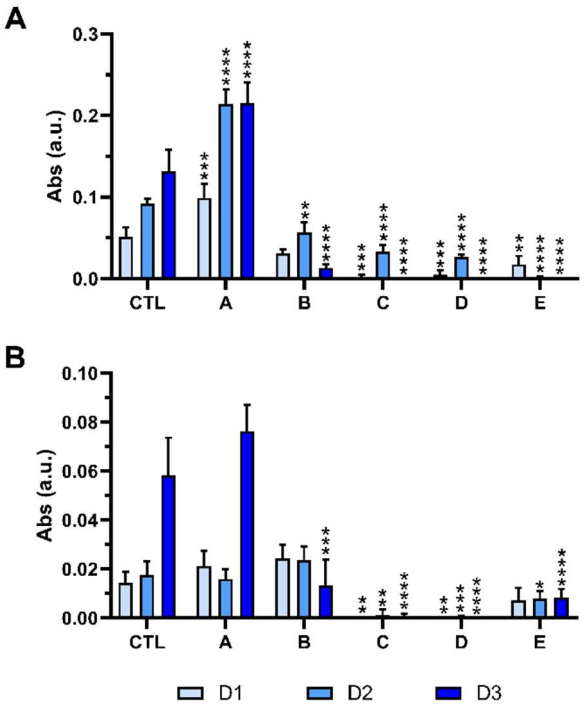

Figure 40 *- Metabolic activity of human keratinocytes (**A**) and fibroblasts (**B**) cultured in the presence of different Films over 3 days. Statistically significant differences are ** ($p < 0.01$), *** ($p < 0.001$), and **** ($p < 0.0001$) in comparison to the negative co*

Representative optical images of cell morphology are shown in Figure 41. Keratinocytes and fibroblasts cultured under CTL conditions exhibited their characteristic morphologies. Keratinocytes displayed a typical polygonal shape, while fibroblasts maintained an elongated, spindle-like appearance. Cells cultured in the presence of Film A preserved morphology and confluence comparable to the control, indicating its cytocompatibility. In contrast, exposure to films B, C, D, and E led to evident morphological alterations, loss of cell

integrity, and a marked reduction in cell density. These observations support the conclusion that films B through E negatively affected cell viability and adherence.

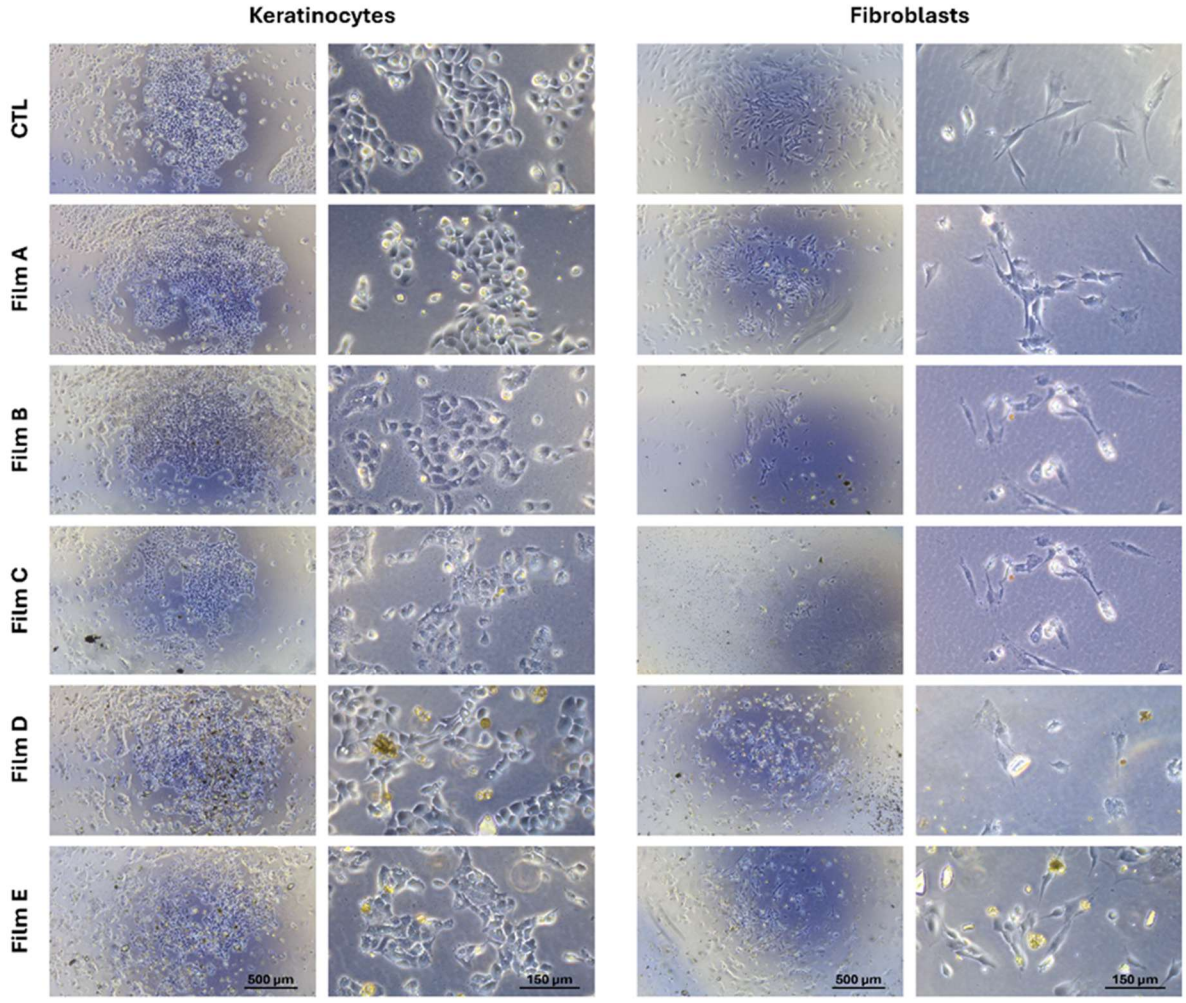

Figure 41 *- Optical images of keratinocytes (left) and fibroblasts (right) cultured in the presence of Films for 1 day.*

To assess whether cell density influenced the observed cytotoxicity, HaCaT cells were seeded at 25000, 50000, and 75000 cells/well (Figure 42). As expected, the absorbance values of the CTL condition increased proportionally with cell density. Film A maintained cytocompatibility across all tested densities, as previously observed. In contrast, films B, C, D, and E consistently exhibited cytotoxic effects, regardless of the initial seeding density, indicating that increasing the number of cells did not mitigate their toxic impact. These results

confirm that the toxicity observed with films B–E is independent of cell density in HaCaT cultures.

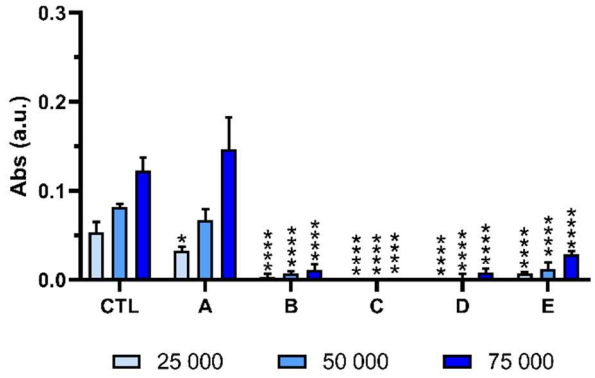

Figure 42 *- Metabolic activity of human keratinocytes at different cell densities cultured in the presence of different Films for 1 day. Statistically significant differences are * ($p < 0.05$) and **** ($p < 0.0001$) in comparison to the negative control for each di*

The variations observed in metabolic activity may be attributed to differences in film dimensions. Although the intended size was 10 × 10 mm, some films were either larger or smaller, leading to variable amounts of material per well. This inconsistency may have influenced the cellular response, as differences in sample quantity among triplicates could impact the observed cytotoxic or cytocompatible effects.

6. CONCLUSIONS AND FUTURE PERSPECTIVES

This study successfully demonstrated effectiveness of using sporopollenin exine capsules (SECs) as a natural micro-carrier system for red and brown propolis extracts, incorporated into alginate-based dressings. The characterization assays, including FTIR, SEM, TGA, UV-Vis, antioxidant assays (DPPH and ABTS), and LC/DAD/ESI-MS^n, enabled a detailed examination of the physicochemical, thermal, morphological, and functional properties of the developed materials.

FTIR analysis confirmed successful interactions between the bioactive compounds and the alginate dressings, while SEM images revealed notable morphological differences, particularly the partial incorporation of SECs and propolis on film surfaces. The TGA results highlighted improved thermal stability in samples containing sporopollenin and/or propolis extracts, especially the SBPF and SRPF films. The UV-Vis light transmittance data suggested reduced UV penetration in films with encapsulated extracts, indicating a potential protective function.

Antioxidant activity analyses showed that all propolis-containing formulations exhibited radical scavenging capacity, with SRPF and SBPF showing better results at this property, likely because of the protective effect of sporopollenin. Moreover, LC/DAD/ESI-MS^n allowed the identification of 35 compounds in BP and 17 in RP, with clear chemical distinctions between flavonoid-rich brown propolis and isoflavonoid-rich red propolis, reinforcing their unique biological signatures. Finally, the films exhibited high flexibility, excellent transparency, and the ability to modulate the drug release profile.

In summary, the results validate the proposed encapsulation strategy as a promising approach for preserving and delivering natural bioactives during the wound healing process. The combination of sporopollenin, propolis, and alginate provides a biodegradable and thermally stable platform with vast potential for pharmaceutical and biomedical applications.

Several future directions are proposed to deepen the understanding and expand the applicability of the developed alginate-based sporopollenin propolis encapsulation dressings. Firstly, a preliminary screening of concentrations is suggested to identify the maximum non-toxic level, which should then be used for the new preparation of films. Antimicrobial activity and inhibition should also be performed.

Long-term stability studies, particularly under varying environmental conditions (humidity, light, temperature), would help determine the shelf life and protective efficacy of the encapsulating and release system over time. Additionally, exploring other natural polymers such as chitosan to obtain a matrix of alginate-chitosan films may enhance the mechanical, barrier, and biodegradability properties of the films.

Chitosan, a biopolymer derived from chitin, has gained attention for its excellent film-forming ability, mucoadhesive properties, and capacity to enhance drug permeation through the skin. A study by Kim et al. (2013) demonstrated that chitosan-based transdermal films loaded with anti-inflammatory drugs showed superior drug retention and sustained release compared to conventional systems. Additionally, chitosan nanoparticles have been used to encapsulate a variety of active compounds, providing targeted delivery and reduced systemic side effects.

In vivo studies should be conducted to evaluate the bioavailability, absorption, and therapeutic effects of the encapsulated propolis extracts in biological models. These analysis would be crucial to confirm the antioxidant and anti-inflammatory potential of red and brown propolis, beyond in vitro assays.

Finally, efforts toward scale-up production, cost-effectiveness analysis, and application testing would be important steps toward industrial and commercial implementation of these sustainable, bioactive delivery systems for wound healing.

8. REFERENCES

Adepu, S., & Ramakrishna, S. (2021). Controlled drug delivery systems: current status and future directions. *Molecules*, *26*(19), 5905. https://doi.org/10.3390/molecules26195905

Agudo, J. E., Pardo, P. J., Sánchez, H., Pérez, Á. L., & Suero, M. I. (2014). A low-cost real color picker based on arduino. *Sensors*, *14*(7), 11943-11956. https://doi.org/10.3390/s140711943

Ahn, M., Cho, W. W., Park, W., Lee, J. S., Choi, M. J., Gao, Q., ... & Kim, B. S. (2023). 3D biofabrication of diseased human skin models in vitro. *Biomaterials Research*, *27*(1), 80. https://doi.org/10.1186/s40824-023-00415-5

Altuntaş, Ü., Güzel, İ., & Özçelik, B. (2023). Phenolic constituents, antioxidant and antimicrobial activity and clustering analysis of propolis samples based on PCA from different regions of Anatolia. *Molecules*, *28*(3), 1121. https://doi.org/10.3390/molecules28031121

Arda, O., Göksügür, N., & Tüzün, Y. (2014). Basic histological structure and functions of facial skin. *Clinics in Dermatology, 32*(1), 3-13. https://doi.org/10.1016/j.clindermatol.2013.05.021

Atalay, F. E., Culum, A. A., Kaya, H., Gokturk, G., & Yigit, E. (2022). Different plant sporopollenin exine capsules and their multifunctional usage. *ACS Applied Bio Materials*, *5*(3), 1348-1360. https://doi.org/10.1021/acsabm.2c00071

Aylanc, V., Ertosun, S., Akyuz, L., Bilican, B. K., Gokdag, S., Bilican, I., ... & Kaya, M. (2020). Natural β-chitin-protein complex film obtained from waste razor shells for transdermal capsaicin carrier. *International Journal of Biological Macromolecules*, *155*, 508-515. https://doi.org/10.1016/j.ijbiomac.2020.03.232

Aylanc, V., Ertosun, S., Peixoto, A. F., Santamaria-Echart, A., Russo-Almeida, P., Vale, N., ... & Vilas-Boas, M. (2025). Development of natural sporopollenin microcapsules: from bee pollen to versatile biomaterials. *Emergent Materials*, 1-16. https://doi.org/10.1007/s42247-025-01002-1

Aylanc, V., Ertosun, S., Russo-Almeida, P., Falcão, S. I., & Vilas-Boas, M. (2022). Performance of green and conventional techniques for the optimal extraction of bioactive compounds in bee pollen. *International Journal of Food Science and Technology*, *57*(6), 3490-3502. https://doi.org/10.1111/ijfs.15672

Aylanc, V., Peixoto, A. F., Vale, N., Freire, C., & Vilas-Boas, M. (2023). Sporopollenin-based bio-microcapsules as green carriers for controlled delivery of pharmaceutical drugs. *Applied Materials Today*, *33*, 101860. https://doi.org/10.1016/j.apmt.2023.101860

Bańkosz, M. (2024). Physicochemical Characterization and Kinetics Study of Polymer Carriers with Vitamin C for Controlled Release Applications. *Materials*, *17*(22), 5502. https://doi.org/10.3390/ma17225502

Bankova, V. S., de Castro, S. L., & Marcucci, M. C. (2000). Propolis: recent advances in chemistry and plant origin. *Apidologie*, *31*(1), 3-15. https://doi.org/10.1051/apido:2000102

Bankova, V. (2005). Chemical diversity of propolis and the problem of standardization. *Journal of ethnopharmacology*, *100*(1-2), 114-117. https://doi.org/10.1016/j.jep.2005.05.004

Banskota, A. H., Tezuka, Y., Prasain, J. K., Matsushige, K., Saiki, I., & Kadota, S. (1998). Chemical constituents of Brazilian propolis and their cytotoxic activities. *Journal of Natural Products*, *61*(7), 896-900. https://doi.org/10.1021/np980028c

Barreto, K. S., Rossi, D., Silva, L. M. G., Veiga, M. I. R. S., Biondo, E. G., Figueiredo, H. Z., Santos, N. de A. R. dos, Castro, G. de, Rodrigues, E. C. G., Carvalho, M. G. P. de, Pedroso, G. G. C., Morelli, J. G., & Dutra, J. M. (2024). CIRURGIA SEM ANTIBIÓTICOS: UM FUTURO POSSÍVEL OU IMPRUDENTE?. *Brazilian Journal of Implantology and Health Sciences*, *6*(10), 1295–1308. https://doi.org/10.36557/2674-8169.2024v6n10p1295-1308

Bechgaard, H., & Nielsen, L. S. (2000). Subcutaneous versus intramuscular injection: A review of the absorption differences. *European Journal of Clinical Pharmacology, 56*(6), 507-510. https://doi.org/10.1007/s002280000178

Bell, V. (2014). *Introdução dos antibióticos em Portugal: ciência, técnica e sociedade (anos 40 a 60 do século XX). Estudo de caso da penicilina* (Doctoral dissertation, Universidade de Coimbra (Portugal)). https://hdl.handle.net/10316/27045

Bernard, S., Benzerara, K., Beyssac, O., Balan, E., & Brown Jr, G. E. (2015). Evolution of the macromolecular structure of sporopollenin during thermal degradation. *Heliyon*, *1*(2). https://doi.org/10.1016/j.heliyon.2015.e00034

Berner, B., & John, V. A. (1994). Pharmacokinetic characterisation of transdermal delivery systems. *Clinical pharmacokinetics*, *26*, 121-134. https://doi.org/10.2165/00003088-199426020-00005

Boateng, J. S., Matthews, K. H., Stevens, H. N., & Eccleston, G. M. (2008). Wound healing dressings and drug delivery systems: a review. *Journal of pharmaceutical sciences*, *97*(8), 2892-2923. https://doi.org/10.1002/jps.21210

Bolognia, J. L. (1995). Aging skin. *The American Journal of Medicine, 98*(1), S99-S103. https://doi.org/10.1016/S0002-9343(99)80066-7

Bowler, P. G., & Davies, B. J. (1999). The microbiology of infected and noninfected leg ulcers. *International Journal of Dermatology, 38*(8), 573-578. https://doi.org/10.1046/j.1365-4362.1999.00738.x

Brasil. Ministério da Agricultura, Pecuária e Abastecimento. (2001). Instrução Normativa nº 3, de 19 de janeiro de 2001: Regulamento técnico para fixação de identidade e qualidade de apitoxina. *Diário Oficial da República Federativa do Brasil*, seção 1, p. 16. https://www.gov.br/agricultura/pt-br/assuntos/inspecao/produtos-animal/empresario/InstruoNormativa_05.2017.pdf?utm_source=chatgpt.com

Camelo-Nunes, I. C., Wandalsen, G. F., Melo, K. C., Naspitz, C. K., & Solé, D. (2004). Prevalência de eczema atópico e sintomas relacionados entre estudantes. *Jornal de Pediatria*, *80*, 60-64.https://doi.org/10.2223/JPED.1135

Cao, R. Z., Zhang, Z. Y., Jiao, J., Gai, Q. Y., Liu, Y., Wang, Y., ... & Fu, Y. J. (2024). A novel surface molecularly imprinted polymer based on the natural biological macromolecule sporopollenin for the specific and efficient adsorption of resveratrol from Polygonum cuspidatum extracts. *International Journal of Biological Macromolecules, 280*, 136168. https://doi.org/10.1016/j.ijbiomac.2024.136168

Cebi, N., Bozkurt, F., Yilmaz, M. T., & Sagdic, O. (2020). An evaluation of FTIR spectroscopy for prediction of royal jelly content in hive products. *Journal of Apicultural Research, 59*(2), 146-155. https://doi.org/10.1080/00218839.2019.1707009

Çelekli, A., Akhras, N., & Bozkurt, H. (2024). Improving antimicrobial activity of brown propolis with incorporation of Arthrospira platensis. *Food and Humanity, 2*, 100191. https://doi.org/10.1016/j.foohum.2023.11.018

Chen, L.-R., Ko, N.-Y., & Chen, K.-H. (2019). Isoflavone supplements for menopausal women: A systematic review. *Nutrients, 11*(11), 2649. https://doi.org/10.3390/nu11112649

Chen, W., Yung, B. C., Qian, Z., & Chen, X. (2018). Improving long-term subcutaneous drug delivery by regulating material-bioenvironment interaction. *Advanced Drug Delivery Reviews, 127*, 20-34. https://doi.org/10.1016/j.addr.2018.01.016

Chen, X., Yu, H., Wang, L., Shen, D., Wang, Y., & Hong, Y. (2023). Glucose-Responsive Microneedle Patch With Variable Crosslinking Density and Flexible Core–Shell Structure for Insulin Delivery. *Advanced Materials Technologies*, *8*(13), 2202124. https://doi.org/10.1002/admt.202202124

Conceição, M., Beserra, F. P., Mejia, J. A. A., Caldas, G. R., Tanimoto, M. H., Luzenti, A. M., ... & Pellizzon, C. H. (2023). Guttiferones: an insight into occurrence, biosynthesis, and their broad spectrum of pharmacological activities. *Chemico-Biological Interactions*, *370*, 110313. https://doi.org/10.1016/j.cbi.2022.110313

Craythorne, E., & Al-Niami, F. (2017). Skin cancer. *Medicine, 45*(7), 431-434. https://doi.org/10.1016/j.mpmed.2017.04.003

da Rosa, C., Bueno, I. L., Quaresma, A. C. M., & Longato, G. B. (2022). Healing potential of propolis in skin wounds evidenced by clinical studies. *Pharmaceuticals*, *15*(9), 1143. https://doi.org/10.3390/ph15091143

de Ávila Reis, N., Filh, C. D. A. S. M., & Timoner, F. R. (2010). Profilaxia em cirurgia dermatológica. *Surgical & Cosmetic Dermatology*, *2*(1), 47-53. https://www.redalyc.org/pdf/2655/265521086010.pdf

Diego-Taboada, A., Beckett, S. T., Atkin, S. L., & Mackenzie, G. (2014). Hollow pollen shells to enhance drug delivery. *Pharmaceutics, 6*(1), 80-96. https://doi.org/10.3390/pharmaceutics6010080

Dornelas-Figueira, L. M., Ricomini Filho, A. P., Junges, R., Åmdal, H. A., Cury, A. A. D. B., & Petersen, F. C. (2023). In Vitro Impact of Fluconazole on Oral Microbial Communities, Bacterial Growth, and Biofilm Formation. *Antibiotics*, *12*(9), 1433. https://doi.org/10.3390/antibiotics12091433

Erdoğan, Ü. (2023). Ultrasonic assisted propolis extraction: characterization by ATR-FTIR and determination of its total antioxidant capacity and radical scavenging ability. *International Journal of Secondary Metabolite, 10*(2), 231-239. https://doi.org/10.21448/ijsm.1167773

Falcão, S. I., Freire, C., & Vilas-Boas, M. (2013). A proposal for physicochemical standards and antioxidant activity of Portuguese propolis. *Journal of the American oil chemists' society, 90*(11), 1729-1741. https://doi.org/10.1007/s11746-013-2324-y

Falcão, S. I., Lopes, M., & Vilas-Boas, M. (2019). A first approach to the chemical composition and antioxidant potential of Guinea-Bissau propolis. *Natural Product Communications, 14*(5), 1934578X19844138. https://doi.org/10.1177/1934578X19844138

Falcão, S. I., Vale, N., Gomes, P., Domingues, M. R., Freire, C., Cardoso, S. M., & Vilas-Boas, M. (2013). Phenolic profiling of Portuguese propolis by LC–MS spectrometry: Uncommon propolis rich in flavonoid glycosides. *Phytochemical Analysis, 24*(4), 309-318. https://doi.org/10.1002/pca.2412

Falcão, S. I., Vale, N., Cos, P., Gomes, P., Freire, C., Maes, L., & Vilas-Boas, M. (2014). In vitro evaluation of Portuguese propolis and floral sources for antiprotozoal, antibacterial and antifungal activity. *Phytotherapy research*, *28*(3), 437-443. https://doi.org/10.1002/ptr.5013

Falcão, S. I., Vilas-Boas, M., Estevinho, L. M., Barros, C., Domingues, M. R., & Cardoso, S. M. (2010). Phenolic characterization of Northeast Portuguese propolis: usual and unusual compounds. *Analytical and bioanalytical chemistry, 396*, 887-897. https://doi.org/10.1007/s00216-009-3232-8

Fea, A. M., Vallino, V., Cossu, M., Marica, V., Novarese, C., Reibaldi, M., & Petrillo, F. (2024). Drug Delivery Systems for Glaucoma: A Narrative Review. *Pharmaceuticals, 17*(9), 1163. https://doi.org/10.3390/ph17091163

Grassi, G., Capasso, G., Gambacorta, E., & Perna, A. M. (2023). Chemical and functional characterization of propolis collected from different areas of South Italy. *Foods, 12*(18), 3481. https://doi.org/10.3390/foods12183481

Guo, S. A., & DiPietro, L. A. (2010). Factors affecting wound healing. *Journal of dental research*, *89*(3), 219-229. https://doi.org/10.1177/0022034509359125

Gupta, N. V., Sharadha, M., Sastri, K. T., Chakraborty, S., Kumar, H., Jain, V., & Dey, S. (2023). Nanoscience for drug delivery in diabetes. In A. Rastegari (Ed.), *Nanoscience Applications in Diabetes Treatment* (pp. 70-101). Bentham Science Publishers. https://doi.org/10.2174/9789815196535123010007

Heym, B., Rimareix, F., Lortat-Jacob, A., & Nicolas-Chanoine, M. H. (2004). Bacteriological investigation of infected pressure ulcers in spinal cord-injured patients and impact on antibiotic therapy. *Spinal Cord, 42*(4), 230-234. https://doi.org/10.1038/sj.sc.3101587

Hoang, H. T., Moon, J.-Y., & Lee, Y.-C. (2021). Natural antioxidants from plant extracts in skincare cosmetics: Recent applications, challenges and perspectives. *Cosmetics, 8*(4), 106. https://doi.org/10.3390/cosmetics8040106

Huang, T., Sun, Z., Heath, D. E., O'Brien-Simpson, N., & O'Connor, A. J. (2024). 3D printed and smart alginate wound dressings with pH-responsive drug and nanoparticle release. *Chemical Engineering Journal, 492*, 152117. https://doi.org/10.1016/j.cej.2024.152117

Ishikawa, T., Matsumura, T., Okimoto, K., Nagashima, A., Shiratori, W., Kaneko, T., ... & Kato, N. (2021). Efficacy of Texture and Color Enhancement Imaging in visualizing gastric mucosal atrophy and gastric neoplasms. *Scientific reports*, *11*(1), 6910. https://doi.org/10.1038/s41598-021-86296-x

Khader, M., & Alany, R. G. (2019). Recent advances in controlled release transdermal drug delivery systems. *International Journal of Pharmaceutics, 564*, 153-170. https://doi.org/10.1016/j.ijpharm.2019.04.030

Kim, J. H., Lim, J. I., & Park, H. K. (2013). Porous chitosan-based adhesive patch filled with poly (l-3, 4-dihydroxyphenylalanine) as a transdermal drug-delivery system. *Journal of Porous Materials, 20*(1), 177-182. https://doi.org/10.1007/s10934-012-9595-3:citation[oaicite:1]{index=1}

Kurek-Górecka, A., Rzepecka-Stojko, A., Górecki, M., Stojko, J., Sosada, M., & Świerczek-Zięba, G. (2013). Structure and antioxidant activity of polyphenols derived from propolis. *Molecules*, *19*(1), 78-101. https://doi.org/10.3390/molecules19010078

Lawrie, G., Keen, I., Drew, B., Chandler-Temple, A., Rintoul, L., Fredericks, P., & Grøndahl, L. (2007). Interactions between alginate and chitosan biopolymers characterized using FTIR and XPS. *Biomacromolecules*, *8*(8), 2533-2541. https://doi.org/10.1021/bm070014y

Lee, K. Y., & Mooney, D. J. (2012). Alginate: Properties and biomedical applications. *Progress in Polymer Science, 37*(1), 106-126. https://doi.org/10.1016/j.progpolymsci.2011.06.003

Leung, D. Y. M., & Bieber, T. (2003). Atopic dermatitis. *The Lancet, 361*(9352), 151-160. https://doi.org/10.1016/S0140-6736(03)12298-9

Leyva-López, N., Lizárraga-Velázquez, C. E., Hernández, C., & Sánchez-Gutiérrez, E. Y. (2020). Exploitation of agro-industrial waste as potential source of bioactive compounds for aquaculture. *Foods*, *9*(7), 843. https://doi.org/10.3390/foods9070843

Liu, D., Ge, Y., Tang, Y., Yuan, Y., Zhang, Q., Li, R., & Xu, Q. (2010). Solid lipid nanoparticles for transdermal delivery of diclofenac sodium: preparation, characterization and in vitro studies. *Journal of microencapsulation*, *27*(8), 726-734. https://doi.org/10.3109/02652048.2010.513456

Liu, L., Zhao, W., Ma, Q., Gao, Y., Wang, W., Zhang, X., ... & Sun, Y. (2023). Functional nano-systems for transdermal drug delivery and skin therapy. *Nanoscale Advances, 5*(6), 1527-1558. https://doi.org/10.1039/D2NA00530A

Marangoni Jr, L., Jamroz, E., Goncalves, S. D. A., da Silva, R. G., Vercelino Alves, R. M., & Vieira, R. P. (2022). Preparation and characterization of sodium alginate films with propolis extract and nano-SiO2. *Food Hydrocolloids for Health, 2*, 8. https://doi.org/10.1016/j.fhfh.2022.100094

Martin, L. J., & Touaibia, M. (2020). Improvement of testicular steroidogenesis using flavonoids and isoflavonoids for prevention of late-onset male hypogonadism. *Antioxidants*, *9*(3), 237. https://doi.org/10.3390/antiox9030237

Martin, N. C., Pirie, A. A., Ford, L. V., Callaghan, C. L., McTurk, K., Lucy, D., & Scrimger, D. G. (2006). The use of phosphate buffered saline for the recovery of cells and spermatozoa from swabs. *Science & justice: journal of the Forensic Science Society*, *46*(3), 179-184. https://doi.org/10.1016/s1355-0306(06)71591-x

Meyer, W., & Seegers, U. (2012). Basics of skin structure and function in elasmobranchs: A review. *Journal of Fish Biology, 80*(5), 1940-1967. https://doi.org/10.1111/j.1095-8649.2011.03207.x

Michalak, M. (2023). Plant extracts as skin care and therapeutic agents. *International Journal of Molecular Sciences, 24*(20), 15444. https://doi.org/10.3390/ijms242015444

Moreno-Rivas, S. C., Ibarra-Gutiérrez, M. J., Fernández-Quiroz, D., Lucero-Acuña, A., Burgara-Estrella, A. J., & Zavala-Rivera, P. (2024). pH-Responsive Alginate/Chitosan Gel Films: An Alternative for Removing Cadmium and Lead from Water. *Gels, 10*(10), 669. https://doi.org/10.3390/gels10100669

Mundargi, R. C., Tan, E. L., Seo, J., & Cho, N. J. (2016). Encapsulation and controlled release formulations of 5-fluorouracil from natural Lycopodium clavatum spores. *Journal of Industrial and Engineering Chemistry*, *36*, 102-108. https://doi.org/10.1016/j.jiec.2016.01.022

Nandiyanto, A. B. D., Oktiani, R., & Ragadhita, R. (2019). How to read and interpret FTIR spectroscope of organic material. *Indonesian Journal of Science and Technology, 4*(1), 97-118. https://ejournal.kjpupi.id/index.php/ijost/article/view/189

Okhale, S. E., Nkwegu, C., Ugbabe, G. E., Ibrahim, J. A., Egharevba, H. O., Kunle, O. F., & Igoli, J. O. (2021). Bee propolis: Production optimization and applications in Nigeria. *Journal of Pharmacognosy and Phytotherapy*, *13*(1), 33-45. http://dx.doi.org/10.5897/JPP2019.0561

Oliveira, L. F. A. D. M. (2021). Nanopartículas de sílica mesoporosa carregadas com extrato de própolis vermelha: síntese, caracterização e avaliação in vitro da atividade antioxidante, antimicrobiana e antiviral. http://www.repositorio.ufal.br/jspui/handle/123456789/8640

Oliveira, R. N., Mancini, M. C., Oliveira, F. C. S. D., Passos, T. M., Quilty, B., Thiré, R. M. D. S. M., & McGuinness, G. B. (2016). FTIR analysis and quantification of phenols and flavonoids of five commercially available plants extracts used in wound healing. *Matéria (Rio de Janeiro)*, *21*, 767-779. https://doi.org/10.1590/S1517-707620160003.0072

Ollerton, J., Winfree, R., & Tarrant, S. (2011). How many flowering plants are pollinated by animals?. *Oikos*, *120*(3), 321-326. https://doi.org/10.1111/j.1600-0706.2010.18644.x

Omar, R. M., Igoli, J., Gray, A. I., Ebiloma, G. U., Clements, C., Fearnley, J., ... & Watson, D. G. (2016). Chemical characterisation of Nigerian red propolis and its biological activity against Trypanosoma brucei. *Phytochemical Analysis*, *27*(2), 107-115. https://doi.org/10.1002/pca.2605

Pacini, E., & Hesse, M. (2005). Pollenkitt–its composition, forms and functions. *Flora-Morphology, Distribution, Functional Ecology of Plants, 200*(5), 399-415. https://doi.org/10.1016/j.flora.2005.02.006

Peixoto, S. R. (2023). *Extraction of bioactive compounds from propolis for application in different matrices in food industry* (Doctoral dissertation). https://hdl.handle.net/1822/87665

Platts-Mills, T. A., & Woodfolk, J. A. (2011). Allergens and their role in the allergic immune response. *Immunological reviews, 242*(1), 51–68. https://doi.org/10.1111/j.1600-065X.2011.01021.x

Pobiega, K., Kot, A. M., Przybył, J. L., Synowiec, A., & Gniewosz, M. (2023). Comparison of the chemical composition and antioxidant properties of propolis from urban apiaries. *Molecules, 28*(18), 6744. https://doi.org/10.3390/molecules28186744

Puizina-Ivic, N. J. A. D. A. (2008). Skin aging. *Acta Dermatovenerologica Alpina Panonica Et Adriatica*, *17*(2), 47. https://skinident.com/fileadmin/img/spanish-pictures/pdf/Skin_Aging.pdf

Raish, M., Kalam, M. A., Ahmad, A., Shahid, M., Ansari, M. A., Ahad, A., ... & Al-Jenoobi, F. I. (2021). Eudragit-coated sporopollenin exine microcapsules (semc) of phoenix dactylifera l. of 5-fluorouracil for colon-specific drug delivery. *Pharmaceutics, 13*(11), 1921. https://doi.org/10.3390/pharmaceutics13111921

Rancan, F., Gaspar, R. S., & Craescu, C. (2023). Silica nanoparticles for enhanced transdermal delivery of anti-inflammatory drugs. *Pharmaceutics, 15*(11), 1372. https://doi.org/10.3390/pharmaceutics15111372

Righi, A. A., Alves, T. R., Negri, G., Marques, L. M., Breyer, H., & Salatino, A. (2011). Brazilian red propolis: unreported substances, antioxidant and antimicrobial activities. *Journal of the Science of Food and Agriculture, 91*(13), 2363-2370. https://doi.org/10.1002/jsfa.4468

Rocha, C. D. L. J. (2009). Histofisiologia e classificação das queimaduras: consequências locais e sistêmicas das perdas teciduais em pacientes queimados. *Rev. interdisciplin. estud. exp. anim. hum.(impr.)*, 140-147. https://pesquisa.bvsalud.org/portal/resource/pt/biblio-964347

Sarapa, A., Peter, A., Buettner, A., & Loos, H. M. (2025). Organoleptic and chemical properties of propolis: a review. *European Food Research and Technology, 1*-22. https://doi.org/10.1007/s00217-025-04708-y

Schaffert, D., & Wagner, E. (2008). Gene therapy progress and prospects: synthetic polymer-based systems. *Gene therapy*, *15*(16), 1131-1138. https://doi.org/10.1038/gt.2008.105

Schiff, M. H., Jaffe, J. S., & Freundlich, B. (2014). Head-to-head, randomised, crossover study of oral versus subcutaneous methotrexate in patients with rheumatoid arthritis: Drug-exposure limitations of oral methotrexate at doses ≥ 15 mg may be overcome with subcutaneous administration. *Annals of the Rheumatic Diseases, 73*(8), 1549-1551. https://doi.org/10.1136/annrheumdis-2014-205228.

Schmitt, J., Apfelbacher, C. J., & Flohr, C. (2011). Eczema. *BMJ Clinical Evidence, 2011*, 1716. https://doi.org/10.1136/bmj.d1716

Silva, B. B., Rosalen, P. L., Cury, J. A., Ikegaki, M., Souza, V. C., Esteves, A., & Alencar, S. M. (2008). Chemical composition and botanical origin of red propolis, a new type of Brazilian propolis. *Evidence-based Complementary and Alternative Medicine*, *5*(3), 313-316. https://doi.org/10.1093/ecam/nem059

Silva, V. C., Silva, A. M., Basílio, J. A., Xavier, J. A., do Nascimento, T. G., Naal, R. M., ... & Goulart, M. O. (2020). New Insights for Red Propolis of Alagoas—Chemical constituents, topical membrane formulations and their Physicochemical and Biological Properties. *Molecules, 25*(24), 5811. https://doi.org/10.3390/molecules25245811

Socha, R., Gałkowska, D., Bugaj, M., & Juszczak, L. (2015). Phenolic composition and antioxidant activity of propolis from various regions of Poland. *Natural Product Research, 29*(5), 416-422. https://doi.org/10.1080/14786419.2014.949705

Soliman, D., Ibrahim, M. A., Mohamed, S. R., Thagfan, F. A., El-khadragy, M. F., Al-Megrin, W. A., ... & Dkhil, M. A. (2023). Lung response to propolis treatment during experimentally induced lung adenocarcinoma. *Journal of Taibah University for Science, 17*(1), 2213411. https://doi.org/10.1080/16583655.2023.2213411

STOJKO, Mateusz; WOLNY, Daniel; WŁODARCZYK, Jakub. Nonwoven releasing propolis as a potential new wound healing method—A review. *Molecules, v. 26*, n. 18, p. 5701, 2021. https://doi.org/10.3390/molecules26185701

Thacharodi, D., & Rao, K. P. (1995). Development and in vitro evaluation of chitosan-based transdermal drug delivery systems for the controlled delivery of propranolol hydrochloride. *Biomaterials*, *16*(2), 145-148. https://doi.org/10.1016/0142-9612(95)98278-M

Touzani, S., Embaslat, W., Imtara, H., Kmail, A., Kadan, S., Zaid, H., ... & Saad, B. (2019). In vitro evaluation of the potential use of propolis as a multitarget therapeutic product: Physicochemical properties, chemical composition, and immunomodulatory, antibacterial, and anticancer properties. *BioMed research international, 2019*(1), 4836378. https://doi.org/10.1155/2019/4836378

Tumbarski, Y., Ivanov, I., Todorova, M., Apostolova, S., Tzoneva, R., & Nikolova, K. (2025). Phenolic Content, Antioxidant Activity and In Vitro Anti-Inflammatory and Antitumor Potential of Selected Bulgarian Propolis Samples. *Biomedicines, 13*(2), 334. https://doi.org/10.3390/biomedicines13020334

Tran, H., Le, T., Le, T., & Nguyen, T. (2016). Burn image classification using one-class support vector machine. In *Context-Aware Systems and Applications: 4th International Conference, ICCASA 2015, Vung Tau, Vietnam, November 26-27, 2015, Revised Selected Papers 4* (pp. 233-242). Springer International Publishing. https://doi.org/10.1007/978-3-319-29236-6_23

Turbiani, F. R., Kieckbusch, T. G., & Gimenes, M. L. (2011). Liberação de benzoato de cálcio de filmes de alginato de sódio reticulados com íons cálcio. *Polímeros*, *21*, 175-181. https://doi.org/10.1590/S0104-14282011005000034

Uzarski, J. S., DiVito, M. D., Wertheim, J. A., & Miller, W. M. (2017). Essential design considerations for the resazurin reduction assay to noninvasively quantify cell expansion within perfused extracellular matrix scaffolds. *Biomaterials, 129*, 163-175. https://doi.org/10.1016/j.biomaterials.2017.02.015

Vieira de Morais, D., Rosalen, P. L., Ikegaki, M., de Souza Silva, A. P., Massarioli, A. P., & de Alencar, S. M. (2021). Active antioxidant phenolics from Brazilian red propolis: An optimization study for their recovery and identification by LC-ESI-QTOF-MS/MS. *Antioxidants, 10*(2), 297. https://doi.org/10.3390/antiox10020297

Vieira, S., Franco, A. R., Fernandes, E. M., Amorim, S., Ferreira, H., Pires, R. A., ... & Neves, N. M. (2018). Fish sarcoplasmic proteins as a high value marine material for wound dressing applications. *Colloids and Surfaces B: Biointerfaces*, *167*, 310-317. https://doi.org/10.1016/j.colsurfb.2018.04.002

Wagner, J., & Horn, R. S. (2012). Pharmacokinetic/pharmacodynamic considerations in the development of controlled-release intravenous drug delivery systems. *Pharmaceutical Research, 29*(7), 1751-1769. https://doi.org/10.1007/s11095-012-0727-4

Zhang, W., Li, X., & Jiang, W. (2020). Development of antioxidant chitosan film with banana peels extract and its application as coating in maintaining the storage quality of apple. *International journal of biological macromolecules*, *154*, 1205-1214. https://doi.org/10.1016/j.ijbiomac.2019.10.275

Zhang, Y., Yu, J., Kahkoska, A. R., Wang, J., Buse, J. B., & Gu, Z. (2019). Advances in transdermal insulin delivery. *Advanced drug delivery reviews*, *139*, 51-70. https://doi.org/10.1016/j.addr.2018.12.006

Zhao, J., & Mao, S. (2021). Tuning the membrane fluidity of liposomes for desirable in vivo fate with enhanced drug delivery. In *Advances in biomembranes and lipid self-assembly* (Vol. 34, pp. 67-106). Academic Press. https://doi.org/10.1016/bs.abl.2021.11.003

Zink, B. S. (2014). Câncer de pele: A importância do seu diagnóstico, tratamento e prevenção. *Revista Hospital Universitário Pedro Ernesto,* 13. https://doi.org/10.12957/rhupe.2014.12256